

ESA Climate Change Initiative (CCI)

Sea Level Budget Closure (SLBC_cci)

Product Description Document D2.3.2
ESA_SLBC_cci_D2.3.2_v1.2

Description of data set and uncertainty assessment,
version 1

Prime & Science Lead: Martin Horwath
Technische Universität Dresden (TUDr)
Martin.Horwath@tu-dresden.de

Technical Officer: Jérôme Benveniste
ESA ESRIIN, Frascati, Italy
Jerome.Benveniste@esa.int

Consortium: Laboratoire d'Etudes en Géophysique et Océanographie Spatiales (LEGOS)
Universität Bremen (UB)
Universität Zürich (UZH)
University of Leeds (UoL)
Goethe-Universität Frankfurt (GUF)
Danmarks Tekniske Universitet, DTU Space, Geodynamics (DTU-GDK)
Danmarks Tekniske Universitet, DTU Space, Geodesy (DTU-GEK)
Nansen Environmental and Remote Sensing Center (NERSC)
University of Reading (UoR)
Mercator Ocean, Toulouse (MerO)



**CCI Sea Level Budget Closure
ESA/ESRIN contract 4000119910/17/I-NB**

Reference: ESA_SLBC_cci_D2.3.2



Version: v1.2

Date: 22.11.2018



Page: 2 of 119

To be cited as:

Novotny, K.; Horwath, M.; Cazenave, A.; Palanisamy, H.; Marzeion, B.; Paul, F.; Döll, P.; Cáceres, D.; Hogg, A.; Shepherd, A.; Otosaka, I.; Forsberg, R.; Barletta, V.R.; Andersen, O.B.; Rannald, H.; Johannessen, J.; Nilsen, J.E.; Gutknecht, B.D.; Merchant, Ch.J.; MacIntosh, C.R.; Old, Ch.; von Schuckmann, K.: *ESA Climate Change Initiative (CCI) Sea Level Budget Closure (SLBC_cci). Product Description Document D2.3.2: Version 1 data sets and uncertainty assessments. Version 1.2, 22 Nov 2018.*

		<p>CCI Sea Level Budget Closure ESA/ESRIN contract 4000119910/17/I-NB</p> <p>Reference: ESA_SLBC_cci_D2.3.2 Version: v1.2 Date: 22.11.2018 Page: 3 of 119</p>
---	---	---

Signatures page

Prepared by	<p style="text-align: center;">Kristin Novotny Project Manager, TUDr Martin Horwath Science Leader, TUDr</p> <p>Anny Cazenave, Hindumathi Palanisamy, LEGOS; Ben Marzeion, UB; Frank Paul, Raymond Le Bris, UZH; Petra Döll, Denise Cáceres, GUF; Anna Hogg, Andrew Shepherd, UOL; Rene Forsberg, DTU-GDK; Ole B. Andersen, Heidi Ranndal, DTU-GEK; Johnny Johannessen, Jan Even O. Nilsen, NERSC; Benjamin D. Gutknecht, TUDr; Christopher John Merchant, Claire Rachel MacIntosh, UoR; Karina von Schuckmann, MerO</p>	Date: 2018-11-22 
Checked by	<p style="text-align: center;">Martin Horwath Science Leader, TUDr</p>	Date: 2018-11-22 
Approved by	<p style="text-align: center;">Jérôme Benveniste Technical Officer, ESA</p>	Date:



**CCI Sea Level Budget Closure
ESA/ESRIN contract 4000119910/17/I-NB**

Reference: ESA_SLBC_cci_D2.3.2

Version: v1.2

Date: 22.11.2018

Page: 4 of 119

		<p>CCI Sea Level Budget Closure ESA/ESRIN contract 4000119910/17/I-NB</p> <p>Reference: ESA_SLBC_cci_D2.3.2 Version: v1.2 Date: 22.11.2018 Page: 5 of 119</p>
---	---	---

Change Log

Issue	Author, Org.	Affected Section	Reason/Description	Status
1.0	M. Horwath / TUDr	All	Document Creation	Released to ESA 2018-08-31
1.1	M. Horwath / TUDr	All	Document revision after review by ESA	Released to ESA 2018-10-25
1.2	M. Horwath / TUDr	All	Document revision after review by ESA	Released to ESA 2018-11-22

Distribution List

Organization	Consortium Member
TUDr	Martin Horwath
LEGOS	Anny Cazenave
UB	Ben Marzeion
UZH	Frank Paul
UoL	Andrew Shepherd, Anna Hogg
DTU- GDK	Rene Forsberg
GUF	Petra Döll
NERSC	Johnny Johannessen
DTU-GEK	Ole B. Andersen
UoR	Christopher Merchant
MerO	Karina von Schuckmann
ESA	Jérôme Benveniste Marco Restano Américo Ambrózio



CCI Sea Level Budget Closure
ESA/ESRIN contract 4000119910/17/I-NB

Reference: ESA_SLBC_cci_D2.3.2

Version: v1.2


Date: 22.11.2018

Page: 6 of 119



		CCI Sea Level Budget Closure ESA/ESRIN contract 4000119910/17/I-NB Reference: ESA_SLBC_cci_D2.3.2 Version: v1.2 Date: 22.11.2018 Page: 7 of 119
---	---	--

Table of Contents

Change Log	5
Table of Contents.....	7
Acronyms and Abbreviations	11
1 Introduction	15
1.1 Purpose and Scope.....	15
1.2 Document Structure.....	15
1.3 Data Structure.....	15
2 Total Sea Level Change	19
2.1 Data access and requirements.....	19
2.2 Algorithms.....	19
2.2.1 Review of scientific background	19
2.2.2 Algorithms	20
2.3 Product Specification	23
2.3.1 Product geophysical data content	23
2.3.2 Coverage and resolution in time and space	23
2.3.3 Product data format	23
2.4 Uncertainty Assessment	24
2.4.1 Sources of error	24
2.4.2 Methodology for uncertainty assessment	24
2.4.3 Results of uncertainty assessment	24
2.4.4 Uncertainty documentation in the data products	24
2.5 References	25
3 Steric Sea Level Change	26
3.1 Data access and requirements.....	26
3.2 Algorithms.....	26
3.2.1 Algorithms	26
3.3 Product Specification	29
3.3.1 Product geophysical data content	29
3.3.2 Coverage and resolution in time and space	29
3.3.3 Product data format	30
3.4 Uncertainty Assessment	30
3.4.1 Sources of error	30
3.4.2 Methodology for uncertainty assessment	31
3.4.3 Results of uncertainty assessment	33
3.4.4 Uncertainty documentation in the data products	35
3.5 References	36
4 Ocean Mass Change	37

		CCI Sea Level Budget Closure ESA/ESRIN contract 4000119910/17/I-NB Reference: ESA_SLBC_cci_D2.3.2 Version: v1.2 Date: 22.11.2018 Page: 8 of 119
---	---	--

4.1	Data Access and Requirements.....	37
4.2	Algorithms.....	38
4.2.1	Review of scientific background	38
4.2.2	Algorithms	40
4.3	Product specification	44
4.3.1	Product geophysical data content	46
4.3.2	Coverage and resolution in time and space	47
4.3.3	Product data format	48
4.3.4	Product grid and projection	48
4.4	Uncertainty assessment.....	49
4.4.1	Sources of error	49
4.4.2	Methodology and Results of Uncertainty Assessment	50
4.4.3	Uncertainty documentation in the data products	52
4.5	Continental Mass Change	53
4.6	References	55
5	Glacier Contribution to Sea Level Change	57
5.1	Data Access and Requirements.....	57
5.2	Algorithms.....	58
5.2.1	Review of scientific background	58
5.2.2	Algorithms	59
5.3	Product Specification	59
5.3.1	Product geophysical data content	59
5.3.2	Coverage and resolution in time and space	61
5.3.3	Product data format	61
5.3.4	Product grid and projection	61
5.4	Uncertainty assessment.....	61
5.4.1	Sources of error	61
5.4.2	Methodology for uncertainty assessment	62
5.4.3	Results of uncertainty assessment	63
5.4.4	Uncertainty documentation in the data products	64
5.5	References	64
6	Ice Sheets Contribution to Sea Level Change.....	65
6.1	Data access and requirements.....	65
6.2	Algorithms.....	67
6.2.1	Review of scientific background	67
6.2.2	Algorithms	68
6.3	Product Specification	72
6.3.1	Product geophysical data content	72
6.3.2	Coverage and resolution in time and space	79
6.3.3	Product data format	80
6.3.4	Product grid and projection	80

		<p>CCI Sea Level Budget Closure ESA/ESRIN contract 4000119910/17/I-NB</p> <p>Reference: ESA_SLBC_cci_D2.3.2 Version: v1.2 Date: 22.11.2018 Page: 9 of 119</p>
---	---	---

6.4	Uncertainty Assessment	81
6.4.1	Sources of error	81
6.4.2	Methodology for uncertainty assessment	82
6.4.3	Results of uncertainty assessment	85
6.4.4	Uncertainty documentation in the data products	85
6.5	References	85
7	Total Land Water Storage Change.....	88
7.1	Data Access and Requirements.....	88
7.2	Algorithms.....	88
7.2.1	Review of scientific background	88
7.2.2	Algorithms	88
7.3	Product Specification	95
7.3.1	Product geophysical data content	95
7.3.2	Coverage and resolution in time and space	99
7.3.3	Product data format	99
7.3.4	Product grid and projection	99
7.4	Uncertainty Assessment	99
7.4.1	Sources of error	99
7.4.2	Methodology for uncertainty assessment	99
7.4.3	Results of uncertainty assessment	100
7.4.4	Uncertainty documentation in the data products	101
7.5	References	102
8	Arctic Sea Level Change	103
8.1	Data Access and Requirements.....	103
8.2	Algorithms.....	103
8.2.1	Review of scientific background	103
8.2.2	Algorithms	104
8.3	Product Specification	107
8.3.1	Product geophysical data content	107
8.3.2	Coverage and resolution in time and space	108
8.3.3	Product data format	108
8.3.4	Product grid and projection	108
8.4	Uncertainty assessment.....	109
8.4.1	Sources of error	109
8.4.2	Methodology for uncertainty assessment	109
8.4.3	Results of uncertainty assessment	110
8.4.4	Uncertainty documentation in the data products	111
8.5	References	111
	Appendix	113



CCI Sea Level Budget Closure
ESA/ESRIN contract 4000119910/17/I-NB

Reference: ESA_SLBC_cci_D2.3.2

Version: v1.2

Date: 22.11.2018

Page: 10 of 119

		<p>CCI Sea Level Budget Closure ESA/ESRIN contract 4000119910/17/I-NB</p> <p>Reference: ESA_SLBC_cci_D2.3.2 Version: v1.2 Date: 22.11.2018 Page: 11 of 119</p>
---	---	--

Acronyms and Abbreviations

Acronym	Explanation
20CRv2	Twentieth Century Reanalysis (V2) (NOAA)
AIS	Antarctic Ice Sheet
ALES, ALES+	Adaptive Leading Edge Subwaveform retracker
AOD	atmospheric and oceanic de-aliasing
AP	Antarctic Peninsula
ASCII	American Standard Code for Information Interchange
ATBD	Algorithm Theoretical Baseline Document
AVISO	Archiving, Validation and Interpretation of Satellite Oceanographic data
CCI	Climate Change Initiative (initiated by ESA)
CECR	Comprehensive Error Characterisation Report
CFSR	NCEP Climate Forecast System Reanalysis
CMC	Continental Mass Change
CNES	Centre National d'Etudes Spatiales
CRU	Climatic Research Unit (University of East Anglia, Norwich, UK)
CRU CL, CRU TS	CRU Timeseries (grids of observed climate)
CSR	Center for Space Research (University of Texas at Austin)
csv	Comma-separated values
DOI	Digital object identifier
DTU	Danmarks Tekniske Universitet
EAIS	East Antarctic Ice Sheet
ECHAM	Max Planck Institute for Meteorology atmospheric general circulation model
ECMWF	European Centre for Medium-Range Weather Forecasts
ECV	Essential Climate Variables
ELA	Equilibrium Line Altitude
EN4	version 4 of the Met Office Hadley Centre "EN" series of data sets of global quality controlled ocean temperature and salinity profiles
Envisat	"Environmental Satellite", Earth-observing satellite operated by ESA
EOS-80	1980 International Equation of State for Seawater
EPSG	European Petroleum Survey Group
EPSG3031	EPSG Projection 3031 - WGS 84 / Antarctic Polar Stereographic
ERA	Earth system ReAnalysis
ERS-1/2	European Remote Sensing Satellite -1/2
ESA	European Space Agency
ESM	Earth System Model
ESRIN	European Space Research Institute
ETOPO5	global 5-minute gridded elevations/bathymetry NOAA product
EWH	equivalent water height

		<p>CCI Sea Level Budget Closure ESA/ESRIN contract 4000119910/17/I-NB</p> <p>Reference: ESA_SLBC_cci_D2.3.2 Version: v1.2 Date: 22.11.2018 Page: 12 of 119</p>
---	---	--

GAA, GAB, GAC, GAD	Names of data products related to GRACE atmospheric and oceanic background models (refer to section 4.2.1)
GFO	GeoSat Follow-On
GFZ	GeoForschungsZentrum Potsdam
GIA	Glacial Isostatic Adjustment
GIS	Greenland Ice Sheet
GMB	Gravimetric Mass Balance / GRACE Mass Balance
GMSL	Global Mean Sea Level
GPCP	Global Precipitation Climatology Centre
GPS / GNSS	Global Positioning System / Global Navigation Satellite System
GRACE	Gravity Recovery and Climate Experiment
GRACE-FO	GRACE-Follow On
GrIS	Greenland Ice Sheet
GSFC	Goddard Space Flight Center
GSSL	Global mean Steric Sea Level
Gt	Gigatons
GUF	Goethe-Universität Frankfurt
GWD	Groundwater depletion
GWS	Groundwater storage
GWSWUSE	submodel of the WaterGAP WGHM
HDF5	Hierarchical Data Format (HDF)
HIRHAM	RCM based on a subset of the HIRLAM and ECHAM models
HIRLAM	High Resolution Limited Area Mode
HYCOM	Hybrid Coordinate Ocean Model
HYOGA	Japanese, means glacier
IB	Inverse Barometer
ICE-4G, ICE-5G, ICE-6G	models of deglaciation history and postglacial relative sea-level history
ICESat	Ice, Cloud, and land Elevation Satellite, part of NASA's Earth Observing System
IMBIE	Ice Sheet Mass Balance Inter-comparison Exercise
ITSG	Institute of Geodesy, Theoretical Geodesy and Satellite Geodesy (TU Graz)
JPL	Jet Propulsion Laboratory
JRA-55	Japanese 55-year ReAnalysis
LARS	Lars Advanced Retracking System
LEGOS	Laboratoire d'Etudes en Géophysique et Océanographie Spatiales
LRM	Low Rate Mode (CryoSat-2)
MBT	Mechanical Bathythermograph
MD5	"Message Digest" (MD), MD5 algorithm can be used as a checksum to verify data integrity
MEaSURES	Making Earth Science Data Records for Use in Research Environments
MerO	Mercator Ocean
MERRA-2	Modern-Era Retrospective analysis for Research and Applications, Version 2

		<p>CCI Sea Level Budget Closure ESA/ESRIN contract 4000119910/17/I-NB</p> <p>Reference: ESA_SLBC_cci_D2.3.2 Version: v1.2 Date: 22.11.2018 Page: 13 of 119</p>
---	---	--

MOG2D	Modèle d'Onde de Gravité à 2 Dimensions
MSS	Mean Sea Surface
MSSL	Mean Steric Sea Level
NASA	National Aeronautics and Space Administration
NCEP	National Centers for Environmental Prediction
NCP	North China Plain
NERSC	Nansen Environmental and Remote Sensing Center
netCDF	Network Common Data Form (to support the creation, access, and sharing of array-oriented scientific data)
NOAA	National Oceanic and Atmospheric Administration
NSIDC	National Snow and Ice Data Center
OBP	Ocean Bottom Pressure
OGGM	Open Global Glacier Model
OMC	Ocean Mass Change
OMCT	Ocean Model for Circulation and Tides
OSTM	Ocean Surface Topography Mission (OSTM) on the Jason-2 satellite
PP	Pulse Peakiness
PSD	Product Specification Document
RADS	Radar Altimetry Database System
RCM	Regional atmospheric Climate Model
RGI	Randolph Glacier Inventory
RMS	Root Mean Square
SAR	Synthetic Aperture Radar
SARIn	SAR Interferometric mode (CryoSat-2)
SARAL	Satellite with ARGos and ALtiKa, cooperative altimetry technology mission of Indian Space Research Organisation (ISRO) and CNES (Space Agency of France)
SELEN	SEa Level EquatioN solver
SH	spherical harmonic
SHA	Steric Height Anomaly
SL	Sea Level
SLA	sea level anomaly
SLBC	Sea Level Budget Closure
SLE, s.l.e.	Sea Level Equivalent
SLR	Satellite Laser Ranging
SSH	Sea Surface Height
SSL	Steric Sea Level
SSLA	Steric Sea Level Anomaly
SSL4SLBC	Steric Sea Level for Sea Level Budget Closure
SST	Sea Surface Temperature
STD	Standard Deviation
TOPAZ	(Towards) an Operational Prediction system for the North Atlantic European coastal Zones

		<p>CCI Sea Level Budget Closure ESA/ESRIN contract 4000119910/17/I-NB</p> <p>Reference: ESA_SLBC_cci_D2.3.2 Version: v1.2 Date: 22.11.2018 Page: 14 of 119</p>
---	---	--

TOPEX	TOPOgraphy EXperiment, part of the TOPEX/Poseidon satellite(joint radar altimetry project, NASA and CNES)
TS	Time Series
TUDr	TU Dresden
TWS	Total Water Storage
TWSA	Total Water Storage Anomaly
UB	Universität Bremen
UK	United Kingdom
UoL	University of Leeds
UoR	University of Reading
UZH	Universität Zürich
v0, v1	version 0/1 data set within SLBC_cci project
VM	model of the radial viscoelastic structure of the Earth (used fo ICE-5G)
w.e.	water equivalent
WAIS	West Antarctic Ice Sheet
WATCH	The WATER and global CHange project
WFDEI	WATCH Forcing Data based on ERA-Interim reanalysis
WGHM	WaterGAP Global Hydrology Model
WGMS	World Glacier Monitoring Service
WGS84	World Geodetic System 1984
WP	Work Package
XBT	Expendable Bathythermograph
XCTD	Expendable Conductivity/Temperature and Depth

		CCI Sea Level Budget Closure ESA/ESRIN contract 4000119910/17/I-NB Reference: ESA_SLBC_cci_D2.3.2 Version: v1.2 Date: 22.11.2018 Page: 15 of 119
---	---	---

1 Introduction

1.1 Purpose and Scope

This document describes the Version 1 (v1) datasets on individual sea level budget components. Starting with the version 0 (v0) data sets at the beginning of the project, these time series have been continuously revised and improved during the project's "preliminary improvement" phase. As a result the v1 data sets were developed, and a description of these data is given by this document. The document (Deliverable D2.3.2), together with the set of related data (D2.3.1) represent an interim result for further discussion and improvements, and a new budget assessment will be performed based on these data.

1.2 Document Structure

Sections 2 to 8 contain the descriptions for the sea level and steric component, the ocean mass component, the glacier contribution, the ice sheet contribution, the land water contribution, and the dedicated datasets for the Arctic area, respectively. Each section has the same subdivision into subsections describing sources of the datasets, algorithms, product specification, uncertainty assessments, and finally the reference list.

University of Reading (UoR) contributes to this project within SSL4SBC_cci. Data provided by UoR are described in this project's document in Section 3.

1.3 Data Structure

All data described in this documentation are stored at a project's data drive at TU Dresden. Access is managed by Kristin Novotny (Kristin.Novotny@tu-dresden.de).

Data files are organized in the following structure:

```

/D2.3_Data_v1_final_2018-09-06_frozen
  /WP212_gmsl_steric_v1
    /Data_LEGOS
      | ts_GMSL_1993_2015_no_seasonal_signal_GIA_applied_TopexA_driftcorrected_v1.nc
    /Data_UoR
      | GSSL_EN4.2.1_1993_2015_v1.nc
      | MSSL_EN.4.2.1_1993_2015_v1.nc
  /WP222_ocean_mass_v1
    /CMC_GraceTimeSeries
      | CMctS_SLBC_cci_v1.00_ITSG2016_2003.00-2016.05_ShFil-0_c21-1_GAD-0_GIA-CaronIvins2018.csv
    /OMC_GraceTimeSeries
      | /ArcticOc

```



**CCI Sea Level Budget Closure
ESA/ESRIN contract 4000119910/17/I-NB**

Reference: ESA_SLBC_cci_D2.3.2
Version: v1.2
Date: 22.11.2018
Page: 16 of 119

AOMCts_SLBCv1.00_ITSG2016_2003.000-2016.050_ShFil-0_c21-1_GAD1-111_GIA-A2013-Ice5Gv2_R2.csv
AOMCts_SLBCv1.00_ITSG2016_2003.000-2016.050_ShFil-0_c21-1_GAD1-111_GIA-CaronIvins2018_R2.csv

/GlobalOc

OMCts_SLBCv1.00_ITSG2016_2003.000-2016.050_ShFil-0_c21-1_GAD1-111_GIA-A2013-Ice5Gv2_R2.csv
OMCts_SLBCv1.00_ITSG2016_2003.000-2016.050_ShFil-0_c21-1_GAD1-111_GIA-CaronIvins2018_R2.csv

/SupplementaryOmcTimeSeries

/arctic

AOMCts_SLBCv1.00_CSRsh_2003.000-2016.050_ShFil-0_c21-1_GAD1-111_GIA-A2013-Ice5Gv2_R2.csv
AOMCts_SLBCv1.00_CSRsh_2003.000-2016.050_ShFil-0_c21-1_GAD1-111_GIA-CaronIvins2018_R2.csv
AOMCts_SLBCv1.00_CSRsh_2003.000-2016.050_ShFil-0_c21-1_GAD1-111_GIA-no_R2.csv
AOMCts_SLBCv1.00_GFZsh_2003.000-2016.050_ShFil-0_c21-1_GAD1-111_GIA-A2013-Ice5Gv2_R2.csv
AOMCts_SLBCv1.00_GFZsh_2003.000-2016.050_ShFil-0_c21-1_GAD1-111_GIA-CaronIvins2018_R2.csv
AOMCts_SLBCv1.00_GFZsh_2003.000-2016.050_ShFil-0_c21-1_GAD1-111_GIA-no_R2.csv
AOMCts_SLBCv1.00_GSFCm_2003.000-2016.050.csv
AOMCts_SLBCv1.00_ITSG2016_2003.000-2016.050_ShFil-0_c21-1_GAD1-111_GIA-no_R2.csv
AOMCts_SLBCv1.00_JPLsh_2003.000-2016.050_ShFil-0_c21-1_GAD1-111_GIA-A2013-Ice5Gv2_R2.csv
AOMCts_SLBCv1.00_JPLsh_2003.000-2016.050_ShFil-0_c21-1_GAD1-111_GIA-CaronIvins2018_R2.csv
AOMCts_SLBCv1.00_JPLsh_2003.000-2016.050_ShFil-0_c21-1_GAD1-111_GIA-no_R2.csv
info.txt

/global

CHAMBERS_ocean_mass_orig.txt
OMCts_SLBCv1.00_CSRsh_2003.000-2016.050_ShFil-0_c21-1_GAD1-111_GIA-A2013-Ice5Gv2_R2.csv
OMCts_SLBCv1.00_CSRsh_2003.000-2016.050_ShFil-0_c21-1_GAD1-111_GIA-CaronIvins2018_R2.csv
OMCts_SLBCv1.00_CSRsh_2003.000-2016.050_ShFil-0_c21-1_GAD1-111_GIA-no.csv
OMCts_SLBCv1.00_GFZsh_2003.000-2016.050_ShFil-0_c21-1_GAD1-111_GIA-A2013-Ice5Gv2_R2.csv
OMCts_SLBCv1.00_GFZsh_2003.000-2016.050_ShFil-0_c21-1_GAD1-111_GIA-CaronIvins2018_R2.csv
OMCts_SLBCv1.00_GFZsh_2003.000-2016.050_ShFil-0_c21-1_GAD1-111_GIA-no_R2.csv
OMCts_SLBCv1.00_GSFCm_2003.000-2016.050.csv
OMCts_SLBCv1.00_ITSG2016_2003.000-2016.050_ShFil-0_c21-1_GAD1-111_GIA-no_R2.csv
OMCts_SLBCv1.00_JPLsh_2003.000-2016.050_ShFil-0_c21-1_GAD1-111_GIA-A2013-Ice5Gv2_R2.csv
OMCts_SLBCv1.00_JPLsh_2003.000-2016.050_ShFil-0_c21-1_GAD1-111_GIA-CaronIvins2018_R2.csv
OMCts_SLBCv1.00_JPLsh_2003.000-2016.050_ShFil-0_c21-1_GAD1-111_GIA-no_R2.csv

/ OMC_GriddedOMC

EWH_OMC-Grid_GSFCm_SLBC-v1.01_1x1.nc
EWH_OMC-Grid_ITSG2016_SLBC-v1.01_1x1_buf300_A2013.nc
EWH_OMC-Grid_ITSG2016_SLBC-v1.01_1x1_buf300_Caron2018.nc
EWH_OMC-Grid_ITSG2016_SLBC-v1.01_1x1_filt_buf300_A2013.nc
EWH_OMC-Grid_ITSG2016_SLBC-v1.01_1x1_filt_buf300_Caron2018.nc
info.txt

OReadme.txt

/WP232_glaciers_v1

glaciers_ensemble_median_rgi_v5_monthly_v1.1.nc

/WP242_icesheets_v1

/AIS_Altim

annual_mean_v1_EAIS.csv
annual_mean_v1_WAIS.csv
AIS_timeseries_and_uncertainty_varying_err_dens.csv
APIS_timeseries_and_uncertainty_varying_err_dens.csv
EAIS_timeseries_and_uncertainty_varying_err_dens.csv
WAIS_timeseries_and_uncertainty_varying_err_dens.csv

/AIS_GMB

AIS_GMB_basin.dat
AIS_GMB_trend.dat



CCI Sea Level Budget Closure
ESA/ESRIN contract 4000119910/17/I-NB

Reference: ESA_SLBC_cci_D2.3.2
Version: v1.2
Date: 22.11.2018
Page: 17 of 119

AIS_GMB_grid.nc

/GIS_Altim

SLBC_GrIS_RA_MB_vers2.nc

SLBC_ICESat_mass_2003_2009_v0.txt

/GIS_GMB

CCI_GMB_RL06_time_series_NO_GIA.zip

(contains GISNN_grace.dat, NN = 00 ... 08)

GIS00_grace.png

README.txt

/WP252_landwater_v1

/globally_average_tws

tws_WaterGAP22c_CRU_mm_irr70_version1_month1992_2015.txt

tws_WaterGAP22c_CRU_mm_irr70_version1_year1992_2015.txt

tws_WaterGAP22c_CRU_mm_irr70_version1_yearinmonth1992_2015.txt

tws_WaterGAP22c_CRU_mm_irr100_version1_month1992_2015.txt

tws_WaterGAP22c_CRU_mm_irr100_version1_year1992_2015.txt

tws_WaterGAP22c_CRU_mm_irr100_version1_yearinmonth1992_2015.txt

tws_WaterGAP22c_WFDEI_CRU_mm_irr70_version1_month1992_2015.txt

tws_WaterGAP22c_WFDEI_CRU_mm_irr70_version1_year1992_2015.txt

tws_WaterGAP22c_WFDEI_CRU_mm_irr70_version1_yearinmonth1992_2015.txt

tws_WaterGAP22c_WFDEI_CRU_mm_irr100_version1_month1992_2015.txt

tws_WaterGAP22c_WFDEI_CRU_mm_irr100_version1_year1992_2015.txt

tws_WaterGAP22c_WFDEI_CRU_mm_irr100_version1_yearinmonth1992_2015.txt

tws_WaterGAP22c_WFDEI_GPCC_mm_irr70_version1_year1992_2013.txt

tws_WaterGAP22c_WFDEI_GPCC_mm_irr70_version1_year1992_2013.txt

tws_WaterGAP22c_WFDEI_GPCC_mm_irr70_version1_yearinmonth1992_2013.txt

tws_WaterGAP22c_WFDEI_GPCC_mm_irr100_version1_year1992_2013.txt

tws_WaterGAP22c_WFDEI_GPCC_mm_irr100_version1_year1992_2013.txt

tws_WaterGAP22c_WFDEI_GPCC_mm_irr100_version1_yearinmonth1992_2013.txt

/gridded_tws

/additional_data

contarea_wghm_wlm.nc

outcell_wghm_wlm.nc

/Q

Q_WaterGAP22c_CRU_irr70_version1.nc

Q_WaterGAP22c_CRU_irr100_version1.nc

Q_WaterGAP22c_WFDEI_CRU_irr70_version1.nc

Q_WaterGAP22c_WFDEI_CRU_irr100_version1.nc

Q_WaterGAP22c_WFDEI_GPCC_irr70_version1.nc

Q_WaterGAP22c_WFDEI_GPCC_irr100_version1.nc

/tws



tws_WaterGAP22c_CRU_mm_irr70_version1.nc

tws_WaterGAP22c_CRU_mm_irr100_version1.nc

tws_WaterGAP22c_WFDEI_CRU_mm_irr70_version1.nc

tws_WaterGAP22c_WFDEI_CRU_mm_irr100_version1.nc

tws_WaterGAP22c_WFDEI_GPCC_mm_irr70_version1.nc

		<p>CCI Sea Level Budget Closure ESA/ESRIN contract 4000119910/17/I-NB</p> <p>Reference: ESA_SLBC_cci_D2.3.2 Version: v1.2 Date: 22.11.2018 Page: 18 of 119</p>
---	---	--

```

| | | tws_WaterGAP22c_WFDEI_GPCC_mm_irr100_version1.nc
| | | README.txt
| | | /WP262_ArcticOcean_v1
| | | /D2.1.1_Arctic_NERSC
| | | topazssh20032015.nc
| | | topazstht20032015.nc
| | | /D2.3.1_Arctic_SLA_DTU
| | | ARCTIC_SLA_v1.1.nc

```

		<p>CCI Sea Level Budget Closure ESA/ESRIN contract 4000119910/17/I-NB</p> <p>Reference: ESA_SLBC_cci_D2.3.2 Version: v1.2 Date: 22.11.2018 Page: 19 of 119</p>
---	---	--

2 Total Sea Level Change

The time series of Global Mean Sea Level (GMSL) change are derived from satellite altimetry observations. The following section describes this product.

2.1 Data access and requirements

The v1 altimetry based GMSL data file consists of GMSL time series from three groups:

- (1) ESA CCI
- (2) AVISO
- (3) NASA/GSFC

These GMSL time series are corrected for the TOPEX A instrumental drift correction over 1993-1998, using 3 different approaches as described in Dieng et al. (2017), Ablain et al. (2017a), and Beckley et al. (2017) (see Section 2.2.1). An ensemble mean of the three time series is also provided along with its corresponding root-mean square (RMS) dispersion with respect to the mean. All three time series together with the ensemble mean have been compiled together as a single netCDF and are provided in the file:

`ts_GMSL_1993_2015_no_seasonal_signal_GIA_applied_TopexA_driftcorrected_v1.nc`

The CCI GMSL time series is available at webpage <http://www.esa-sealevel-cci.org/>, access to the data directory (password) can be got by e-mail as stated on the web page. The AVISO time series can be downloaded at <https://www.aviso.altimetry.fr>. The Beckley et al. (2017) time series can be found at http://podaac.jpl.nasa.gov/dataset/MERGED_TP_J1_OSTM_OST_ALL_V4.2/.

2.2 Algorithms

2.2.1 Review of scientific background

To the above 3 GMSL time series, the TOPEX A instrumental drift correction has been applied. An instrumental aging of the TOPEX A altimeter placed in the TOPEX/Poseidon mission impacted significant wave height estimates (Hayne and Hancock, 1998) from January 1993 to early 1999. As a result, TOPEX A was switched off and replaced by the redundant TOPEX B altimeter in February 1999. It was earlier assumed that the GMSL derived from TOPEX A altimeter was not impacted by the instrumental problem. However, by comparing tide gauge data with TOPEX A sea level time series, Valladeau et al. (2012) put this in question but did not quantify this effect. In a later study, by interpolating altimetry based sea level data at tide

		<p>CCI Sea Level Budget Closure ESA/ESRIN contract 4000119910/17/I-NB</p> <p>Reference: ESA_SLBC_cci_D2.3.2 Version: v1.2 Date: 22.11.2018 Page: 20 of 119</p>
---	---	--

gauge sites, Watson et al. (2015) estimated the trend of differences between altimetry and vertical land motion corrected tide gauge records. Based on this method, over 1993-1998 time span, the TOPEX A drift correction was estimated to (1.5 ± 0.5) mm/yr. Other recent studies since then have also estimated this correction using different methodologies, and confirmed its significant impact on GMSL and therefore on sea level budget (Ablain et al., 2017a; Dieng et al., 2017; Beckley et al., 2017). They showed in particular an acceleration in the global mean sea level rate when the TOPEX A drift correction is accounted for. The description of the drift correction methodology involved in these data sets can be found in Section 2.2.2.

2.2.2 Algorithms

The Dieng et al. (2017) GMSL time series uses version 2.0 of the European Space Agency/ESA Climate Change Initiative/CCI ‘Sea Level’ project and combines data from the TOPEX/Poseidon, Jason-1/2, GFO, ERS-1/2, Envisat, CryoSat-2 and SARAL/Altika missions and is based on a new processing system with dedicated algorithms and adapted data processing strategies (Ablain et al., 2015, 2017b; Quartly et al., 2017; Legeais et al., 2018). It is averaged over 82°N and 82°S latitudinal range. The CCI sea level product has been validated using different approaches including a comparison with tide gauge records as well as to ocean re-analyses and climate model outputs. Taking advantage of the good agreement between GMSL and sum of sea level components beyond 1998, Dieng et al. (2017) estimated the TOPEX A drift by least squares adjustment of a linear function to the differences between GMSL time series and sum of sea level components over 1993-1998. This methodology produced a drift trend value of (1.5 ± 0.5) mm/yr, in agreement with that of Watson et al. (2015). This GMSL time series will henceforth be called ESA CCI based Dieng et al., 2017 GMSL time series.

The Ablain et al. (2017a) GMSL time series is based on the AVISO sea level data, henceforth called AVISO based Ablain et al., 2017a GMSL time series, that combines sea level measurements from TOPEX/Poseidon, Jason-1 and Jason-2 averaged over 66°N-66°S latitudinal range. All necessary instrumental and geophysical corrections have been applied. The TOPEX A drift correction from Ablain et al. (2017a) involves comparison of the altimetry based sea level time series with tide gauges and the filters out the differences by applying a Lanczos low pass filter. Various issues have been investigated to enable an accurate drift correction estimate of the Ablain et al. (2017a) time series. The TOPEX A drift value based on this methodology corresponds to (1.0 ± 1.0) mm/yr over January 1993 to July 1995 and (3 ± 1.0) mm/yr over August 1995 to February 1999.

The GMSL time series from Beckley et al. (2017) consists of GMSL variations computed at the NASA Goddard Space Flight Center (GSFC) under the auspices of the NASA MEaSUREs program. The GMSL was generated using the Integrated Multi-Mission Ocean Altimeter Data for Climate Research. It combines Sea Surface Heights from TOPEX/Poseidon, Jason-1, and

		<p>CCI Sea Level Budget Closure ESA/ESRIN contract 4000119910/17/I-NB</p> <p>Reference: ESA_SLBC_cci_D2.3.2 Version: v1.2 Date: 22.11.2018 Page: 21 of 119</p>
---	---	--

OSTM/Jason-2 to a common terrestrial reference frame with all inter-mission biases, range and geophysical corrections applied and placed onto a georeferenced orbit.

Concerning the TOPEX A drift, Beckley et al. (2017) specify that the drift is likely an artificial one introduced into the system as an independent correction based on an internal instrument calibration (called the Cal-mode correction) affecting only the TOPEX A altimeter. Beckley et al. (2017) therefore removed the Cal-mode corrections applied to the original TOPEX A data. The resulting GMSL over 1993-1998, henceforth called NASA based Beckley et al., 2017 GMSL, agrees reasonably well with the corrected CCI based GMSL from Dieng et al. (2017) and AVISO based Ablain et al. (2017 a) GMSL time series.

To all GMSL time series, the Glacial Isostatic Adjustment (GIA) correction (-0.3 mm/yr, Peltier 2004) has been taken into account. While this correction was included in the AVISO and NASA based GMSL time series downloaded, it was applied later on for CCI time series. Annual and semi-annual signals were already removed from the downloaded AVISO and NASA products, while for CCI GMSL time series they were removed through a least squares fit of 12 month and 6 month period sinusoids. A 60 day smoothing has also already been performed on these GMSL time series.

Figure 2.1 displays the three CCI, AVISO and NASA GMSL time series over 1993-2015. The time series have been corrected for the TOPEX A drift (1993-1998) based on different methodologies as described by Dieng et al. (2017), Ablain et al. (2017a) and Beckley et al. (2017). The differences between the time series in the time period 1993-1998 as seen in Figure 2.1 is expected, and is caused by the different methods in assessing the drift correction, none of which is for now 100% confident of taking into account the exact drift to be corrected. Figure 2.2 shows the ensemble mean of the three above mentioned time series. The uncertainty at each time step is estimated as the RMS of the dispersion of each time series from the mean.

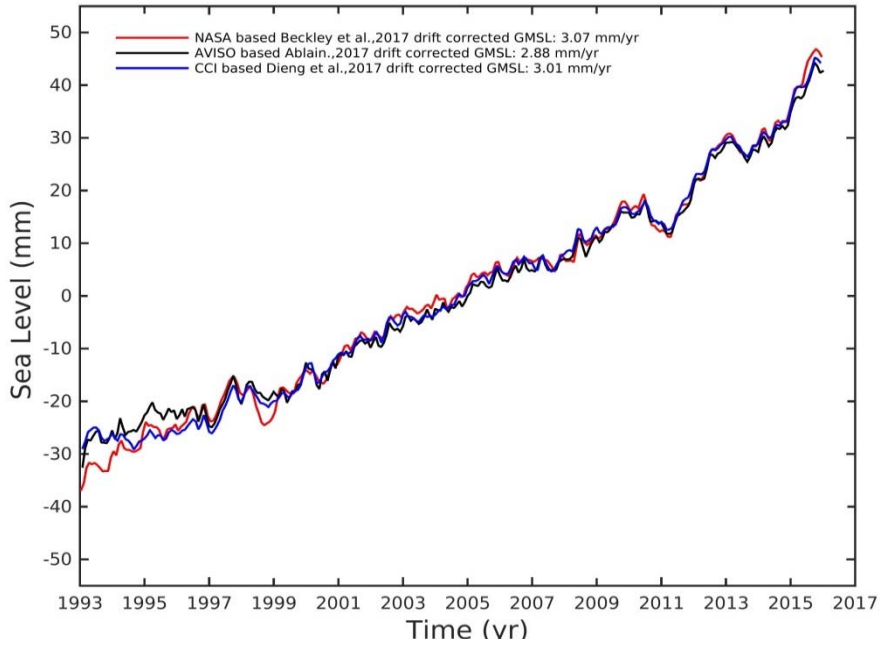


Figure 2.1: CCI, AVISO and NASA GMSL time series over 1993-2015 based on Dieng et al. (2017), Ablain et al. (2017a) and Beckley et al. (2017) TOPEX A drift corrections applied over 1993-1998.

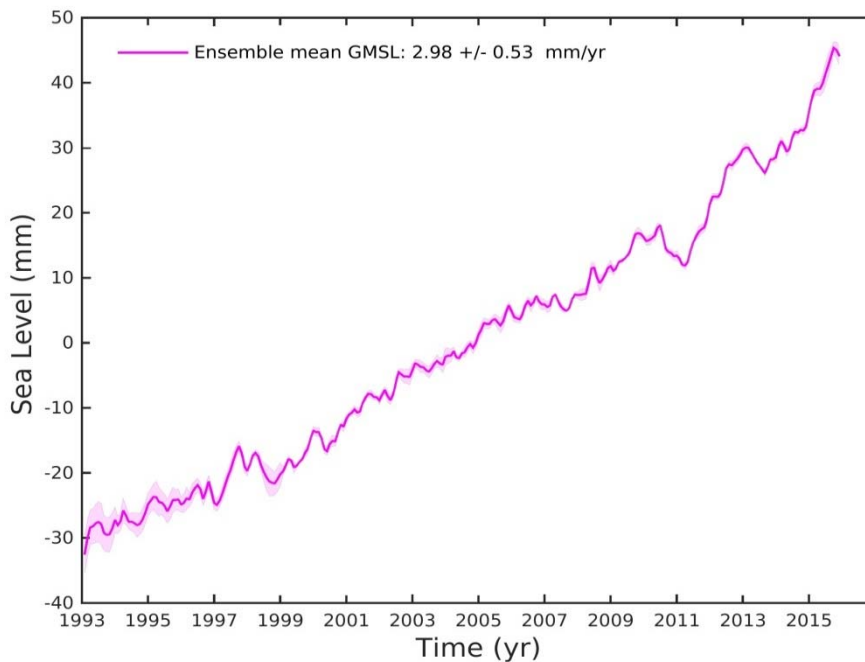


Figure 2.2: Ensemble mean of the 3 GMSL time series in Figure 2.1. The shaded error bar corresponds to the RMS of the dispersion of each time series from the mean

		<p>CCI Sea Level Budget Closure ESA/ESRIN contract 4000119910/17/I-NB</p> <p>Reference: ESA_SLBC_cci_D2.3.2 Version: v1.2 Date: 22.11.2018 Page: 23 of 119</p>
---	---	--

2.3 Product Specification

2.3.1 Product geophysical data content

(1) Global mean sea level data

file name:

ts_GMSL_1993_2015_no_seasonal_signal_GIA_applied_TopexA_driftcorrected_v1.nc

Geophysical Variable	Name in product	Unit
Global mean sea level anomaly	ts_Beckley_et_al ts_Ablain_et_al ts_CCI_Dieng_et_al ts_Ensemble_mean RMS_Ensemble_mean	mm
Time	Time	Decimal year

2.3.2 Coverage and resolution in time and space

The AVISO based Ablain et al. (2017a) (*ts_Ablain_et_al*) and NASA based Beckley et al. (2017) (*ts_Beckley_et_al*) GMSL series have been averaged over 66°N and 66°S latitudes and are at a monthly time resolution.

The CCI-based Dieng et al. (2017) GMSL time series (*ts_CCI_Dieng_et_al*) has been averaged over 82°N and 82°S latitudes and is also at monthly time resolution.

All the GMSL time series cover the period from January 1993 to December 2015.

2.3.3 Product data format

The various GMSL time series have been stored as a single netCDF4 file. The variables are one dimensional array with dimension corresponding to time steps.

		<p>CCI Sea Level Budget Closure ESA/ESRIN contract 4000119910/17/I-NB</p> <p>Reference: ESA_SLBC_cci_D2.3.2 Version: v1.2 Date: 22.11.2018 Page: 24 of 119</p>
---	---	--

2.4 Uncertainty Assessment

2.4.1 Sources of error

Currently none of the processing groups provide errors for GMSL time series at each time step. However, the processing groups have identified and discussed sources of errors in GMSL trend estimation that include errors due to geophysical corrections, instrumental drifts and other systematic errors (Ablain et al., 2015, 2017 b; Dieng et al, 2017; Quartly et al., 2017; Legeais et al., 2018).

2.4.2 Methodology for uncertainty assessment

In the v1 data, we have provided an uncertainty estimate at each time step for the ensemble mean of the three GMSL time series based on the root mean square (RMS) of the dispersion of each of the three GMSL time series from the ensemble mean. This calculation based on Dieng et al. (2017) provides (at least partially) the random error when no other uncertainty estimate is available over each time step.

For the estimation of trend error, values provided by each of the three GMSL groups have been considered. These also include the systematic errors. For the ensemble mean data, the trend error was estimated as the RMS of trend errors from the three GMSL time series plus error due to dispersion from the mean (as described in detail by Dieng et al., 2017; see also Bevington and Robinson, 1969; Kirkup, 1994).

2.4.3 Results of uncertainty assessment

As mentioned in Section 2.4.1, the processing groups only provide GMSL trend uncertainty based on various geophysical corrections, instrumental drifts and other systematic errors. This accounts to +/- 0.5 mm/yr (with a confidence interval of 90%) for both CCI and AVISO based GMSL time series and +/- 0.4 mm/yr for the NASA based GMSL time series. Refer to the articles mentioned in Section 2.4.1 for more information.

2.4.4 Uncertainty documentation in the data products

Refer to data format and file content in Section 2.3.1. There is no uncertainty given for the SSH values at each time step in the individual GMSL time series. We however have provided an uncertainty estimate at each time step for the ensemble mean data based on root mean square. (RMS) of the dispersion of each of the three GMSL time series from the ensemble mean as mentioned in Section 2.4.2.

		<p>CCI Sea Level Budget Closure ESA/ESRIN contract 4000119910/17/I-NB</p> <p>Reference: ESA_SLBC_cci_D2.3.2 Version: v1.2 Date: 22.11.2018 Page: 25 of 119</p>
---	---	--

2.5 References

- Ablain, M., et al. (2015): Improved sea level record over the satellite altimetry era (1993–2010) from the climate change Initiative project, *Ocean Sci.*, 11, 67–82, doi:10.5194/os-11-67-2015.
- Ablain M., R. Jugier, L. Zawadzki, and N. Taburet (2017a): The TOPEX-A Drift and Impacts on GMSL Time Series. *AVISO Website*. October 2017. https://meetings.aviso.altimetry.fr/fileadmin/user_upload/tx_ausyclsseminar/files/Poster_OSTST17_GMSL_Drift_TOPEX-A.pdf.
- Ablain, M., J. F. Legeais, P. Prandi, M. Marcos, L. Fenoglio-Marc, H. B. Dieng, J. Benveniste, and A. Cazenave (2017b): Altimetry-based sea level at global and regional scales, *Surv. Geophys.*, 38, 7–31, doi:10.1007/s10712-016-9389-8.
- Beckley, B. D., P. S. Callahan, D. W. Hancock, G. T. Mitchum, and R. D. Ray (2017): “On the ‘Cal-Mode’ Correction to TOPEX Satellite Altimetry and Its Effect on the Global Mean Sea Level Time Series.” *Journal of Geophysical Research, C: Oceans* 122 (11):8371–84. <https://doi.org/10.1002/2017jc013090>.
- Bevington, P. R., and D. K. Robinson (1969): *Data Reduction and Error Analysis for the Physical Sciences*, 320 pp., McGraw Hill, New York.
- Dieng, H.B, A. Cazenave, B. Meyssignac, and M. Ablain (2017): New estimate of the current rate of sea level rise from a sea level budget approach, *Geophysical Research Letters*, 44, doi:10.1002/2017GL073308.
- Hayne G. S., and D. W. Hancock (1998): Proceedings of the TOPEX/Poseidon/Jason-1 Science Working Team Meeting.
- Kirkup, L. (1994): *Experimental Methods. An Introduction to the Analysis and Presentation of Data*, 216 pp., Wiley, New York.
- Legeais J.F., Ablain M., Zawadzki L., Zuo H., Johannessen J.A., Scharffenberg M.G., Fenoglio-Marc L., Fernandes J., Andersen O.B., Rudenko S., Cipollini P., Quartly G.D., Passaro M., Cazenave A., and Benveniste J. (2018): An improved and homogeneous altimeter sea level record from the ESA Climate Change Initiative, *Earth Syst. Sci. Data*, 10, 281–301, doi: 10.5194/essd-10-281-2018.
- Peltier W.R. (2004): Global glacial isostasy and the surface of the ice-age Earth: the ICE-5G (VM2) model and GRACE, *Annual Review of Earth and Planetary Sciences* 32:111.
- Quartly G.D., Legeais J.F., Ablain M., Zawadzki L., Fernandes J., Rudenko S., Carrère L., García P.N., Cipollini P., Andersen O.B. , Poisson J.C. , Sabrina Mbajon Njiche S.M., Cazenave A., and Benveniste J. (2017): A new phase in the production of quality-controlled sea level data, *Earth Syst. Sci. Data*, 9, 557–572, doi: 10.5194/essd-9-557-2017.
- Valladeau, G., J. F. Legeais, M. Ablain, S. Guinehut, and N. Picot (2012): Comparing altimetry with tide gauges and Argo profiling floats for data quality assessment and mean sea level studies, *Mar. Geod.*, 35, 20–41.
- Watson, C. S., N. J. White, J. A. Church, M. A. King, R. J. Burgette, and B. Legresy (2015): Unabated global mean sea level over the satellite altimeter era, *Nat. Clim. Change*, doi: 10.1038/NCLIMATE2635.

		<p>CCI Sea Level Budget Closure ESA/ESRIN contract 4000119910/17/I-NB</p> <p>Reference: ESA_SLBC_cci_D2.3.2 Version: v1.2 Date: 22.11.2018 Page: 26 of 119</p>
---	---	--

3 Steric Sea Level Change

3.1 Data access and requirements

The v1 product consists of a time series of monthly mean Steric Sea Level Anomaly (SSLA) fields and a time series of monthly global mean SSLA. The corresponding data files are:

- MSSL_EN.4.2.1_1993_2015_v1.nc
- GSSL_EN.4.2.1_1993_2015_v1.nc

The product is available on Jasmin from the ESA SST CCI public pages, at http://gws-access.ceda.ac.uk/public/esacci-sst/slbc_cci/.

Input:



- ARGO, XBT and XCTD profiles, processed onto common vertical levels (method von Schuckmann and Le Traon, 2011), data from the UK Met Office EN4.2.1 Profiles archive
- 1993-2015 climatology fields of Temperature and Salinity (T,S) data generated from MetOffice EN4.2.1 Analyses archive
- Bathymetry from ETOPO 5
- Equation of state for seawater, EOS-80

3.2 Algorithms

3.2.1 Algorithms

Steric height or anomaly fields must be gridded to form a spatially resolved product. This product uses a box averaging method, at 5°, monthly resolution, rather than interpolation. The method is derived from that described in detail in von Schuckmann and Le Traon (2011). The spatial resolution is selected to correspond to the resolutions at which mass balance can be assessed from GRACE, and is close to the statistical limit for the approach in terms of available profile data over the 1993-2015 period.

In the von Schuckmann and Le Traon (2011) method, the profiles of (T,S) data are converted into vertically integrated estimates of the steric height anomaly. These are then binned into 5° x 5° latitude-longitude cells, and a weighted average is calculated following the method of Bretherton (1976). The Bretherton method also provides an estimate of the uncertainty in the

		<p>CCI Sea Level Budget Closure ESA/ESRIN contract 4000119910/17/I-NB</p> <p>Reference: ESA_SLBC_cci_D2.3.2 Version: v1.2 Date: 22.11.2018 Page: 27 of 119</p>
---	---	--

weighted cell average SSLA. However, this approach does not allow a full account of the sources of uncertainty to be made.

The revised method developed at UoR takes into account the uncertainty in the original observations of (T,S), the uncertainty in the climatological (T,S) data, the effects of error correlation, and the spatial and temporal representivity of the sparse profile data within a cell. The weighted cell average steric anomalies are calculated on a layer-by-layer basis where the weights depend on the uncertainties in the data, these are then summed to give the mean cell SSLA and an associated uncertainty is calculated using the weights and an error covariance matrix.

The revised mathematical formulation of the SSLA is given by

$$\begin{aligned}
\Delta h &= \sum_l \Delta h_l \\
&= \sum_l \mathbf{w}_l^T \mathbf{x}_l \\
&= \mathbf{w}^T \mathbf{x}
\end{aligned} \tag{Eq. 3.1}$$

where \mathbf{x}_l are the SHA for the observations and climatology in layer l of the cell, and the \mathbf{w}_l are the corresponding averaging weights for the values in the layer.

The SHA for each data value i in a given cell level l , $\Delta h_{l,i}$, is given by

$$\Delta h_{l,i} = \left(\frac{1}{\rho_{l,i}} - \frac{1}{\rho_{l,clim}} \right) \rho_0 \Delta z_l \quad (\text{units: m})$$

where $\rho_{l,i}$ are the observed densities in the layer, $\rho_{l,clim}$ is the climatological density in the layer, ρ_0 is a reference density (commonly set to 1000 kg m⁻³), and Δz_l is the vertical thickness of the layer.

The layer weights, \mathbf{w}_l , are given by

$$\mathbf{w}_l = \frac{\mathbf{S}_{x_l}^{-1} \mathbf{i}}{\mathbf{i}^T \mathbf{S}_{x_l}^{-1} \mathbf{i}}$$



where \mathbf{S}_{x_l} is the block of the covariance matrix \mathbf{S}_x that corresponds to the data in cell layer l , and \mathbf{i} is a vector of ones of length equal to the number of SHA values in the cell layer.

The uncertainty corresponding to the SSLA as calculated by Eq. 3.1 is given by

$$\mathbf{u}_{\Delta h} = (\mathbf{w}^T \mathbf{S}_x \mathbf{w})^{0.5} \tag{Eq. 3.2}$$

The estimation of the SSLA and the corresponding uncertainty requires the construction of the error covariance matrix \mathbf{S}_x from the uncertainty information. This is described in Section 3.4.

The global mean SSLA for month n is obtained as the deep-ocean weighted area average of the cell values (see Eq. 3.1):

		<p>CCI Sea Level Budget Closure ESA/ESRIN contract 4000119910/17/I-NB</p> <p>Reference: ESA_SLBC_cci_D2.3.2 Version: v1.2 Date: 22.11.2018 Page: 28 of 119</p>
---	---	--

$$\langle h_n \rangle = \frac{\sum_{j=1}^{ncell} (\Delta h_j \times A_j)}{\sum_{j=1}^{ncell} (A_j)} \quad (\text{Eq. 3.3})$$

where A_j is the area of each cell, and $ncell$ is the number of cells. The uncertainty in the global mean SSLA defined by Eq. 3.3 associated with filled cells σ_n , is given by the area weighted average of the cell uncertainties ($\sigma_j = u_{\Delta h,j}$) (Eq. 3.2), defined as

$$\sigma_n = \sqrt{\frac{\sum_{n=1}^{ncell} (\sigma_j \times A_j)^2}{\frac{N_{eff}}{N} (\sum_{j=1}^{ncell} (A_j))^2}} \quad (\text{Eq. 3.4})$$

The factor $\frac{N_{eff}}{N}$ accounts for the non-independence of adjacent cells. If errors in cells were independent, the effective number of independent values, N_{eff} would equal the actual number $N = ncell$ and this factor would equal 1. For wholly correlated errors, $N_{eff}=1$, and the uncertainty is larger. The true situation is that there is less than one degree of freedom per cell, but not complete error correlation. The factor $\frac{N_{eff}}{N}$ has been parameterised using synthetic data (MacIntosh et al., 2017), and depends on the number of filled cells.

An estimate of uncertainty associated with empty cells is defined by a simple linear function of the uncertainty with respect to the fraction of cells that are empty, with gradient derived from synthetic data as above (MacIntosh et al., 2017).

The filled and empty cell uncertainties are close to independent in the synthetic data. Accordingly, they are combined in quadrature to form the estimate of the total global mean SSLA uncertainty.

		CCI Sea Level Budget Closure ESA/ESRIN contract 4000119910/17/I-NB Reference: ESA_SLBC_cci_D2.3.2 Version: v1.2 Date: 22.11.2018 Page: 29 of 119
---	---	---

3.3 Product Specification

3.3.1 Product geophysical data content

- (1) Global mean steric sea level data (time series)

GSSL_EN4.2.1_1993_2015_v1.nc

Geophysical Variable	Name in product	Unit
Global mean steric sea level anomaly	global_ssla	mm
Time	time	days relative to epoch 1993-01-01
Uncertainty associated with filled cells	filled_uc	mm
Uncertainty associated with empty cells	empty_uc	mm
Total global SSLA uncertainty	total_uc	mm

- (2) Mean steric sea level field data

MSSL_EN4.2.1_1993_2015_v1.nc

Geophysical Variable	Name in product	Unit
Time	time	days relative to epoch 1993-01-01
Latitude	lat	degrees north
Longitude	lon	degrees east
Steric sea level anomaly	ssla	mm
SSLA uncertainty	error	mm
Number of profiles in box; considered missing if count <10	count	
Cell ocean fraction	weight_continent	
Global mean ssla, implied value for empty cells	mean_ssla	mm
Standard deviation of filled cells / uncertainty estimate for empty cells	stddev_ssla	mm

3.3.2 Coverage and resolution in time and space

The gridded v1 product is mapped onto the full globe at a spatial resolution of 5° x 5°. There are gaps in the maps where there were no available observations. The coverage is worst at the start of the time record where the data are predominantly in the northern hemisphere, by the end of the record there is virtually full global coverage.

		<p>CCI Sea Level Budget Closure ESA/ESRIN contract 4000119910/17/I-NB</p> <p>Reference: ESA_SLBC_cci_D2.3.2 Version: v1.2 Date: 22.11.2018 Page: 30 of 119</p>
---	---	--

The temporal resolution of the gridded and global average time series is monthly, covering the period from January 1993 to December 2015.

3.3.3 Product data format

Data are stored in netCDF4 format. All of the variables in the GSSL file are 1-dimensional arrays where the dimension is time. For the MSSL file the variables *ssla*, *error* and *count* are 3-dimensional arrays where the dimensions are in the order (time,lat,lon), *lat* and *lon* are 1-dimensional arrays with dimensions lat and lon respectively, lastly *time*, *mean_ssla* and *std_ssla* are 1-dimensional arrays with dimension time.

Data are provided in an equal-angle lat/lon grid with a spatial resolution of $5^{\circ} \times 5^{\circ}$. The grid cell edges are at 5° degree meridians (e.g. longitudes = {0, 5, 10 ... 355, 360}) and the grid cell centres are at 2.5° meridians (e.g. longitudes = {2.5, 7.5 ... 352.5, 357.5}).

3.4 Uncertainty Assessment

3.4.1 Sources of error

The overall uncertainty in a climate dataset can be decomposed into structural uncertainty and value uncertainty (Thorne et al., 2005). Decisions regarding the construction of a dataset may influence both structural and value uncertainty. The dispersion of outcomes that could arise for all well-justified choices reflects the structural uncertainty. Value uncertainty is the total remaining uncertainty given the structural choice made for constructing the dataset. It can, in principle, be formally propagated.

The sources of uncertainty present in estimates of global mean ocean quantities from profile data can largely be divided into three main categories: (1) uncertainty in the profile level data, (2) uncertainty due to the choice of climatology or other background, and (3) uncertainty due to the mapping procedure. This last can be further subdivided into intra- and inter-cell uncertainty, often discussed as representativeness and large-scale errors, respectively (e.g. Kennedy, 2014).

In principle, a full uncertainty model for gridded, interpolated or integrated SSL estimates can be built beginning with a single profile (e.g. MacIntosh et al., 2017), and propagating the errors through successive operations. Error propagation when many error sources are correlated or exhibit strongly non-Gaussian behaviour is complex, but can be addressed systematically for environmental observations (e.g. Mittaz et al., in prep) using standard methods from metrology (uncertainty propagation and Monte Carlo methods).

3.4.2 Methodology for uncertainty assessment

The uncertainty in the monthly mean SSLA in a given $5^\circ \times 5^\circ$ cell is defined by Eq. 3.2. To compute the uncertainties we need a definition of the error covariance matrix \mathbf{S}_x . This matrix can be separated into the measurement uncertainties and representation uncertainties, giving

$$\mathbf{S}_x = \mathbf{S}_{x_m} + \mathbf{S}_{x_r} \quad (\text{Eq. 3.5})$$

The appropriate construction of these two matrices allows the various sources of uncertainty to be propagated through to the uncertainty in the cell mean SSLA.

The total measurement uncertainty consists of the measurement bias and measurement noise. The initial data used in the calculation of the SSLA are profiles of observed (T,S) and a climatology of (T,S). The observed profiles are a collection of ARGO float, XBT, and XCTD data. From the literature we find the values of expected uncertainty in the (T,S) values as given in Table 3.1. For the purposes of this analysis we assume that these uncertainty values represent the measurement bias, and that the measurement noise is negligible. The ARGO data used are delayed mode where the (T,S) have been corrected for fall rate offsets, and the XBT and XCTD data have all had similar bias corrections applied to compensate for fall rate effects.

The climatology data have been generated from the monthly (T, S) fields given in the EN4.2.1 analyses data. The uncertainty in the climatology (T, S) is taken to be the de-trended inter-annual variability for every cell layer in every horizontal grid cell. It is assumed that the inter-annual variability represents the climatology measurement noise, and that the measurement bias is negligible.



The measurement error covariance model for a given profile is given by

$$\mathbf{S}_{x_{m,p}} = \mathbf{U}_b \mathbf{J} \mathbf{U}_b^T + \mathbf{U}_n \mathbf{I} \mathbf{U}_n^T$$

where \mathbf{U}_b is a diagonal matrix containing the measurement bias for each profile layer, \mathbf{U}_n is a diagonal matrix containing the measurement noise for each profile layer, \mathbf{J} is a matrix of ones which allows for the correlation in bias between layers, and \mathbf{I} is the identity matrix. This structure is replicated for every profile of data in the cell to give the measurement error covariance matrix, \mathbf{S}_{x_m} in Eq. 3.5. Given that we are going to be processing the data layer-by-layer this matrix is constructed in layer order instead of profile order.

Table 3.1: (T, S) instrument uncertainty values from literature.

Variable	XBT	XCTD	ARGO
T	$\pm 0.2 \text{ }^\circ\text{C}$	$\pm 0.03 \text{ }^\circ\text{C}$	$\pm 0.002 \text{ }^\circ\text{C}$
S	-	$\pm 0.03 \text{ psu}$	$\pm 0.01 \text{ psu}$

		<p>CCI Sea Level Budget Closure ESA/ESRIN contract 4000119910/17/I-NB</p> <p>Reference: ESA_SLBC_cci_D2.3.2 Version: v1.2 Date: 22.11.2018 Page: 32 of 119</p>
---	---	--

The representivity error covariance model in Eq. 3.5 is given by

$$\mathbf{S}_{x_r} = \mathbf{U}_r \mathbf{R}_r \mathbf{U}_r^T \quad (\text{Eq. 3.6})$$

where \mathbf{U}_r is the uncertainty for a randomly selected space-time location of a measurement in a grid cell and is given by the magnitude of the variability within the space-time cell, and \mathbf{R}_r is the representivity error correlation matrix. \mathbf{U}_r is assumed to be known, and has the same value for all observations corresponding to a given layer (determined by an estimate of the intra-month-cell variability for that layer). The level of correlation in the representivity error between a given pair observations in a layer will depend upon how close they are in space and time, this correlation will decay over some spatial and temporal scale. There will also be a degree of intra-cell-month vertical correlation in the representivity error between layers. Therefore, the model for the error correlation matrix for a given pair of observations in Eq. 3.6 is given by

$$[R_r]_{l_p, l_{p'}} = \exp\left(-\frac{|d_p - d_{p'}|}{\Delta_d} - \frac{|t_p - t_{p'}|}{\Delta_t}\right) r_{l, l'} \quad (\text{Eq. 3.7})$$

where $|d_p - d_{p'}|$ is the magnitude of the horizontal spatial separation, $|t_p - t_{p'}|$ is the magnitude of the temporal separation, Δ_d and Δ_t are the spatial and temporal decorrelation length scales, and $r_{l, l'}$ is the between layer error correlation coefficient. Given the sparsity in space and time of the (T,S) observations, the values for \mathbf{U}_r and $r_{l, l'}$ will be determined from synthetic data in the first instance. These values will need to be scaled in some way to represent the real data.

Initially we have assumed a spatial decorrelation length scale of 2.5° and temporal decorrelation length scale of 10 days. This will need to be refined based on an appropriate set of observational data.

As summarized in Section 3.2.1, the uncertainty in global mean SSLA is made up from the uncertainty associated with the filled cells and the uncertainty due to there being cells with no data available to estimate the cells monthly SSLA (i.e. empty cells). The uncertainty due to the filled cells is given by Eq. 3.4. The linear form used to define the empty cell uncertainty is

$$u_{empty} = -3.144 \text{Frac}_{filled} + 3.144 \text{ (mm)} \quad (\text{Eq. 3.8})$$

As described in Section 3.2.1, in the global mean total uncertainty for each month is the quadratic sum of the filled (Eq. 3.4) and empty cell (Eq. 3.8) uncertainties (i.e. there is an implicit assumption that the two quantities are independent), given by

$$u_{tot} = \sqrt{u_{filled}^2 + u_{empty}^2}$$

3.4.3 Results of uncertainty assessment

Figure 3.1 shows the global mean SSLA calculated using the revised layer-by-layer method covering the period from January 1993 to December 2015. To improve spatial coverage and profile density, the XBT and XCTD data have been included in the analysis for the years 1993 to 2003, for 2004 to 2015 only ARGO data are used. The effect of both the improvement in measurement quality and the increase in measurement density can be seen in the reduction in error total over time, as shown in Figure 3.2.

A simple unweighted linear trend was fitted to the time series giving an average trend in steric sea level rise of 1.63 cm/decade over the 23 year period. This simple fit will be strongly controlled by the early part of the data record where the data quality is poor (XBT predominantly) and the spatial distribution of data is strongly biased to the northern hemisphere. A better estimate could be obtained by applying an error weight linear least squares fit, this gives a trend of 1.48 cm/decade which is closer to, but higher than, values from the literature for this time period.

At this point in time it has not been possible to produce useful estimates of the U_r or $r_{l,l'}$ matrices (see Eq. 3.6 and Eq. 3.7). Therefore, the v1 SSLA product delivered currently only includes the uncertainties due to the profile measurement errors, and not the intra-cell representivity errors. The software tools developed to implement this new methodology has the code structures required to include the representivity in the computation, but currently

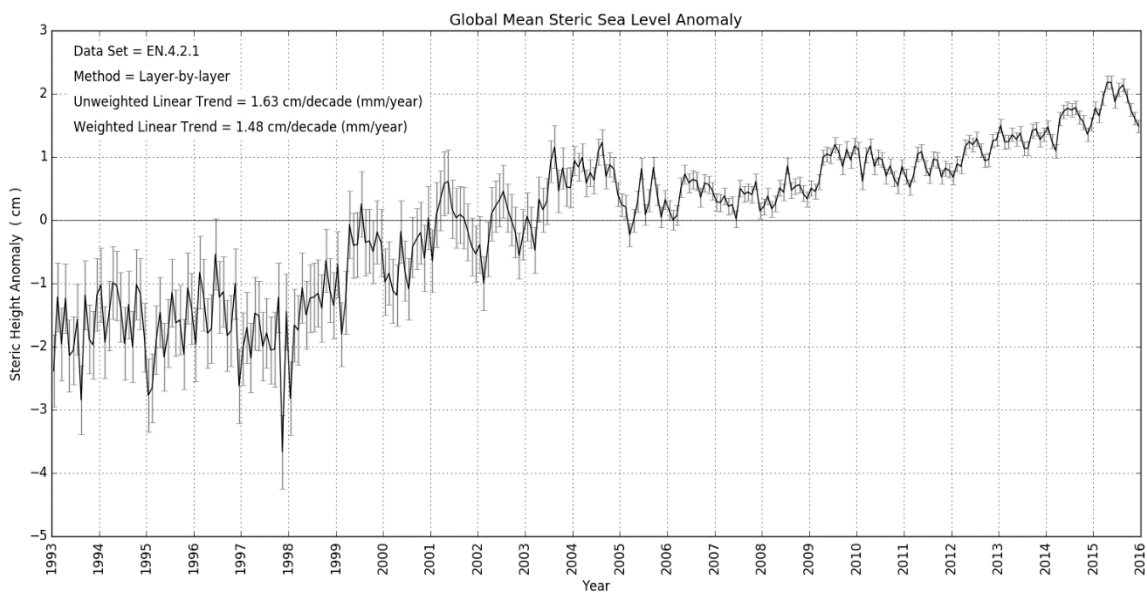


Figure 3.1: Global mean steric sea level anomaly and uncertainty from layer-by-layer method.

the U_r matrix is set to zero everywhere, and the correlation between layers is set to zero, i.e. $r_{l,l'}$ is a diagonal matrix of ones. In this sense the full calculation is carried out, but the S_{x_r} (Eq. 3.6) matrix is always zero everywhere, so does not contribute to the uncertainties.

It should also be noted that the XBT data only provide profiles of the temperature. In this case the climatological salinity profile data are used in the calculation of the sea water density. Therefore, the XBT data only provide the thermosteric component. Hence, the early part of the time record will be dominated by thermosteric only values, while the latter half of the series provides the full steric (i.e. thermosteric + halosteric) anomaly.

Due to issues with memory limitation and the way in which the process is currently ordered, for the later part of the time series it was necessary to restrict the number of profiles in a given cell. A code restructuring will be needed to allow the inclusion of all profiles in the more recent years, alternatively we may be able to increase the horizontal spatial resolution and/or decrease the vertical layer resolution to reduce the size of the matrices constructed during the process.

The XBT and XCTD data used in this version of the SSLA product have not as yet been checked for issues with quality, so it is possible that more rigorous screening may be required for the final version (v2) of the data product. A full implementation of the representivity covariance matrix will most likely result in an overall increase in the uncertainty values, but should not have a significant impact on the values of the SSLA (the layer-averaging weights are a function

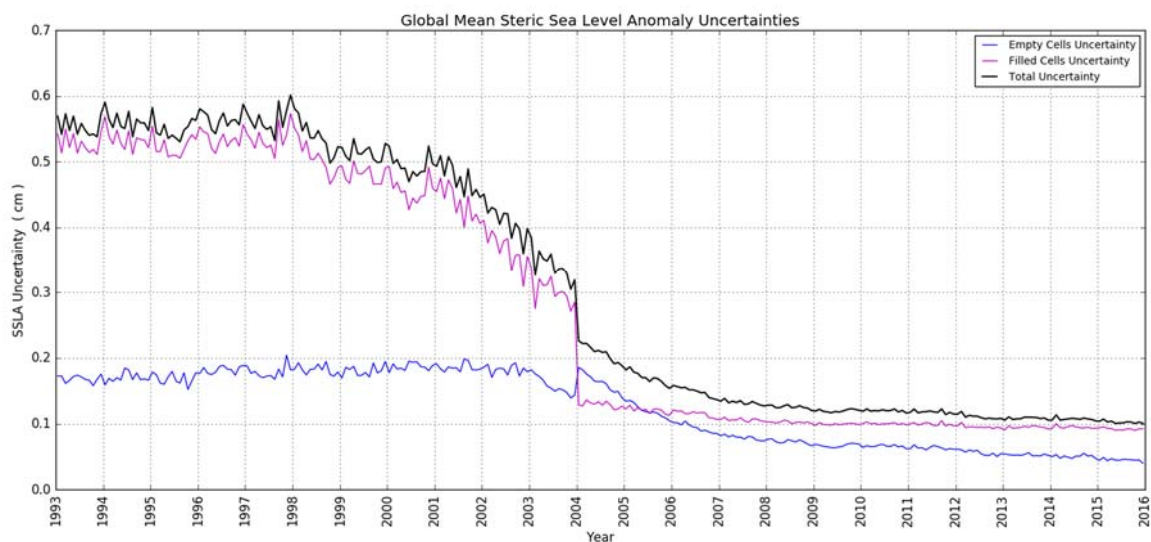


Figure 3.2: Total uncertainty and two components of uncertainty in the global mean steric sea level anomaly. Black: total uncertainty. Red: uncertainty of the steric sea level anomaly averaged across filled cells, by propagation of cell-level uncertainty estimates. Blue: additional uncertainty from existence of empty cells (reflecting the fact that the value used as a global estimate is derived from only the sample of cells with data).

of the uncertainty associated with each observation). The parameters (e.g. empty cell uncertainty, N_{eff}) used in calculating the global averages also need to be re-calculated using synthetic data processes with the new revised method of estimating the uncertainties.

The code has been set up so that it is possible to apply the above process to the depth integrated SHA data, which is effectively equivalent to have a single layer 2000 m thick. This allows a similar calculation to the von Schuckmann and Le Traon (2011) method. Figure 3.3 shows a comparison of the layer-by-layer with the depth integrated analysis. In general, the two lines fall within error bounds. The differences in the SSLA values are due to the subtly different layer weightings that get propagated through to the total SSLA in the layer-by-layer method.

3.4.4 Uncertainty documentation in the data products

Three uncertainty values are returned with the GSSL data, these are the uncertainty from the filled grid cells (i.e. cells where data were available), the uncertainty associated with the empty cells (i.e. cells where no data were available), and the total uncertainty in the global mean SSLA. The total uncertainty value represents the uncertainty in the global mean SSLA.

The uncertainty values for the MSSL gridded data are provided at the grid cell level. The uncertainty value given is the estimated total uncertainty for the monthly average SSLA in the grid cell.

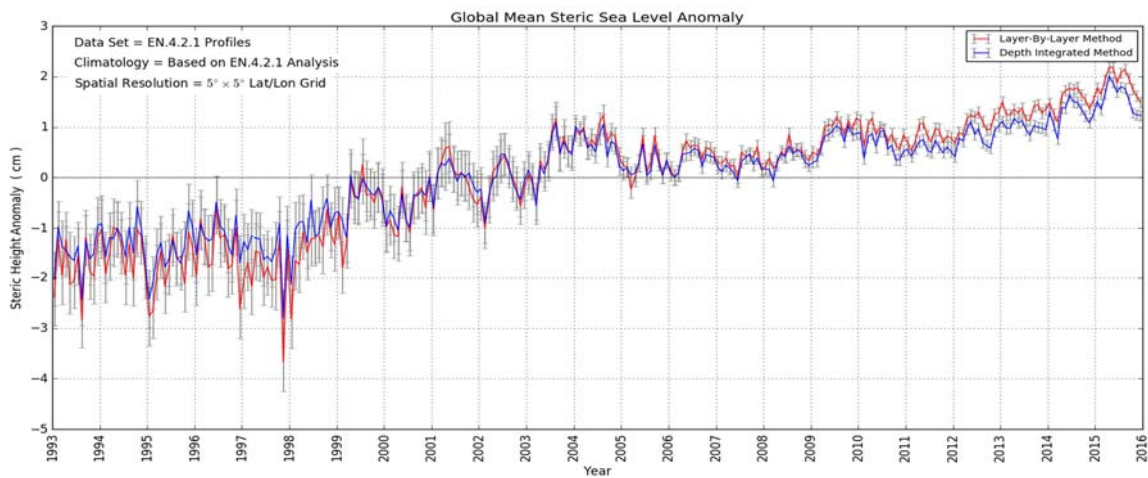


Figure 3.3: Comparison of the layer-by-layer and depth integrated global SSLA.

		<p>CCI Sea Level Budget Closure ESA/ESRIN contract 4000119910/17/I-NB</p> <p>Reference: ESA_SLBC_cci_D2.3.2 Version: v1.2 Date: 22.11.2018 Page: 36 of 119</p>
---	---	--

3.5 References

- Bretherton F, Davis R, and Fandry C (1976): A technique for objective analysis and design of oceanic experiments applied to mode-73, *Deep-Sea Res.*, 23, 559-582.
- Kennedy J J (2014): A review of uncertainty in in situ measurements and data sets of sea surface temperature, *Rev. Geophys.*, 52, 1–32, doi:10.1002/2013RG000434.
- Leuliette, E. W., and L. Miller (2009): Closing the sea level rise budget with altimetry, Argo, and GRACE, *Geophys. Res. Lett.*, 36, L04608, doi: 10.1029/2008GL036010.
- MacIntosh C R, Merchant C J and von Schuckmann K (2017), Uncertainties in steric sea level change estimation during the satellite altimeter era: concepts and practices. *Surveys in Geophysics*, 38 (1). ISSN 0169-3298 doi: 10.1007/s10712-016-9387-x.
- Mittaz, J. et al., Applying Principles of Metrology to Historical Earth Observations from Satellites, in prep.
- Thorne P W, Parker D E, Christy J R, and Mears C A (2005): Uncertainties in climate trends: Lessons from Upper-Air Temperature Records. *BAMS* 86: 1437-1442 doi:10.1175/BAMS-86-10-1437.
- von Schuckmann K, Gaillard F, and Le Traon P-Y (2009): Global hydrographic variability patterns during 2003-2008. *Journal of Geophysical Research*, 114, 1-17, doi: 10.1029/2008JC005237.
- von Schuckmann K, and Le Traon P-Y (2011): How well can we derive Global Ocean Indicators from Argo data? *Ocean Sci.*, 7:783-791, doi: 10.5194/os-7-783-2011.
- Willis, J K, Chambers D P, and Nerem S R (2008): Assessing the globally averaged sea level budget on seasonal to interannual timescales. *Journal of Geophysical Research*, 110, C06015, doi: 10.1029/2007JC004517.

		<p>CCI Sea Level Budget Closure ESA/ESRIN contract 4000119910/17/I-NB</p> <p>Reference: ESA_SLBC_cci_D2.3.2 Version: v1.2 Date: 22.11.2018 Page: 37 of 119</p>
---	---	--

4 Ocean Mass Change

Time-variable ocean- and continental mass products are derived from quasi-monthly solutions from the Gravity Recovery And Climate Experiment (GRACE) satellite mission (Tapley et al. 2004). While the processing and inversion approaches of the products involved differ considerably, the common setting is such that mass redistributions in the Earth-/Ocean system cause changes in the gravity field that are observed with the GRACE satellites. Here, these changes are expressed as temporal changes of mass per surface area in kg/m² near the Earth's surface, or equivalently, temporal changes of *equivalent water height (EWH)* in millimetres water equivalent (mm w.e.). The changes are expressed relative to an arbitrary reference state, e.g. the temporal mean state over the period 2004–2009. The EWH is a *hypothetical* layer of fresh water which would cause the observed change in gravity at each data point, respectively.

4.1 Data Access and Requirements

The following products are considered for SLBC_cci version 1 (v1):

- **ITSG Grace2016 [Main SLBC_cci v1 product]**
Institution: Institut für Geodäsie, TU Graz
Product Source: <https://www.tugraz.at/institute/ifg/downloads/gravity-field-models/itsg-grace2016/>
Reference: Klinger et al. (2016), Mayer-Gürr et al. (2016)
- **CSR/GFZ/JPL Release 5 [Supplementary SLBC_cci v1 product]**
GRACE Release 5 data from the official GRACE processing centres at CSR Texas, GFZ Potsdam and JPL, CA.
- **GSFC Mascons v02.4 [Supplementary SLBC_cci v1 product]**
Institution: Goddard Space Flight Center (NASA)
Product Source: <https://neptune.gsfc.nasa.gov/gngphys/index.php?section=470>
Reference: Luthcke et al. (2013)
- **Don Chambers' global mean OMC time-series [Supplementary SLBC_cci v1 product]**
An updated version of the file provided in SLBC_cci version 0.
Product Source: Personal communication
Reference: Johnson and Chambers (2013); Chambers and Bonin (2012)

		<p>CCI Sea Level Budget Closure ESA/ESRIN contract 4000119910/17/I-NB</p> <p>Reference: ESA_SLBC_cci_D2.3.2 Version: v1.2 Date: 22.11.2018 Page: 38 of 119</p>
---	---	--

CSR- and JPL Mascon products are not considered in this version 1 delivery, as they do not meet the SLBC_cci processing standard regarding C_{21}, S_{21} - and GAD-/atmospheric mean pressure corrections. They may be included again for the final version 2 assessment as an optional supplementary product after further processing and thorough review.

Data from GRACE Release 6 or from the GRACE-FO mission are not part of the SLBC_cci deliverables, yet.

4.2 Algorithms

4.2.1 Review of scientific background

Global solutions of Earth's gravity field are commonly represented by the coefficients (so-called Stokes coefficients) of a spherical harmonic (SH) expansion up to a specific maximum SH degree (Wahr et al. 1998). GRACE processing centres typically analyse Level-1 GRACE data (including the GRACE K-band ranging data, on-board GPS data and accelerometer data) to estimate a set of Stokes coefficients on a monthly basis ("monthly SH solutions").

Following the "atmospheric and oceanic de-aliasing" (AOD) approach, modelled short-term atmospheric and oceanic mass variations (as well as tidal mass variations) are accounted for as part of the background model within the gravity field estimation procedure (Flechtner et al. 2014, Dobslaw et al. 2013). Therefore, these variations are not included in the monthly solutions. In order to retain the full mass variation effect in the ocean domain, the respective monthly averages of the AOD fields need to be added back to the monthly solutions. These monthly averages are provided by the analysis centres of the GRACE Science and Data System. They have adopted the following nomenclature for those products: GAA products for the atmospheric mass variations, GAB products for the oceanic mass variations, and GAC products for the sum of the two. As an additional series of products, GAD products contain the sum of atmospheric surface pressure effects and ocean mass effects over the ocean domain (advised for comparisons with ocean bottom pressure observations). Different options of restoring mass variations in the oceanic domain exist for different oceanic applications of GRACE (compare section "De-aliasing products and ocean-only mascons" in the GSFC mascon description at <https://neptune.gsfc.nasa.gov/gngphys/index.php?section=470>). The SLBC_cci v1 OMC time-series processed from CSR-, GFZ-, GSFC-, ITSG- and JPL- data have the GAD product consequently restored and the spatial mean of atmospheric surface pressure over the full ocean removed in order to be consistently comparable to steric-corrected altimetry data.

GRACE is insensitive to surface mass displacement components of SH degree one (mass exchange between hemispheres). Swenson et al. (2008) have proposed an approach to derive the degree-one components by combining the GRACE information for degree $n \geq 2$ with ocean

		<p>CCI Sea Level Budget Closure ESA/ESRIN contract 4000119910/17/I-NB</p> <p>Reference: ESA_SLBC_cci_D2.3.2 Version: v1.2 Date: 22.11.2018 Page: 39 of 119</p>
---	---	--

model output. This approach is widely applied. GRACE has also a reduced sensitivity to the C_{20} component of the gravity field (dynamic flattening term). Therefore, GRACE-based C_{20} components are commonly replaced by results from satellite laser ranging. Specifically, the mascon solution by GSFC as well as the spherical harmonic-based results by D. Chambers and the products generated within SLBC_cci (based on ITSG Grace2016 and the 'official' CSR/GFZ/JPL RL05 Level-2 products) all follow the approach of adding degree-one terms and replacing C_{20} in the way described here – see related references given in Section 4.3.1.

Wahr et al. (2015) showed that pole-tide corrections to compensate for the response of the solid Earth and oceans to the Earth's polar motion (affecting coefficients of degree 2 and order 1: C_{21} , S_{21}) are not sufficiently modelled during GRACE RL05 processing. They recommend an additional correction to be applied to the GRACE Release 5 Level-2 products. We included this correction in our SLBC_cci v1 processing.

The task of determining changes in the mass distribution from changes of Earth's exterior gravity field has no unique solution. Uniqueness can be enforced by the assumption that the mass redistribution occurs in terms of surface mass changes in a "thin" layer on the Earth's surface, comprising the hydrosphere, atmosphere and cryosphere. In this way, global grids of surface mass variations can be calculated from the temporal variations of the gravity field.

Mass redistribution processes in the Earth interior, in particular glacial isostatic adjustment (GIA) or seismic events, cannot be subsumed in the concept of surface load changes. Therefore, they need to be corrected prior to the conversion of gravity field changes to surface mass changes. This is usually done by using results from geophysical modelling.

Due to the attenuation of short wavelength (= high SH degree) gravity field patterns with height, the sensitivity of GRACE rapidly decreases with SH degree. In other words, GRACE errors increase with SH degree. On top of this general error characteristics, GRACE errors exhibit distinct correlation patterns, which show up as north-south striping features and are related to the orbital geometry. In consequence, GRACE analyses for temporal surface mass change often involve filtering (spatial smoothing) leading to spatial resolutions limited to 300-500 km. Advanced filter approaches (Swenson and Wahr, 2006; Kusche, 2007) account for the complex, non-isotropic GRACE error structure. For the determination of mass change over global-average integration kernels, however, the non-application of smoothing filters may prevent leakage effects that would occur otherwise (e.g., Johnson and Chambers, 2013).

Based on grids of surface mass changes (generated by involving the corrections mentioned above), the total mass change over an area (e.g. the global ocean) is derived by spatial integration with an appropriate weight function. Equivalently, a respective linear functional may be applied in the spherical harmonic domain. The reduced spatial resolution causes leakage effects: Mass changes in coastal regions cannot be uniquely assigned to either the land side or the ocean side of the coastline. Since hydrological (or glaciological) changes on the land

		<p>CCI Sea Level Budget Closure ESA/ESRIN contract 4000119910/17/I-NB</p> <p>Reference: ESA_SLBC_cci_D2.3.2 Version: v1.2 Date: 22.11.2018 Page: 40 of 119</p>
---	---	--

side tend to have larger amplitudes than oceanic mass changes on the ocean side, a buffer zone of a few hundred kilometres is typically masked out from the ocean integration kernel (Chambers, 2009). Conversely, for estimating continental water or ice mass changes, a respective buffer zone may be added to the integration kernel. In this case, leakage effects due to oceanic mass changes in this buffer zone need to be considered.

Mascon approaches are a way to enforce a sharp separation between mass changes on either side of coastlines. Mascons (mass concentrations) are direct parametrisations of (localised) surface mass anomalies. Level-1-based mascon solutions directly estimate mascon magnitudes from the Level-1 GRACE data, without involving global gravity field solutions as an intermediate step. Geographically dependent constraints on the spatio-temporal variance and covariance of mass changes can be employed.

Similar mascon approaches can be followed based on SH gravity field solutions as intermediate ("pseudo-observation") products. This becomes even more attractive when realistic error variance-covariance information of the SH solutions is accounted for. In this way SH solution-based mascon approaches are a flexible way of incorporating both signal covariance information and error covariance information, without the burden of complete Level-1 data processing.

4.2.2 Algorithms

ITSG-Grace2016 based products

ITSG-Grace2016 (Klinger et al. 2016; Mayer-Gürr et al. 2016) is a series of monthly global SH gravity field solutions. Methodological advancements of the processing by TU Graz include the co-estimation of daily variations (in order to reduce aliasing from short-term variations into the monthly solutions) and the incorporation of temporal instrument error covariances.

RL05- and ITSG GRACE2016 unconstrained monthly solutions are available in different resolutions between degree 60 and 120, where a higher degree means higher spatial resolution. The model choice is a trade-off between higher resolution and an increased noise level. High noise levels require smoothing filters, but we found smoothed solutions to be unsuitable for OMC trend determination due to signal dampening (cf. trends of filtered SLBC_cci version 0 time series). Hence, for reasons of considerable signal-to-noise ratio and consistency with comparable OMC solutions, a lower resolution model (with a corresponding lower noise level) was chosen that can be integrated over an un-smoothed global ocean kernel. Here we use the series of solutions expanded up to SH degree 60.

These SH solutions are further processed at TU Dresden to derive global grids of surface mass changes.

		<p>CCI Sea Level Budget Closure ESA/ESRIN contract 4000119910/17/I-NB</p> <p>Reference: ESA_SLBC_cci_D2.3.2 Version: v1.2 Date: 22.11.2018 Page: 41 of 119</p>
---	---	--

GAD is restored and the mean atmospheric surface pressure effect over the entire Global Ocean is removed (i.e. OBP with correction of IB-effect approximation, comparable to steric-corrected and IB-corrected sea level anomaly measurements; cf. D1.2 "Update on Science Requirements", Novotny et al., 2018). Here, we use the mean of GAD over the ocean area to represent the mean atmospheric surface pressure effect, which is justified as the ocean mass component in GAD is mass-conserving. Effectively, adding the GAD change averaged over the global ocean and subtracting the atmospheric effect averaged over the global ocean would cancel each other out. However, due to the application of coastal buffer zones, we treat both effects separately. More specifically, in conjunction with known artificial drifts in the GAD fields we find it preferable to calculate the GAD by averaging over the entire ocean, rather than over the buffered ocean area. Calculating the GAD averages only over the buffered area leads to a final OMC trend that is on the order of 0.1 to 0.2 mm/yr higher than for our preferred approach. Similar findings are discussed by Uebbing et al. (2018).

Since degree zero of GAD is not provided with the available ITSG data, we replaced C_{00} in the ITSG GAD coefficients with those from CSR by linear interpolation in time. From all coefficients, their mean value over the same period as the GRACE solution is subtracted.

GIA is removed using two different GIA modelling results from

- a) A et al. (2013, based on ICE-5G glaciation history from Peltier, 2004) and
- b) Caron et al. (2018).

We also provide OMC time-series without GIA effect correction applied as a supplementary product.

Degree one components (centre of mass, geocentre motion) are added from the data set based on Swenson et al. (2008) and are freely available at ftp://podaac.jpl.nasa.gov/allData/tellus/L2/degree_1/deg1_coef.txt.

C20 ("flattening" of the Earth) is replaced by results from satellite laser ranging (SLR) after Cheng et al., 2013.

Different from the version 0 product, we now also corrected C_{21}/S_{21} coefficients (pole tide) as suggested by Wahr et al. (2015) for RLO5 products. With applying this correction, global OMC trends are 0.1 mm/yr smaller than without applying this correction.

As the most effective modification related to version 0, we changed the SLBC_cci version 1 OMC processing towards an un-smoothed ocean kernel in order to avoid damping effects from Gauss- and Swenson-filtering. This applies to all v1 integrated OMC time-series and to the ITSG-based $1^\circ \times 1^\circ$ gridded time-series products. In addition, optional Swenson-filtered (Swenson and Wahr, 2006) and smoothed (Gaussian 300 km) $1^\circ \times 1^\circ$ gridded time-series are

		<p>CCI Sea Level Budget Closure ESA/ESRIN contract 4000119910/17/I-NB</p> <p>Reference: ESA_SLBC_cci_D2.3.2 Version: v1.2 Date: 22.11.2018 Page: 42 of 119</p>
---	---	--

provided as well, but users should be aware that smoothed grids are subject to damping effects and will lead to lower integrated OMC trends.

Time series of total ocean mass change are derived by the weighted integral of surface mass variations over all oceanic cells. For this integration, a 300 km buffer is applied along the ocean margins to avoid leakage from land mass change. The integral is subsequently scaled by the ratio between total ocean area and the integrated area (i.e. total ocean area minus buffer area).

CSR/GFZ/JPL GRACE RL05 based products

The SLBC_cci version 1 OMC integrated time-series include products based on the 'official' monthly GRACE Level-2 solutions from Release 5 (5a for GFZ) in the form of spherical harmonic coefficients. The mass change products for SLBC_cci v1 were processed in exactly the same way as described for the ITSG Grace2016 based deliverable (see above), except that the GAD restore step could be processed with the C_{00} of the dedicated GAD data files, respectively. The initial SH solutions are further processed at TU Dresden to derive global grids of surface mass changes, from which the OMC time-series are derived by weighted integration over the 300 km buffered ocean kernel.

GSFC Mascons v02.4 (SLA)

The GSFC v02.4 mascon solution (Luthcke et al. 2013) is a global equal area (1 arc-degree) mascon solution based on Level-1 GRACE data. Anisotropic constraints on the signal covariance were applied.

Different versions, w.r.t. GIA corrections and re-addition of signal components are published. For the SLBC_cci v1 purposes, the "GSFC.ocn.200301_201607_v02.4_SLA-GeruoA" version is chosen. The following description refers to this version.



Degree-one components are added from the data set based on Swenson et al. (2008) and are freely available at ftp://podaac.jpl.nasa.gov/allData/tellus/L2/degree_1/deg1_coef.txt.

C_{20} is replaced by results from satellite laser ranging (Cheng et al., 2013).

C_{21}/S_{21} ("pole-tides") trends are corrected following Wahr et al., 2015.

GAD is restored and the mean atmospheric pressure removed, i.e. the global ocean average of GAD is subtracted in addition, in order to account for changes of the integrated atmospheric masses over the ocean domain. This makes the GSFC mascon based SLBC_cci v1 product comparable to steric-corrected and IB-corrected sea level anomalies, while the old SLBC_cci v0 product was rather consistent with ocean bottom pressure measurements instead.

Different versions, w.r.t. GIA corrections and re-addition of signal components are published. For the SLBC_cci v1 purposes, the "GSFC.ocn.200301_201607_v02.4_SLA-GeruoA" variant is chosen.

		<p>CCI Sea Level Budget Closure ESA/ESRIN contract 4000119910/17/I-NB</p> <p>Reference: ESA_SLBC_cci_D2.3.2 Version: v1.2 Date: 22.11.2018 Page: 43 of 119</p>
---	---	--

The treatment of atmospheric and oceanic background models is complicated by the fact that GSFC uses a different set of background models (namely, ECMWF for the atmosphere and MOG2D for the ocean) than the members of the GRACE Science and Data System CSR and JPL (which use ECMWF for the atmosphere but OMCT for the Ocean). To reach consistency, the difference between the background models was first accounted for by adding ECMWF+MOG2D and subtracting GAC, and subsequently, GAD was restored.

The above mentioned corrections and re-additions are entirely included in the mascon solution provided by GSFC. Time series of total ocean mass change for SLBC_cci v1, however, are derived by TUDr by the weighted integral over all oceanic points using the ocean-land point-set mask provided by GSFC specific to their Mascon solutions. We strictly used the area information provided with the GSFC data set and rescaled the resulting mass change to a standard ocean surface area as given in the version 1 file headers, respectively. Also, in this product, the Caspian Sea is not counted as a part of the Global Ocean.

Chambers' global ocean mass change time series

Time series result from applying an un-smoothed averaging kernel over the Global Ocean to series of global SH GRACE solutions from the three 'official' centres at CSR Texas, GFZ Potsdam and JPL, CA.

Degree one components are added from the data set based on Swenson et al. (2008) and are freely available at ftp://podaac.jpl.nasa.gov/allData/tellus/L2/degree_1/deg1_coef.txt.

C20 is replaced by results from satellite laser ranging (Cheng et al. 2013).

The data are not corrected for pole tides (C_{21}/S_{21}), which may result in Global OMC trends ~ 0.1 mm/yr higher than with the correction applied.

A 300 km buffer along the coastlines of continents and large islands is applied.

GAD is restored and the mean atmospheric pressure effect has been removed. It is not documented whether the mean atmospheric pressure has been calculated over the entire ocean or over a buffered ocean area, which is relevant -- see discussion in conjunction with "ITSG2016-based products".

We provide the supplementary updated data set "as is" without any further processing by TUDr.

4.3 Product specification

Time series of OMC are plotted in Figure 4.1 (global ocean) and Figure 4.2 (Arctic Ocean).

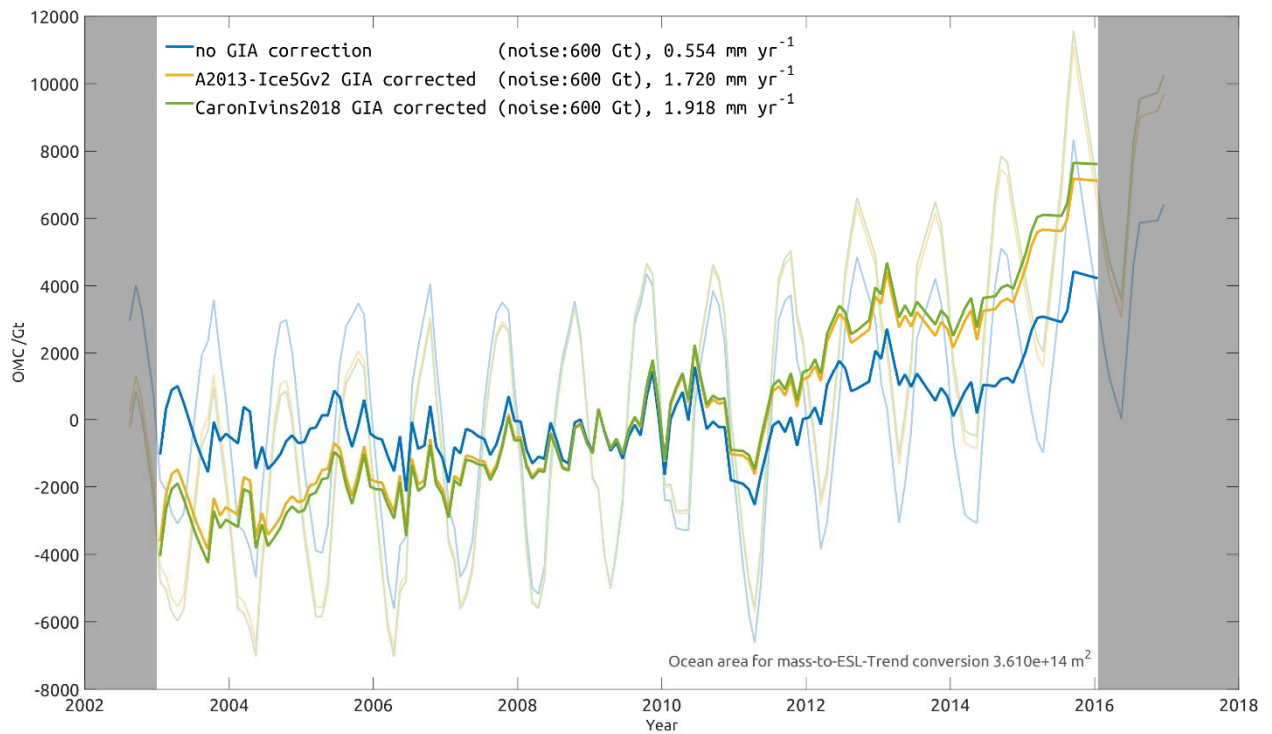


Figure 4.1: Ocean mass change from ITSG-Grace2016 monthly solutions up to degree 60 over the unsmoothed Global Ocean integration kernel. Degree 1 is added, C_{20} replaced, C_{21}, S_{21} corrected, GAD restored and atmospheric mean pressure over the entire Global Ocean removed. The three colours represent GIA corrections after A et al. (2013, yellow), Caron et al. (2018, green) and without GIA correction (blue). The pale coloured curves represent the time-series including seasonal variation, while the bold lines have the full- and semi-annual cycle removed. Note that there are missing months, in particular towards the end of the time series, despite the graphical representation of the time series by continuous lines.

All lines plotted in the figure are centered at their respective mean value over the observation period. That means, all curves come together about the mean time of the observation period. Due to the different trend of each time series, differences between the lines get naturally larger at the edges of the observation period as time goes forward/backward from the temporal center point.

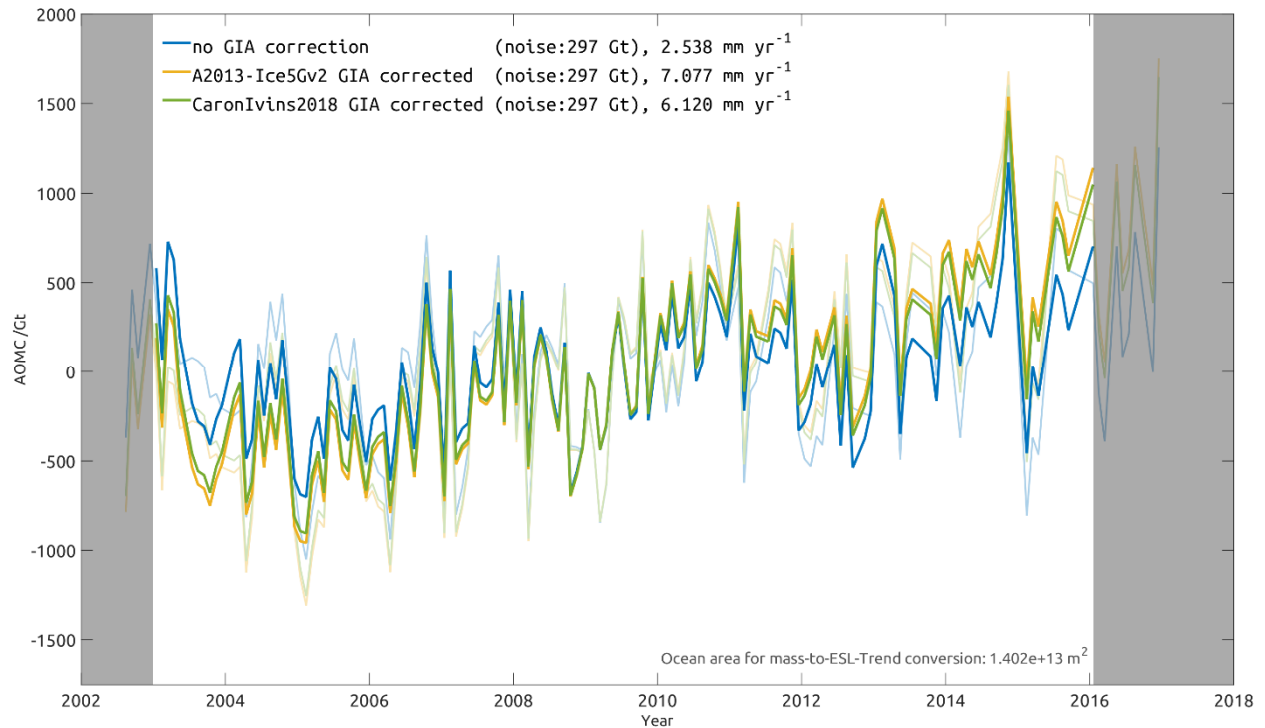


Figure 4.2: Arctic Ocean mass change from ITSG-Grace2016 monthly solutions up to degree 60 over the un-smoothed Arctic Ocean integration kernel. Degree 1 is added, C_{20} replaced, C_{21}, S_{21} corrected, GAD restored and atmospheric mean pressure over the entire Global (sic!) Ocean removed. The three colours represent GIA corrections after A et al. (2013, yellow), Caron et al. (2018, green) and without GIA correction (blue). The pale coloured curves represent the time-series including seasonal variation, while the bold lines have the full- and semi-annual cycle removed. Note that there are missing months, in particular towards the end of the time series, despite the graphical representation of the time series by continuous lines. All lines plotted in the figure are centered at their respective mean value over the observation period. That means, all curves come together about the mean time of the observation period. Due to the different trend of each time series, differences between the lines get naturally larger at the edges of the observation period as time goes forward/backward from the temporal center point.

		CCI Sea Level Budget Closure ESA/ESRIN contract 4000119910/17/I-NB Reference: ESA_SLBC_cci_D2.3.2 Version: v1.2 Date: 22.11.2018 Page: 46 of 119
---	---	---

4.3.1 Product geophysical data content

Ocean Mass Change Grids SLBCv1

Files: EWH_OMC-Grid_SSSS_SLBC-v1.VV_RxR[_filt][_bufBB][_GG].nc

with	SSSS	...	GSFC, ITSG
	VV	...	sub-version number, starting with 'v1.01' for grids
	RxR	...	resolution 1° by 1° (1x1)
and for ITSG			
in addition	'filt'	...	only present if smoothing was applied
	'bufBB'	...	for the applied leakage buffer, e.g. 300 km: 'buf300'
	'GG'	...	for the GIA correction applied

Product source (for ITSG data):

<https://www.tugraz.at/institute/ifg/downloads/gravity-field-models/itsg-grace2016/>

Product source (for GSFC Mascon data):

<https://neptune.gsfc.nasa.gov/gngphys/index.php?section=470>

Content (grid files)

Geophysical Variable	Name in product	Unit
change in ocean mass	EWH	kg/m ² (corresponds to mm w.e.)
Time	time_dec	Decimal year
Longitude	lon	degree east
Latitude	lat	degrees_north

OMC time series files

In addition to the gridded products, times series of ocean mass data are provided as text files (comma-separated values, csv).

Files: [A]OMCts_SLBCv1.VV_SS_YY_ShFilt-{0,1}_c21-{0,1}_GAD{0,1}-{111,...}_GIA-{GG}[_R2].csv

with	[A]	...	File for the Arctic Ocean, if present
	VV	...	sub-version number; starts with 'v1.00' for OMC time-series

		<p>CCI Sea Level Budget Closure ESA/ESRIN contract 4000119910/17/I-NB</p> <p>Reference: ESA_SLBC_cci_D2.3.2 Version: v1.2 Date: 22.11.2018 Page: 47 of 119</p>
---	---	--

- SS ... Solution source center string, one of {ITSG2016, GSFCm, CSRsh, GFZsh, JPLsh}
- YY ... Mass mean subtracted over values falling in this time period (see also info in file header for the exact center-of-epoch time)
- GG ... Name of GIA correction applied; one of {A2013-Ice5Gv2, CaronIvins2018, no}
- [_R2] ... Optional string; if present, the surface mass integration was done over a sphere with an WGS84 ellipsoid equal area radius (so called 'R2')

Several logical switches (1: true, 0: false) have a meaning as follows:

- ShFilt ... smoothing applied
- c21 ... C21/S21 correction applied
- GAD ... GAD restored; with '111' meaning "GAD processing active, GAD was restored and the atmospheric mean subtracted"

Content: column description (content, unit)

col 1: TIME (year.decimal)

col 2: mass (ocean mass minus mean_OceanMass) (Gigatonnes)

Please consider using the information given in the file header!

File: CHAMBERS__ocean_mass_orig.txt

Product Source: Pers. comm.

Content: column description (content, unit)

col 1: TIME (year.decimal)

col 2-4: Mean ocean mass (in mm of equivalent mean sea level)

col 2: CSR, col 3: GFZ, col 4: JPL

col 5: standard error

Please note the comments given in the file header.

4.3.2 Coverage and resolution in time and space

OMC time-series

- Mass change given in Gt (1 Gt = 10¹² kg) with respect to a standard ocean surface area of 3.61e+14 m² (Global Ocean) or 1.4e+13 m² (Arctic Ocean).

		<p>CCI Sea Level Budget Closure ESA/ESRIN contract 4000119910/17/I-NB</p> <p>Reference: ESA_SLBC_cci_D2.3.2 Version: v1.2 Date: 22.11.2018 Page: 48 of 119</p>
---	---	--

- Time is given in decimal years. Each time-stamp gives the mid-time of the function value's epoch. In most cases, this is mid-of-month, but may vary with increasing time when GRACE solutions were no longer processed every consecutive month.
- Period: second half of 2002 – end of 2016, please refer to the individual files. Please consider to use data in the agreed SLBC_cci time period (2003–2015) and compute your own mean-period value reduction if needed.

SLBC_cci v1 Gridded OMC time-series

GSFC- and ITSG solution series were interpolated onto the grid format defined for SLBC_cci v1:

- EWH given in mm (equivalent to kg/m², assuming a water density of 1000 kg/m³) over the ocean, 'NaN' else.
- 1° x 1° geographic grid (pix-reg)
- The grids derived from ITSG Grace2016 SH have an additional 300 km coastal leakage buffer applied, the GSFC-Mascon based version not.
- Time is given in decimal years.
- Periods are identical to the original data sets.
- ITSG Grace2016 based grids are available with either A et al. (2013) or Caron et al. (2018) GIA correction; as well as with and without smoothing filters applied.

The grids derived from GSFC-Mascons are to be considered the main gridded product for SLBC_cci version 1 analysis.

4.3.3 Product data format

Time series of integrated mass changes (global and Arctic north of 65(!)°N) are given as ASCII formatted two-column, comma-separated CSV-files. Please consider information given in the file header. Each CSV file's header ends with the string '# EOH' (end-of-header).

Time series of gridded mass changes are given in the netCDF-4 classic format.

4.3.4 Product grid and projection

SLBC_cci v1 1°x1° global grid, pixel-registration; one grid per time dimension.

		<p>CCI Sea Level Budget Closure ESA/ESRIN contract 4000119910/17/I-NB</p> <p>Reference: ESA_SLBC_cci_D2.3.2 Version: v1.2 Date: 22.11.2018 Page: 49 of 119</p>
---	---	--

4.4 Uncertainty assessment

4.4.1 Sources of error

GRACE errors: Errors in the GRACE observations as well as in the modelling assumptions applied during GRACE processing propagate into GRACE results on surface mass redistribution and in particular into GRACE-based ocean mass change products (“GRACE errors”). GRACE errors need to be damped in some way, either by filtering (in the case of approaches starting from a SH solution) or by applying regularization methods (in the case of mascon approaches). The loss of spatial resolution implied by approaches to reduce GRACE errors causes leakage errors, in turn.

Errors in C_{20} and Degree-1 terms: The GRACE satellites are insensitive to lower degrees coefficients (degree 1 or 'geocentre motion', C_{20} or 'flattening') of spherical-harmonics representations of the Earth's gravity field and its changes. These terms are usually derived by employing observations and modeling approaches other than GRACE. Because of their very large scale nature and possible systematic effects (including possible systematic errors in linear trends), errors of these components are particularly important for global ocean mass change applications. The related uncertainties are likely in the order of 0.1 – 0.2 mm/yr (cf. Quinn and Ponte 2010 for degree-one term uncertainty effects). As these coefficients are replaced with secondary products during our processing, we account for uncertainties that arise from the low-degree replacements applied to the ITSG2016 and other SH solutions during the SLBC version 1 processing, accordingly.

Effects of Glacial Isostatic Adjustment (GIA) are known to be a huge source of signal and error for mass change estimates: Post-glacial rebound of the Earth's crust, flexural effects, viscous back-flow of mantle material and other effects may introduce untargeted mass-change signals in GRACE data and need to be removed from them. GIA effects are usually corrected based on geophysical GIA models. Current models show strong discrepancies. As the models are based on a non-ideal data distribution space- and time-wise, and as the modelling shows considerable variability in its parameter space, the impact of GIA is among the fundamental uncertainties of GRACE-based ocean mass changes. The uncertainty is in the order of a few tens of mm/yr, and it is correlated to GIA-based uncertainties of altimetry-based GMSL changes and to GIA-based uncertainties in GRACE based ice sheet mass changes (Quinn and Ponte 2010, Chambers et al. 2010, Tamisiea 2011, Rietbroek et al. 2016).

Leakage errors: For SLBC version 1, we consider the additional uncertainty category of leakage-errors, which arise from the vanishing sensitivity of GRACE to small spatial scales (high SH degrees) or, respectively, by the necessity to dampen GRACE errors at small spatial scales: For OMC analyses, GRACE data are used only up to a certain spherical-harmonics degree and order (here: 60; ~333 km half-wavelength). At these longer wavelengths, a

		<p>CCI Sea Level Budget Closure ESA/ESRIN contract 4000119910/17/I-NB</p> <p>Reference: ESA_SLBC_cci_D2.3.2 Version: v1.2 Date: 22.11.2018 Page: 50 of 119</p>
---	---	--

significantly large gravity-change signal from the continents (e.g. ice-mass loss of the GIS) leaks into areas over the ocean close to the source and superimposes the actual signal caused by OMC. Hence, leakage errors can be described as errors in correctly assigning gravity field changes to the geographic location of surface mass changes. The problem is aggravated by the fact that surface mass changes on the land side (continental hydrology or continental ice mass changes) are often significantly larger than ocean mass changes. Differences in methods to avoid (or repair) leakage effects can amount to a several tenths of mm w.e./yr in regional OMC estimates (e.g. Kusche et al. 2016).

In order to avoid integrating mass-changes over areas holding such leakage-signals, we make use of an ocean kernel that 'buffers' out the closest 300 km surrounding continents, large island (20,000 km²) globally and medium-scale islands (2,000 km²) at high latitudes ($>|50^\circ|$). The OMC result for the such-derived 'inner' ocean becomes subsequently re-scaled to the standard surface area of the target area (3.61e+14 m² for the Global Ocean). Furthermore, users should be aware that potential signal content from fingerprint-effects (i.e. near-coast ocean mass loss through decreasing gravitational acceleration from ice-masses) may partially be omitted in SLBC version 1 OMC time-series as a side-effect of the application of coastal buffer zones.

Uncertainty of corrections: Others. Other corrections, with their specific uncertainties, include the correction for rotational feedback effects (polar tides) to long-term mass re-distributions, and corrections for atmospheric mass variations.

4.4.2 Methodology and Results of Uncertainty Assessment

We separate the error into two components distinguished by their temporal characteristics:

- noise, considered temporally uncorrelated, with equal variance for each month
- systematic errors of the linear trend.

We note that this treatment simplifies the situation by not considering autocorrelated errors other than errors that evolve linearly with time.

The standard deviation of the noise is estimated from the OMC time series themselves. For that aim, the time series are high-pass filtered in the temporal domain. The filtered time series are assumed to be dominated by the high-pass filtered noise. The variance of these filtered time series is calculated. It is subsequently scaled by a factor that accounts for the dampening of white noise variance imposed by the high-pass filtering.

The assessed noise component of the uncertainty comprises uncorrelated errors from all sources listed in Section 4.4.1, (except for GIA which is considered purely linear in time).

		<p>CCI Sea Level Budget Closure ESA/ESRIN contract 4000119910/17/I-NB</p> <p>Reference: ESA_SLBC_cci_D2.3.2 Version: v1.2 Date: 22.11.2018 Page: 51 of 119</p>
---	---	--

The systematic errors of the linear trends are assumed to originate from the sources Degree-1, C20, GIA, and leakage. The related uncertainties are assessed for each source individually. The analysis of systematic errors of the linear trends follows the same approach as described by Nagler et al. (2018) for the ESA CCI Antarctica project with GRACE Mass Balance derived changes over Antarctica (cf. Section 6 and the Comprehensive Error Characterisation Report, Nagler et al., 2018). For the v1 products based on ITSG2016 (and CSR/GFZ/JPL) spherical harmonics this is done as follows. Results are summarized in Table 4.1.

- Degree-1 errors have been assessed through an intercomparison of different degree-1 time-series and the distribution of their effect on the OMC trend. The assessed standard uncertainty for degree 1 is **0.136 mm/yr** for the Global OMC trend and 1.238 mm/yr for the Arctic OMC trend (north of 65 degrees N).
- C20 uncertainties have been assessed through an intercomparison of different C20 time-series and the distribution of their effect on the OMC trend. The assessed standard uncertainties are 0.051 mm/yr for the Global OMC trend and 0.694 mm/yr for the Arctic OMC trend, respectively.
- In order to estimate uncertainties that arise from GIA corrections, we analysed the distribution of OMC trends with different GIA models from A et al. (2013, ICE-5G-VM2), Peltier et al. (2015, ICE-6G_C-VM5a) and Caron et al. (2018). We do no longer include the ICE-4G-VM2 model (Peltier et al., 1994) in this analysis, for we agree with suggestions made within the project that successor-models by the same authors would inherently be an improved update of the predecessors. Including those older models would thus unnecessarily increase the uncertainty range. The assessed standard uncertainties for GIA corrections in SLBC_cci version 1 are **0.135 mm/yr** for the Global OMC trend and **0.489 mm/yr** for the Arctic OMC trend, respectively.
- In order to estimate the error that arises from leakage-buffering and rescaling during processing, we performed an extensive study based on synthetic mass change data, namely the updated ESA Earth System Model (ESM; Dobslaw et al., 2015). Synthetic data of the ESM was processed according to the settings of the SLBC_cci v1 OMC time-series setting (pseudo-observed) and then compared with the full-resolution ESM data (pseudo-true) over the identical target area and time, respectively. The RMS of misfits between pseudo-observed and pseudo-true OMC trends for a set of different 9–12 years long time frames gives us the estimate of the leakage error. The assessed standard uncertainty coming from this effect is **0.136 mm/yr** for the Global OMC trend and **0.588 mm/yr** for the Arctic OMC trend.

		CCI Sea Level Budget Closure ESA/ESRIN contract 4000119910/17/I-NB Reference: ESA_SLBC_cci_D2.3.2 Version: v1.2 Date: 22.11.2018 Page: 52 of 119
---	---	---

4.4.3 Uncertainty documentation in the data products

Several lines about uncertainty characterisation are placed in the header of each self-processed OMC time-series file. Specifically, the noise component (in Gt) and systematic uncertainty of the linear trend (in Gt/yr) are given individually. The GIA component of the systematic linear trend uncertainty is given explicitly, in addition. [Due to automated processing this is also the case for supplementary files without GIA correction applied, but can be ignored in that case]. The file header specifically describes to combine the uncertainties in the form of



$$\sigma_{\text{total}}^2(t) = \sigma_{\text{noise}}^2(t) + (\sigma_{\text{trend}} * (t-t_0))^2$$

for time-series of mass change $m(t)-m(t_0)$ with respect to a reference time t_0 .

The Global OMC time-series data file from Chambers has a standard error given in the last (5th) column for each epoch.

Table 4.1: Estimated standard uncertainties for different trend solutions

Error Component	Estimation procedure	Assessed Standard Uncertainty (Global)	Assessed Standard Uncertainty (Arctic)
Noise GRACE solution: ITSG and {CSR / GFZ / JPL}	Estimation of STD of white noise component of time series	1.662 mm 600.0 Gt {1.894/2.232/2.034} mm {683.7/805.5/734.2} Gt	21.23 mm 297.6 Gt {22.25/23.96/22.86} mm {312.0/335.9/320.6} Gt
Trend uncertainty Degree 1	Intercomparison of different degree-1 time-series	0.136 mm/yr 49.1 Gt/yr	1.238 mm/yr 17.4 Gt/yr
Trend uncertainty C ₂₀	Intercomparison of different C ₂₀ time-series	0.051 mm/yr 18.4 Gt/yr	0.694 mm/yr 9.7 Gt/yr
Trend uncertainty GIA	Intercomparison of different models	0.135 mm/yr 48.7 Gt/yr	0.489 mm/yr 6.9 Gt/yr
Trend uncertainty Leakage	Synthetic model data analysis (ESM)	0.136 mm/yr 49.1 Gt/yr	0.588 mm/yr 8.2 Gt/yr
Combined trend Uncertainty	Root Sum Square	0.240 mm/yr 86.8 Gt/yr	1.612 mm/yr 22.6 Gt/yr

		<p>CCI Sea Level Budget Closure ESA/ESRIN contract 4000119910/17/I-NB</p> <p>Reference: ESA_SLBC_cci_D2.3.2 Version: v1.2 Date: 22.11.2018 Page: 53 of 119</p>
---	---	--

4.5 Continental Mass Change

A preliminary time series with GRACE mass change over continents (continental mass change, CMC) without Antarctica and Greenland is provided in the case of the SLBC_cci version 1 release. It comprises ITSG Grace2016 based mass-change time-series over continental area (Land-Water-Mask provided by GUF and modified by TUDr).

The data processing is similar to the OMC time-series processing as described above (degree 1 added, C_{20} replaced, C_{21}/S_{21} corrected, GIA corrected with Caron et al., 2018, but omission of the GAD restore step). As GRACE cannot distinguish between mass changes coming from hydrology or ice, the product is considered to be jointly compared with both components.

Following the motivation of the above mentioned leakage problem for OMC determination, an 'inverse buffering' principle applies here for the CMC: Leaking signal that is attributed to the land side but appears to occur over the near-coast ocean (in the buffer zone), needs to be integrated with the 'continental' surface mass changes together, in order to correctly be counted as part of the continental mass change. We therefore expanded the provided continental Land-Water-Mask by several half-degree grid cells (as a function of latitude) so that the modified part of the mask matches a 300 km buffer.

However, the mass change derived from integration over the added buffer cells must not be added without further processing as it also includes the mass change signal of the ocean itself. To counteract the superposition, we subtract the monthly mean value of the Global Ocean multiplied by the area of the buffer cells, respectively; assuming that the actual ocean mass change therein is adequately close to the global mean OMC. The resulting integrated and corrected signal is attributed to the initial Land-Water-Mask area only and represents the global mean continental mass change from hydrology and ice mass changes, excluding Antarctica and Greenland (Figure 4.3).

Integration scheme:

$$CMC = \text{Int}_{\text{ContArea}}(\text{ewh}) + \text{Int}_{\text{BufArea}}(\text{ewh}) - \frac{\text{BufArea}}{\text{OcAreaBuffered}} * \text{Int}_{\text{OcAreaBuffered}}(\text{ewh})$$

with CMC: Continental Mass Change in kg,

$\text{Int}_{\text{ABC}}(\text{ewh})$: Integration of surface mass over area ABC

ContArea: Continental Area (from the provided mask)

BufArea: Area of inverse buffer over ocean

OcAreaBuffered: Area of the buffered ocean, i.e. full ocean minus buffer

Equivalent mean water height changes over the continental area or over the global ocean can then be derived by dividing the CMC by *ContArea* or the Global Ocean area, respectively.

For a future release, a clearer separation of the Canada/Greenland transition and the peripheral glaciers has to be accomplished. The effect of mass change signals from very large earthquakes on the integrated time-series has yet to be assessed. Further potential for improvement lies in a more consistent treatment of AOD1b background models and a thorough uncertainty estimation.

File name:

CMCTs_SLBC_cci_v1.00_ITSG2016_2003.00-2016.05_ShFil-0_c21-1_GAD-0_GIA-CaronIvins2018.csv

Format: comma-separated two-column CSV file. First column is decimal years, second column is mass value in Gt minus the mean between 2003 and 2016.05 .

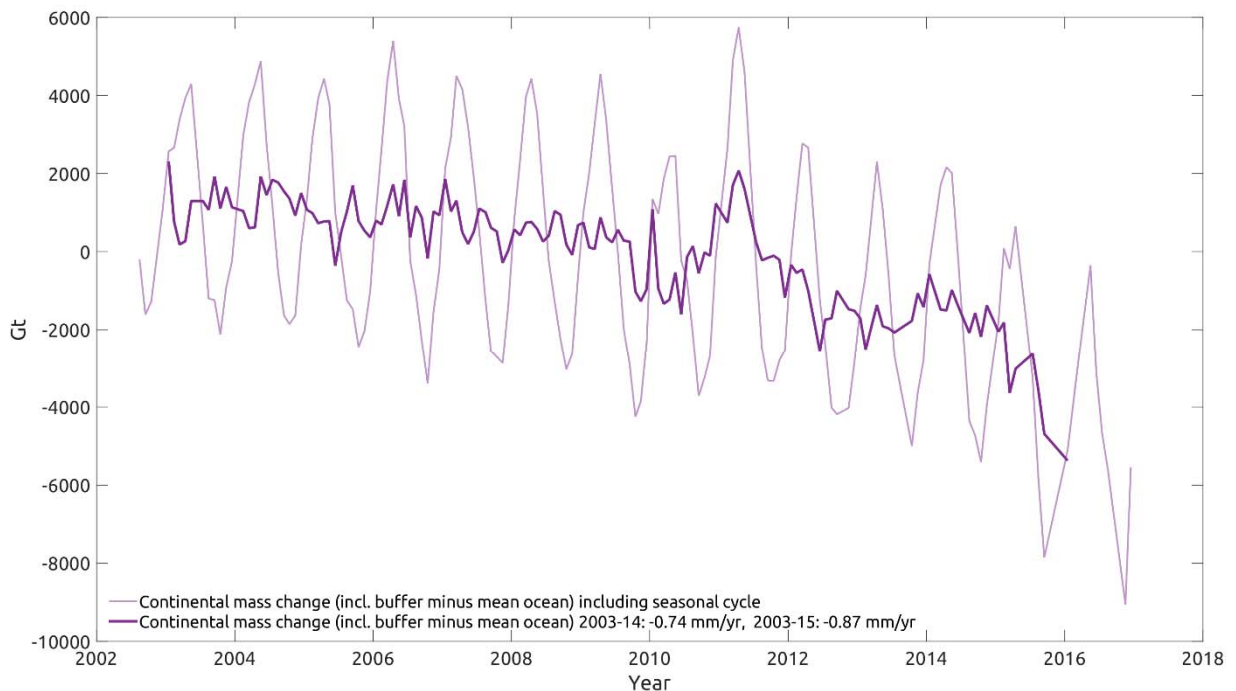


Figure 4.3: Continental mass change (excluding Greenland and Antarctica) from ITSG-Grace2016 monthly solutions up to degree 60 over an un-smoothed continental integration kernel. Degree 1 is added, C_{20} replaced and C_{21}, S_{21} corrected. GIA correction after Caron et al. (2018) was applied. The pale coloured curve represents the time series including seasonal variation, while the bold curve has the full- and semi-annual cycle removed. Note that there are missing months, in particular towards the end of the time series, despite the graphical representation of the time series by continuous lines.

		<p>CCI Sea Level Budget Closure ESA/ESRIN contract 4000119910/17/I-NB</p> <p>Reference: ESA_SLBC_cci_D2.3.2 Version: v1.2 Date: 22.11.2018 Page: 55 of 119</p>
---	---	--

4.6 References

- A, G., Wahr, J., and Zhong, S. (2013): Computations of the viscoelastic response of a 3-D compressible Earth to surface loading: an application to Glacial Isostatic Adjustment in Antarctica and Canada. *Geophysical Journal International*, 192(2), 557–572. doi: 10.1093/gji/ggs030.
- Caron, L., Ivins, E. R., Larour, E., Adhikari, S., Nilsson, J., and Blewitt, G. (2018): GIA model statistics for GRACE hydrology, cryosphere, and ocean science. *Geophysical Research Letters*, 45, 2203–2212. doi: 10.1002/2017GL076644.
- Chambers, D. P. (2009): Calculating trends from GRACE in the presence of large changes in continental ice storage and ocean mass, *Geophysical Journal International*, 176(2), 415–419. doi: 10.1111/j.1365-246X.2008.04012.x.
- Chambers, D. P., J. Wahr, M. E. Tamisiea, and R. S. Nerem (2010): Ocean mass from GRACE and glacial isostatic adjustment, *J. Geophys. Res.*, 115, B11415, doi: 10.1029/2010JB007530.
- Chambers, D. P., and J. A. Bonin (2012): Evaluation of Release-05 GRACE time-variable gravity coefficients over the ocean, *Ocean Sci.*, 8, 859–868, doi: 10.5194/os-8-859-2012.
- Cheng, M.K., B. D. Tapley, and J. C. Ries(2013): Deceleration in the Earth's oblateness, *Jour. Geophys. Res.*, V118, 1-8, doi: 10.1002/jgrb.50058, 2013.
- Dobslaw, H., Flechtner, F., Bergmann-Wolf, I., Dahle, C., Dill, R., Esselborn, S., ... , and Thomas, M. (2013): Simulating high-frequency atmosphere-ocean mass variability for dealiasing of satellite gravity observations: AOD1B RL05. *Journal of Geophysical Research: Oceans*, 118(7), 3704–3711. doi: 10.1002/jgrc.20271.
- Dobslaw, H., Bergmann-Wolf, I., Dill, R., Forootan, E., Klemann, V., Kusche, J., and Sasgen, I. (2015): The updated ESA Earth System Model for future gravity mission simulation studies, *Journal of Geodesy*, 89, 5, 505–513, doi: 10.1007/s00190-014-0787-8.
- Flechtner, F., Dobslaw, H., and Fagiolini, E. (2014): *AOD1B product description document for product release 05 (Rev. 4.2, May 20, 2014)*. Technical Note, GFZ German Research Centre for Geosciences Department, 1.
- Johnson, G. C., and D. P. Chambers (2013): Ocean bottom pressure seasonal cycles and decadal trends from GRACE Release-05: Ocean circulation implications, *J. Geophys. Res. Oceans*, 118, 4228–4240, doi: 10.1002/jgrc.20307.
- Klinger, B., Mayer-Gürr, T., Behzadpour, S., Ellmer, M., Kvas, A., and Zehentner, N. (2016): The new ITSG-Grace2016 release. *Geophys. Res. Abstr.*, 18, EGU2016–11547.
- Kusche, J. (2007): Approximate decorrelation and non-isotropic smoothing of time-variable GRACE-type gravity field models. *Journal of Geodesy*, 81(11), 733–749, doi: 10.1007/s00190-007-0143-3.
- Kusche, J., Uebbing, B., Rietbroek, R., Shum, C. K., and Khan, Z. H. (2016): Sea level budget in the Bay of Bengal (2002–2014) from GRACE and altimetry. *Journal of Geophysical Research: Oceans*, 121, 1194–1217, doi: 10.1002/2015JC011471.
- Luthcke, S. B., Sabaka, T. J., Loomis, B. D., Arendt, A. A., McCarthy, J. J., and Camp, J. (2013): Antarctica, Greenland and Gulf of Alaska land-ice evolution from an iterated GRACE global mascon solution. *J. Glac.*, 59(216), 613–631. doi: 10.3189/2013JoG12J147.
- Mayer-Gürr, T., Behzadpour, S., Ellmer, M., Kvas, A., Klinger, B., and Zehentner, N. (2016): ITSG-Grace2016 - Monthly and Daily Gravity Field Solutions from GRACE. *GFZ Data Services*. doi: 10.5880/icgem.2016.007.
- Nagler et al. (2018): ST-UL-ESA-AISCCI-CECR-001_v3.0.pdf: Comprehensive Error Characterisation Report (CECR). An update for the GMA part is given under https://data1.geo.tu-dresden.de/ais_gmb/source/ST-UL-ESA-AISCCI-CECR-Draft_GMB.pdf.

		<p>CCI Sea Level Budget Closure ESA/ESRIN contract 4000119910/17/I-NB</p> <p>Reference: ESA_SLBC_cci_D2.3.2 Version: v1.2 Date: 22.11.2018 Page: 56 of 119</p>
---	---	--

- Novotny, K.; Horwath, M., Cazenave, A., Palanisamy, H., Marzeion, B., Paul, F., Döll, P., Cáceres, D., Hogg, A., Shepherd, A., Forsberg, R., Sørensen, L., Barletta, V.R., Andersen, O.B., Rannald, H., Johannessen, J., Nilsen, J.E., Gutknecht, B.D., Merchant, Ch.J., MacIntosh, C.R., Old, Ch., and von Schuckmann, K. (2018): *ESA Climate Change Initiative (CCI) Sea Level Budget Closure (SLBC_cci) Science Requirements Updated and Preliminary Thoughts on Roadmap. Version 1.0, 05.06.2018.*
- Peltier, W. R. (1994): Ice Age Paleotopography. *Science*, 265(5169), 195–201. doi: 10.1126/science.265.5169.195.
- Peltier, W. R. (2004): Global glacial isostasy and the surface of the ice-age Earth: the ICE-5G (VM2) model and GRACE. *Annu. Rev. Earth Planet. Sci.*, 32, 111-149, doi: 10.1146/annurev.earth.32.082503.144359.
- Peltier, W. R., Argus, D. F., and Drummond, R. (2015): Space geodesy constrains ice age terminal deglaciation: The global ICE-6G_C (VM5a) model: Global Glacial Isostatic Adjustment. *J. Geophys. Res. Solid Earth*, 120(1), 450–487. doi: 10.1002/2014JB011176.
- Quinn, K.J, and Ponte, R.M. (2010): Uncertainty in ocean mass trends from GRACE. *Geophys J In*, 181 (2): 762-768. doi: 10.1111/j.1365-246X.2010.04508.x.
- Rietbroek, R, Brunnabend, S-E, Kusche, J, Schröter, J, and Dahle, C (2016):-Revisiting the contemporary sea-level budget on global and regional scales. *PNAS* 2016 113 (6) 1504-1509, doi: 10.1073/pnas.1519132113.
- Swenson, S., and Wahr, J. (2006): Post-processing removal of correlated errors in GRACE data. *Geophysical Research Letters*, 33(8), doi: 10.1029/2005GL025285.
- Swenson S., Chambers D., and Wahr J. (2008): Estimating geocenter variations from a combination of GRACE and ocean model output. *Journal of Geophysical Research: Solid Earth*, 113(B8), doi: 10.1029/2007JB005338.
- Tamisiea, M.E. (2011): Ongoing glacial isostatic contributions to observations of sea level change. *Geophys J Int.*, 186 (3): 1036-1044. doi: 10.1111/j.1365-246X.2011.05116.x.
- Tapley, B. D., Bettadpur, S., Watkins, M., and Reigber, C. (2004): The gravity recovery and climate experiment: Mission overview and early results. *Geophys. Res. Lett.*, 31, L09607. doi: 10.1029/2004GL019920.
- Uebbing, B., Lück, Ch., Rietbroek, R., Kusche, J., and Landerer, F.W. (2018): *Reconciling Global Ocean Mass Timeseries from GRACE and Swarm*. Presentation at the GRACE / GRACE-FO Science Team Meeting, Potsdam, October 9-11, 2018.
- Wahr, J., M. Molenaar, and F. Bryan (1998): Time variability of the Earth's gravity field: Hydrological and oceanic effects and their possible detection using GRACE, *J. Geophys. Res.*, 103(B12), 30205–30229, doi:10.1029/98JB02844.
- Wahr, J., Nerem, R. S., and Bettadpur, S. V. (2015): The pole tide and its effect on GRACE time-variable gravity measurements: Implications for estimates of surface mass variations. *Journal of Geophysical Research: Solid Earth*, 120(6), 4597-4615, doi: 10.1002/2015JB011986.

		<p>CCI Sea Level Budget Closure ESA/ESRIN contract 4000119910/17/I-NB</p> <p>Reference: ESA_SLBC_cci_D2.3.2 Version: v1.2 Date: 22.11.2018 Page: 57 of 119</p>
---	---	--

5 Glacier Contribution to Sea Level Change

5.1 Data Access and Requirements

The glacier evolution model used to calculate glacier mass changes and their contribution to sea level (Marzeion et al. 2012) requires (1) global glacier outlines, (2) atmospheric boundary conditions, and (3) measured mass balances (for calibration and validation) as an input. These datasets are freely available from the following sites: Glacier outlines are taken from the Randolph Glacier Inventory (RGI) version 5.0 (updated from Pfeffer et al. 2014) that provides an initial extent for each of the world's glaciers and is available from glims.org/RGI.

Atmospheric boundary conditions were obtained from 7 different global reanalysis products/gridded observational data sets:

- CRU gridded climate data version 4.01 (updated from Harris et al. 2014) that are available from http://browse.ceda.ac.uk/browse/badc/cru/data/cru_ts/ in combination with the spatially higher resolved climatological dataset CRU CL 2.0 (updated from New et al. 2002) that can be obtained from <https://crudata.uea.ac.uk/cru/data/hrg/tmc/>.
- The 20th Century Reanalysis version 2 (20CRv2, Compo et al., 2011) that is available from https://www.esrl.noaa.gov/psd/data/20thC_Rean/. Only anomalies were taken from this dataset, the climatology was obtained from the spatially higher resolved CRU CL 2.0 data set mentioned above. Since this reanalysis only includes data up to 2012, the remaining years were filled using CRU TS version 4.01 (see above).
- The Climate Forecast System Reanalysis (CFSR, Saha et al., 2014) that is available from <https://rda.ucar.edu/datasets/ds093.2/>. Only anomalies were taken from this dataset, the climatology was obtained from the spatially higher resolved CRU CL 2.0 data set mentioned above. Since this reanalysis only includes data between 1979 and 2010, the remaining years were filled using CRU TS version 4.01 (see above).
- The ERA-20C reanalysis (ERA20C, Poli et al., 2016) that is available from <http://apps.ecmwf.int/datasets/data/era20c-moda/levtype=sfc/type=an/>. Only anomalies were taken from this dataset, the climatology was obtained from the spatially higher resolved CRU CL 2.0 data set mentioned above. Since this reanalysis only includes data up to 2010, the remaining years were filled using CRU TS version 4.01 (see above).
- The ERA-Interim reanalysis (ERA-Interim, Dee et al., 2011) that is available from <http://apps.ecmwf.int/datasets/data/interim-full-moda/levtype=sfc/>. Only anomalies were taken from this dataset, the climatology was obtained from the

		<p>CCI Sea Level Budget Closure ESA/ESRIN contract 4000119910/17/I-NB</p> <p>Reference: ESA_SLBC_cci_D2.3.2 Version: v1.2 Date: 22.11.2018 Page: 58 of 119</p>
---	---	--

spatially higher resolved CRU CL 2.0 data set mentioned above. Since this reanalysis only includes data starting in 1979, the remaining years were filled using CRU TS version 4.01 (see above).

- The Japanese 55-year reanalysis (JRA55, Kobayashi et al., 2015) that is available from <https://rda.ucar.edu/datasets/ds628.1/>. Only anomalies were taken from this dataset, the climatology was obtained from the spatially higher resolved CRU CL 2.0 data set mentioned above. Since this reanalysis only includes data between 1958 and 2014, the remaining years were filled using CRU TS version 4.01 (see above).
- The Modern-Era Retrospective analysis for Research and Applications, Version 2 (MERRA-2, Gelaro et al., 2017) that is available from <https://disc.gsfc.nasa.gov/datasets?keywords=%22MERRA-2%22&page=1&source=Models%2FAnalyses%20MERRA-2>. Only anomalies were taken from this dataset, the climatology was obtained from the spatially higher resolved CRU CL 2.0 data set mentioned above. Since this reanalysis only includes data starting in 1980, the remaining years were filled using CRU TS version 4.01 (see above).

The model is calibrated and validated using observations of glacier mass balance from the collections of the World Glacier Monitoring Service (WGMS, 2016) that are available from wgms.ch.

5.2 Algorithms

5.2.1 Review of scientific background

The objective of model-based estimates of glacier mass change is to complement observations of glaciers with observations of the state of the atmosphere and physical understanding of glacier mass balance. While there is a growing number of glacier models being developed and used for projecting future glacier change, there is currently only one that allows to reconstruct past and reproduce current glacier change on the global scale, while also accounting for glacier geometry change (Marzeion et al., 2012). We will use this model for all calculations, as a specific aim of this project is also the globally consistent reconstruction of former glacier extents and their contribution to sea level. Special constraints such as storage of water in endorheic basins or potential future lakes forming in overdeepenings of currently still glacier covered glacier beds have to be considered separately.

		<p>CCI Sea Level Budget Closure ESA/ESRIN contract 4000119910/17/I-NB</p> <p>Reference: ESA_SLBC_cci_D2.3.2 Version: v1.2 Date: 22.11.2018 Page: 59 of 119</p>
---	---	--

5.2.2 Algorithms

The model uses global fields of temperature and precipitation rates to estimate the glacier mass balance. Changes in glacier geometry are modeled following an area-volume-time scaling approach, enabling the model to account for various feedbacks between glacier geometry and mass balance. Glacier geometries obtained through remote sensing (from the RGI) are used to initiate the model, as well as validate results and obtain error characteristics. From the time of initialization, the model is run forward by using volume changes obtained from the mass balance module to calculate changes in glacier area, length, and terminus altitude. Glacier changes prior to the time of initialization are obtained using an iterative process: the model is also run forward during the time preceding the initialization. However, to find the correct starting conditions, the model iteratively searches for that state of the glacier at the beginning of the model run, which results in the observed state of the glacier at the time of glacier observation (i.e., at the time the glacier outlines were obtained). A detailed description of the model is found in Marzeion et al. (2012).

The procedure described above was repeated for all seven forcing data sets, in order to obtain an ensemble estimate of the glacier mass change. Local (i.e., glacier-specific) parameters were re-calibrated and cross-validated following the procedure described in Marzeion et al. (2012). After gridding the results of all ensemble members onto the regular grid described below, the median of the ensemble was calculated at each grid cell. This median value is provided in the data files.

5.3 Product Specification

5.3.1 Product geophysical data content

Two variables are given:

1. Glacier mass change is calculated in the unit m water equivalent (w.e.) and multiplied with glacier area (in m²) and water density (1000 kg m⁻³) to obtain the mass of water in Gt. This is the temporally accumulated mass contribution of glaciers within each grid cell to sea-level change. Mass loss of glaciers is counted positive (see Figure 5.1 and Figure 5.2). Regional or global values of glacier mass change can be obtained by summing over the region of interest.
2. Uncertainties of glacier mass change are originally also in the unit m w.e. and are converted to Gt. These uncertainties are obtained from the cross-validation of the model using annual values. To obtain the monthly values, it is assumed that each

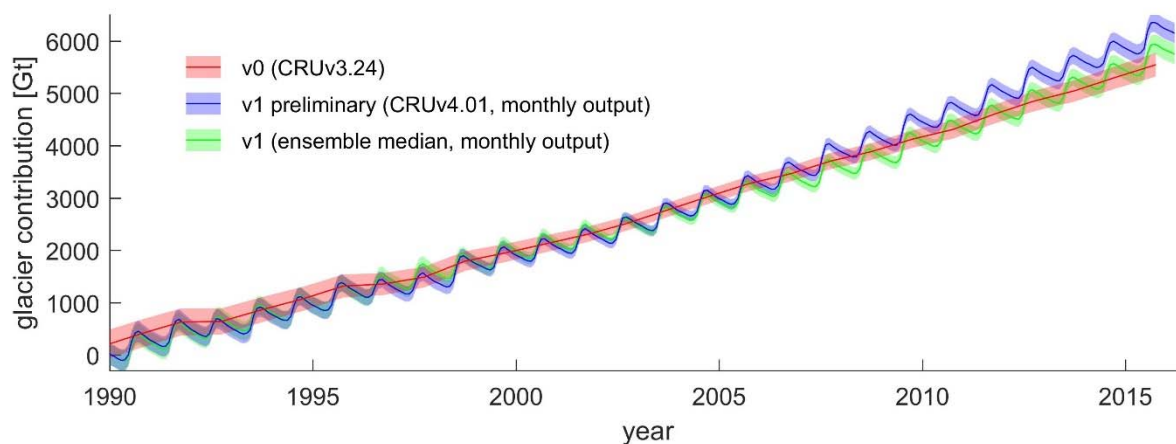


Figure 5.1: Comparison of the temporally accumulated contribution of glaciers to sea-level change of data product version 0, the preliminary version 1, and final version 1.

month of the mass balance year contributes equally to the annual uncertainty. The uncertainties are accumulated temporally forward and backward from the initialization year of each glacier, and then accumulated spatially for all glaciers contained within each grid cell. The value from 1. (see above) \pm this uncertainty indicates the 5th to 95th percentile of the uncertainty band. Regional or global values of the uncertainty can be obtained by taking the square root of the sum of the squares of these uncertainties over the region of interest. To convert the given uncertainties to standard uncertainties, the numbers have to be divided by 1.645. The underlying assumption of a normal distribution of errors is supported by the uncertainty assessment.

Data are provided with the file

glaciers_ensemble_median_rgi_v5_monthly_v1.1.nc

Geophysical Variable	Name in product	Unit
Time	time	decimal year
Latitude	lat	degrees north
Longitude	lon	degrees east
Glacier mass change	accumulated glacier mass loss [Gt]	Gt
Uncertainty of glacier mass change (half-width of 90% confidence interval)	uncertainty of accumulated glacier mass loss [Gt]	Gt

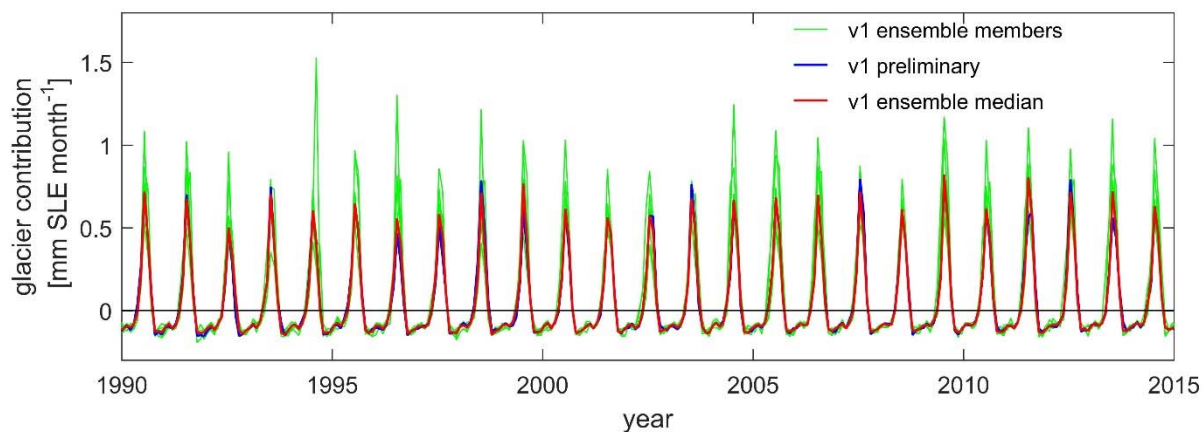


Figure 5.2: Comparison of the monthly contribution of glacier to sea-level change between the preliminary and final data product version 1. The individual ensemble members are shown for information, but not included in the data product.

5.3.2 Coverage and resolution in time and space

Data coverage is global, but excluding peripheral glaciers in Greenland and Antarctica. Data are provided starting 1979 through to 2016. The resolution in space is half a degree and the resolution in time is one month.

5.3.3 Product data format

The data are provided in netcdf4 format.

5.3.4 Product grid and projection

Data are provided on a rectangular grid. Latitude and longitude values of the grid correspond to the center of the grid cell. Each glacier is assigned to that grid cell that contains its center point (as given in the RGIv5.0), even if the glacier stretches across several grid cells.

5.4 Uncertainty assessment

5.4.1 Sources of error

The most relevant sources of error are:

1. uncertainty in the initialization data set (i.e., errors in glacier outlines);
2. simplification of physics in the model (concerning both the mass balance module and the simple representation of ice dynamics);

		<p>CCI Sea Level Budget Closure ESA/ESRIN contract 4000119910/17/I-NB</p> <p>Reference: ESA_SLBC_cci_D2.3.2 Version: v1.2 Date: 22.11.2018 Page: 62 of 119</p>
---	---	--

3. uncertainty in the forcing data (i.e., scarce observations of temperature and precipitation near glaciers that impact the aggregated climate data as well as the reanalysis data used),
4. uncertainty in the observations of glacier mass balance used to calibrate the model,
5. uncertainty in the model calibration.

Uncertainties increase forward and backward in time relative to the year of model initialization, which is typically around the year 2000 (but differs for glaciers individually), since then the model's results depend on the modeled rather than observed glacier geometries, which become more uncertain. This increasing uncertainty is included in the error propagation. On considerably larger time scales, particularly time periods preceding the satellite era, the uncertainty of the atmospheric data used as boundary conditions for the glacier model increases. In principle, this increased uncertainty should be detectable during the validation, but since there are very few validation data points (i.e., in situ glacier mass balance observations) available preceding the satellite era, there is no robust signal of an increased uncertainty detectable. However, we don't believe this unquantified uncertainty is a significant contributor during the period considered here 1979 to 2016, and if so, only in the first few years.


5.4.2 Methodology for uncertainty assessment

The total uncertainty of the resulting glacier mass change estimates is determined using a leave-one-glacier-out cross validation of the glacier model. In this procedure, the out-of-sample uncertainties of the model are measured by:

1. calibrating the model based on glacier observations, but withholding from the calibration all observations from one glacier;
2. running the model for that glacier and determine model error;
3. repeat the above two steps for all glaciers with available mass balance observations.

A total of 255 glaciers with 3997 observed mass balance years was used in this procedure.

As uncertainties in the estimated mass balance feed back to the modeled glacier geometry, these uncertainty estimates were then propagated through the entire model chain, forward and backward in time relative to the year of model initialization. The obtained uncertainty estimates of temporally integrated glacier area and volume change were then validated once more using observations of glacier area and volume change.

		<p>CCI Sea Level Budget Closure ESA/ESRIN contract 4000119910/17/I-NB</p> <p>Reference: ESA_SLBC_cci_D2.3.2 Version: v1.2 Date: 22.11.2018 Page: 63 of 119</p>
---	---	--

5.4.3 Results of uncertainty assessment

Compared to version 0 and the preliminary version 1 of the data product, we now use an ensemble approach, particularly to reduce – as far as possible – error source 3 listed above. The glacier-specific model parameters were recalibrated for each of the ensemble members. Since the observations-driven ensemble member is only extended in time, and provided in monthly instead of annual resolution compared to version 0, the uncertainty measures are identical.

The validation of the other individual ensemble members showed that contrary to expectations, the systematic differences in the different data sets used as boundary conditions (as listed above) are large enough to warrant a recalibration of the global model parameters as well (this concerns, in particular, the lapse rates and correction factors for precipitation). This re-calibration will be added to the list of tasks for version 2 of the data product. The most pessimistic assumption is that this re-calibration (and new validation) will indicate that all six added reanalysis-driven ensemble members perform weaker than the observation-driven ensemble member. In that case, the optimal estimation of the glacier contribution would be identical with the observation-driven ensemble member, and the uncertainties would remain unchanged as well. We therefore decided to provide the uncertainties in version 1 of the data product based on this most pessimistic scenario. However, based on experience, we expect the ensemble median to perform best in the global validation. We therefore decided to provide the ensemble median as our best estimate for the glacier contribution. In total, we therefore provide a conservative estimate of uncertainties (as detailed below), that we expect to improve in version 2.

The global mean temporal correlation between modeled and observed mass balances of individual glaciers is 0.60 with a standard deviation of 0.39 between the different glaciated regions. The skill score global mean is 0.34, with a regional standard deviation of 0.27. The mean model bias in the mass balance is indistinguishable from zero (global mean value of 5 mm w.e.). The mean root mean square error of modeled mass balances for individual glaciers is 736 mm w.e. The model errors are spatially and temporally uncorrelated. While the model results for any given individual glacier are therefore quite uncertain, the relative error becomes smaller for ensembles of glaciers (e.g. all glaciers within a grid cell, on a mountain range, or globally).

Since errors grow forward and backward relative to the time of model initialization, and since model initialization occurs at different years for different glaciers (depending on the year the glacier geometry was observed), the uncertainties of rates of mass change are not trivially to derive from the uncertainties of accumulated glacier mass changes. Since validation is only possible of mass balances accumulated within a year, we only provide the uncertainty of accumulated mass balances in the data file.

		<p>CCI Sea Level Budget Closure ESA/ESRIN contract 4000119910/17/I-NB</p> <p>Reference: ESA_SLBC_cci_D2.3.2 Version: v1.2 Date: 22.11.2018 Page: 64 of 119</p>
---	---	--

5.4.4 Uncertainty documentation in the data products

The delivered data file contains gridded data of the uncertainty for temporally accumulated mass change (in Gt). See Section 5.3.1.

5.5 References

- Compo, G.P., J.S. Whitaker, P.D. Sardeshmukh, N. Matsui, R.J. Allan, X. Yin, B.E. Gleason, R.S. Vose, G. Rutledge, P. Bessemoulin, S. Brönnimann, M. Brunet, R.I. Crouthamel, A.N. Grant, P.Y. Groisman, P.D. Jones, M. Kruk, A.C. Kruger, G.J. Marshall, M. Maugeri, H.Y. Mok, Ø. Nordli, T.F. Ross, R.M. Trigo, X.L. Wang, S.D. Woodruff, and S.J. Worley (2011): The Twentieth Century Reanalysis Project. *Quarterly J. Roy. Meteorol. Soc.*, 137, 1-28.
- Dee, D. P., Uppala, S. M., Simmons, A. J., Berrisford, P., Poli, P., Kobayashi, S., ... and Bechtold, P. (2011): The ERA-Interim reanalysis: Configuration and performance of the data assimilation system. *Quarterly Journal of the royal meteorological society*, 137(656), 553-597.
- Gelaro, R., McCarty, W., Suárez, M. J., Todling, R., Molod, A., Takacs, L., ... and Wargan, K. (2017): The modern-era retrospective analysis for research and applications, version 2 (MERRA-2). *Journal of Climate*, 30(14), 5419-5454.
- Harris, I. P. D. J., Jones, P. D., Osborn, T. J., and Lister, D. H. (2014): Updated high-resolution grids of monthly climatic observations—the CRU TS3. 10 Dataset. *International Journal of Climatology*, 34(3), 623-642.
- Kobayashi, S., Ota, Y., Harada, Y., Ebata, A., Moriya, M., Onoda, H., ... and Miyaoka, K. (2015): The JRA-55 reanalysis: General specifications and basic characteristics. *Journal of the Meteorological Society of Japan*. Ser. II, 93(1), 5-48.
- Marzeion, B.; Jarosch, A. H.; Hofer, M. (2012): Past and future sea-level change from the surface mass balance of glaciers. *The Cryosphere* 6 (6), 1295–1322, doi: 10.5194/tc-6-1295-2012.
- New, M., Lister, D., Hulme, M., and Makin, I. (2002): A high-resolution data set of surface climate over global land areas. *Climate Research*, 21(1), 1-25.
- Pfeffer, W. T., Arendt, A. A., Bliss, A., Bolch, T., Cogley, J. G., Gardner, A. S., ... and Miles, E. S. (2014). The Randolph Glacier Inventory: a globally complete inventory of glaciers. *Journal of Glaciology*, 60(221), 537-552.
- Poli, P., Hersbach, H., Dee, D. P., Berrisford, P., Simmons, A. J., Vitart, F., ... and Trémolet, Y. (2016): ERA-20C: An atmospheric reanalysis of the twentieth century. *Journal of Climate*, 29(11), 4083-4097.
- Saha, S., Moorthi, S., Wu, X., Wang, J., Nadiga, S., Tripp, P., ... and Ek, M. (2014): The NCEP climate forecast system version 2. *Journal of Climate*, 27(6), 2185-2208.
- WGMS (2016): *Fluctuations of Glaciers Database*. World Glacier Monitoring Service, Zurich, Switzerland. DOI: 10.5904/wgms-fog-2016-08. Online access: <http://dx.doi.org/10.5904/wgms-fog-2016-08>.

		CCI Sea Level Budget Closure ESA/ESRIN contract 4000119910/17/I-NB Reference: ESA_SLBC_cci_D2.3.2 Version: v1.2 Date: 22.11.2018 Page: 65 of 119
---	---	---

6 Ice Sheets Contribution to Sea Level Change

Time series for the Greenland Ice Sheet (GrIS) and for the Antarctic Ice Sheet (AIS) are provided. All ice sheet methods and data are documented in the respective ESA CCI Greenland Ice Sheet and Antarctica Ice Sheet documentation.

6.1 Data access and requirements

For the GrIS, three datasets describing the mass variation and changes of the polar ice sheets are available. Note, that the GrIS mass changes from lidar altimetry are the version 0 data as delivered in D2.1.

(1) Greenland Ice Sheet mass changes from GRACE

The data set described here is the time series of mass changes of the Greenland Ice Sheet derived from GRACE data. The product is publicly available as one of the ECVs of the Greenland Ice Sheet CCI, and hence is described in depth in the various documents (deliverables) of this programme. Therefore, it will not be described as thoroughly here. The summary here is based on the reference documents from the Greenland Ice Sheet CCI.

The GRACE-derived time series for Greenland is available for free download at <http://products.esa-icesheets-cci.org/products/downloadlist/GMB/> (for product specifications see Sørensen et al. (2017)).

At this site, four products are available: two generated by TU Dresden and two by DTU Space. The data submitted here are the ones derived by DTU Space.

GRACE data are available from different processing centres, in particular the GIS CCI products are available for the release RLO6 provided by CSR and the ITSG-Grace2016 release provided by TU Graz (www.tugraz.at/institute/ifg/downloads/gravity-field-models/itsg-grace2016). For the v1 data submitted here we make use of the CSR RLO6 release provided by CSR, which includes spherical harmonic coefficients up to degree $l_{max}=96$.

Moreover, for the v1 data submitted here we do not include the GIA correction.

(2a) Greenland Ice Sheet mass changes from lidar altimetry

The data set described here is the mean mass loss grid for the Greenland Ice Sheet in the time period 2003-2009 derived from ICESat laser altimetry and snow/firn modelling. This is the data set that has been submitted to the IMBIE 2016 intercomparison exercise (except that here the full grid is provided, for IMBIE the sum over the different basins was provided). The data product is an updated version of what was published in Sørensen et al. (2011). This document

		<p>CCI Sea Level Budget Closure ESA/ESRIN contract 4000119910/17/I-NB</p> <p>Reference: ESA_SLBC_cci_D2.3.2 Version: v1.2 Date: 22.11.2018 Page: 66 of 119</p>
---	---	--

explains the basic information and highlights updates, for details please refer to Sørensen et al. (2011).

The ICESat mass change data evaluation follows Sasgen et al. (2012), Sørensen et al. (2011) with an update of the ICESat data to the product release 34. In addition, the GIA- and firn-corrections have also been updated.

The mass change grid is derived from elevation changes derived from ICESat laser altimetry data release 34 available through NSIDC (http://nsidc.org/data/icesat/data_releases.html#rel34-alt).

The Firn model is forced by output data from the RCM HIRHAM5 model (Langen et al., 2015; Lucas-Picher et al., 2012).

The mass change grid data product is not currently available for download as it was specifically created for use in the IMBIE 2016 (<http://imbie.org/imbie-2016/>).

(2b) Greenland Ice Sheet mass changes from radar altimetry

The data set described here is the annual mean mass loss for the GrIS in the period of ESA radar altimetry (1992-2017). The data are calibrated using the 2003-2009 data from ICESat laser altimetry and snow/firn modelling to both account for firn changes and radar penetration. The combined radar volume change data-series is published in Simonsen and Sørensen (2017) and Sørensen et al. (2018). This document explains the basic information and highlights updates in the conversion of radar volume change to mass change, for details regarding the volume change estimates we refer to the two publications above.

(3) Antarctic Ice Sheet mass changes from GRACE

The data set described here is the time series of mass changes of the Antarctic Ice Sheet derived from GRACE data. The product is publicly available as one of the ECVs of the Antarctic Ice Sheet CCI, and hence is described in depth in the various documents (deliverables) of this project. The relevant documents are available at ftp://anon-ftp.ceda.ac.uk/neodc/esacci/ice_sheets_antarctica/docs/, <http://esa-icesheets-antarctica-cci.org/index.php?q=documents> (Folders “Task 1 Requirements” and “Task 2 Algorithms” and “Task 3 System Evolution”) namely

- ST-UL-ESA-AISCCI-ATBD-001_v3.0.pdf: Algorithm Theoretical Baseline Document (ATBD)
- ST-UL-ESA-AISCCI-CECR-001_v3.0.pdf: Comprehensive Error Characterisation Report (CECR). An update for the GMA part is given under https://data1.geo.tu-dresden.de/ais_gmb/source/ST-UL-ESA-AISCCI-CECR-Draft_GMB.pdf
- ST-UL-ESA-AISCCI-PSD-001_v2.0.pdf: Product Specification Document (PSD; Hogg et al., 2018)

		<p>CCI Sea Level Budget Closure ESA/ESRIN contract 4000119910/17/I-NB</p> <p>Reference: ESA_SLBC_cci_D2.3.2 Version: v1.2 Date: 22.11.2018 Page: 67 of 119</p>
---	---	--

- ST-UL-ESA-AISCCI-PUG-001_v1.4.pdf: Product User Guide (PUG)

The datasets are available from ftp://anon-ftp.ceda.ac.uk/neodc/esacci/ice_sheets_antarctica/data/gravimetric_mass_balance/.

In addition, the datasets and the documentation can be obtained at the interactive geodetic data portal of TU Dresden at https://data1.geo.tu-dresden.de/ais_gmb/index.html.

The products provided here within SLBC v1 are an update of the products provided within SLBC v0. The v1 data are copies of the of Antarctic_cci GMB data updated in January 2018.

(4) Antarctic Ice Sheet mass changes from altimetry

The data set described here is the time series of ice mass loss for the East Antarctic Ice Sheet, the West Antarctic Ice Sheet and the Antarctic Peninsula for the time period 1992-2016 derived from radar altimetry and a time evolving ice density mask. Data from the 2010-2016 is published in McMillan et al., (2014), and the full 25 year time series is in the publication process. This document explains the basic information about the dataset, for details of the plane fit method, please refer to (McMillan et al., 2014).

The mass change time series is derived from surface elevation change generated by processing Level 2 elevation measurements provided by ESA, and acquired by multiple radar altimetry satellite missions, ERS-1, ERS-2, ENVISAT and CryoSat-2. The lateral limit used for both the Greenland and Antarctic ice sheet CCI can be found at the following link (<http://imbie.org/imbie-2016/>), and this has been provided to the Glaciers and Ice Caps CCI project team.

6.2 Algorithms

6.2.1 Review of scientific background

Ice Sheet mass changes from GRACE (Greenland and Antarctica)

The GRACE mission has two identical space crafts flying about 220 km apart in a near-polar orbit originally at 480 km above the Earth. GRACE maps the Earth's gravity field by making accurate measurements of the distance between the two satellites, using GPS and a microwave ranging system. GRACE-derived solutions of the Earth's time variable gravity field are available from different processing facilities like CSR, GFZ or JPL. With a typical temporal resolution of one month, GRACE Level-2 products allow the investigation of seasonal and inter-annual variations in addition to long-term changes (Horwath et al., 2012). A comprehensive review of scientific background is found in Khvorostovsky et al. (2016).

		<p>CCI Sea Level Budget Closure ESA/ESRIN contract 4000119910/17/I-NB</p> <p>Reference: ESA_SLBC_cci_D2.3.2 Version: v1.2 Date: 22.11.2018 Page: 68 of 119</p>
---	---	--

Greenland Ice Sheet mass changes from lidar altimetry

Satellite laser altimetry and radar altimetry, respectively, is used to derive elevation changes of the GrIS for the given time period. The elevation changes are interpolated to cover the entire ice sheet. The elevation changes are corrected for any elevation change signal that is not associated with ice mass loss (GIA, elastic uplift and changes in firn compaction), and finally converted into grid point mass changes using assumptions on ice/snow densities. This procedure is described in detail in Sørensen et al. (2011).

Greenland Ice Sheet mass changes from radar altimetry

Satellite radar altimetry is used to derive elevation changes of the GrIS for the given time period. The elevation changes are interpolated to cover the entire ice sheet. The elevation changes are corrected for any elevation change signal that is not associated with ice mass loss (GIA, elastic uplift and changes in firn compaction), by calibrating the radar mass change series by the observations from ICESat (above).

Antarctic Ice Sheet mass changes from altimetry

The scientific background is described in the Antarctic Ice Sheet Climate Change Initiative (AIS_CCI) Algorithm Theoretical Basis Document (ATBD) (Nagler et al., 2018a).

6.2.2 Algorithms

Greenland Ice Sheet mass changes from GRACE

Methods used for the inference of ice sheet mass changes from GRACE data is an inversion approach as in Barletta et al. (2013). The mass inversion method has been adopted for the GMB product generation, within the GIS CCI.

A detailed description of the method and associated algorithms is provided in Sect. 6.3.1 of Khvorostovsky et al. (2016).

Greenland Ice Sheet mass changes from lidar altimetry

Elevation change method:

Several methods for deriving elevation changes from repeat laser altimetry exist. Here, we have used M3 of Sørensen et al. (2011), which was also used in Sasgen et al. (2012).

Correction for Glacial Isostatic Adjustment:

The ICE-6g rates of radial displacement (UP; Peltier et al., 2015) have been interpolated from the $0.2^\circ \times 0.2^\circ$ grid posting given in the drad.12mgrid.nc dataset available at <http://www.atmos.physics.utoronto.ca/~peltier/data.php>.

		<p>CCI Sea Level Budget Closure ESA/ESRIN contract 4000119910/17/I-NB</p> <p>Reference: ESA_SLBC_cci_D2.3.2 Version: v1.2 Date: 22.11.2018 Page: 69 of 119</p>
---	---	--

Correction for elastic uplift

The instantaneous elastic vertical displacement is applied following Sørensen et al. (2011). It is obtained from a suitably modified version of the code SELEN 2.9 (Nielsen et al., 2014; Spada and Stocchi, 2007).

Correction for changes in air content in the firn:

The firn model follows Simonsen et al. (2013), which include a parameterization of melt water retention. The firn model is forced by the HIRHAM5 regional climate model (Langen et al., 2015; Lucas-Picher et al., 2012), which have been updated with a new and improved surface scheme compared to the version used in Nielsen et al. (2014) (Sasgen et al., 2012; Sørensen et al., 2011).

Conversion from Volume to Mass:

The volume to mass conversion is done by the appropriate density.

Greenland Ice Sheet mass changes from radar altimetry

Elevation change method:

The volume change method is derived following Simonsen and Sørensen (2017) and Sørensen et al. (2018).

Conversion from Volume to Mass, including the appropriate corrections:

The mass change estimate is derived in a three-step procedure:

- 1) The coverage of the radar altimetry is limited to ice sheets slopes less than 1.5 degrees. To estimate the volume change of the entire GrIS, the volume change is extrapolated using nearest-neighbor interpolation. This will underestimate the volume change in the fast losing areas for GrIS and is in need of calibration.
- 2) Following the methodology of Sørensen et al. (2011) the volume change is converted into mass change by the appropriate density.
- 3) As the radar volume shown in Figure 6.1, is not accounting for the correction terms given above and the radar also are biased by changing scattering horizon in the firn column (Nilsson et al., 2015). It was decided to account for all of the terms at once by calibrating the mass change rate during the ICESat era.

Antarctic Ice Sheet mass changes from GRACE

The Antarctic Ice Sheet GMB products are derived from the spherical harmonic monthly solution series by ITSG-Grace2016 by TU Graz (Klinger et al. 2016; Mayer-Gürr et al. 2016) following a regional integration approach with tailored integration kernels that account for

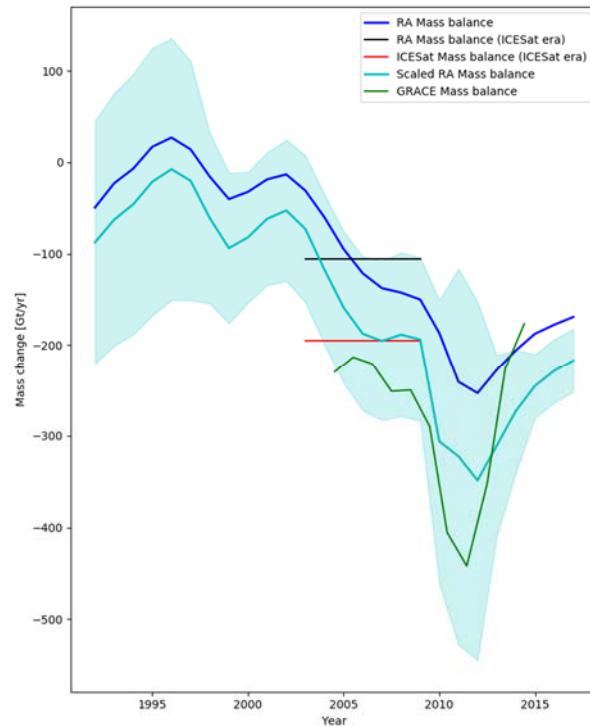


Figure 6.1: GrIS volume change estimates, including the raw (blue) mass change from radar altimetry. The horizontal black line indicates the average radar altimetry rate during the ICESat era, the red line indicates the average rate measured by ICESat. The calibrated radar altimetry mass change rate is shown with uncertainties in cyan. For reference the GRACE mass change rate is shown in green.

both the GRACE error structure and the information on different signal variance levels on the ice sheet and on the ocean (Horwath and Groh 2016).

Antarctic Ice Sheet mass changes from altimetry

The algorithm for elevation changes is described in the Antarctic Ice Sheet Climate Change Initiative (AIS_CCI) Algorithm Theoretical Basis Document (ATBD) (Nagler et al., 2018a) and is summarized here.

Elevation change method

Several methods for deriving elevation changes from repeat laser altimetry exist. Here, we have employed the plane fit method (McMillan et al., 2014). The plane fit method (McMillan, et al., 2014) is an adaption of the along track method which can be applied to satellites which operate in both short 27-35 day orbit repeat periods (such as the main operational periods of Envisat, ERS-1,2 and Sentinel-3A,B) and long 369 day repeat periods where measurements do not exactly repeat within monthly time scales such as CryoSat-2.

The plane fit method grids both ascending and descending measurements in a regular polar stereographic grid instead of gridding separately along track. It derives a surface elevation

		<p>CCI Sea Level Budget Closure ESA/ESRIN contract 4000119910/17/I-NB</p> <p>Reference: ESA_SLBC_cci_D2.3.2 Version: v1.2 Date: 22.11.2018 Page: 71 of 119</p>
---	---	--

change estimate at the center of each grid cell by applying a surface model to the measurements within that cell and has been shown in the CCI round robin experiments to perform as well or better than other along track methods for all missions (except Envisat's drifting phase from Oct 2010- Apr 2012, where special techniques are required for all methods) and hence is the primary along track method chosen for the Antarctic CCI. Another advantage of the plane fit method is that SEC results are produced on the same grid as the SEC output product and hence do not require re-gridding which can introduce an additional error and reduce accuracy.

Correction for Glacial Isostatic Adjustment

A post-glacial rebound (PGR) correction was applied to all the residual heights in each selected cell. The correction used was the IJ05_R2 correction, from Ivins et al. (2013).

Treatment of unobserved areas

New methods of estimating the SEC of the unobserved regions of the ice sheets have been developed, both between a satellite's ground tracks and beyond the latitude limits of the satellite's orbit.

- Polar hole filling: beyond the orbit limits, SEC is estimated from an annular region, 80°S-81°S. Most drainage basins within that region are treated together but Zwally basin 18 is a special case: its snow area is treated separately, and its ice area, which includes the Kamb Ice Stream, is used to estimate all unobserved ice, since the unobserved ice area is continuous.
- Between-tracks: the between-track estimates are based on spatially-limited triangulation, followed by a velocity-guided interpolation (using BISICLES) on the ice sheet margins, i.e. within 100km of the coast, and mean estimates elsewhere

Derivation of Height Time Series

Time series calculations used the dz and dt values retained after the model-fitting stage and aggregated in 140-day epochs, which were only calculated for grid cells that were observed by satellite. Time series can be calculated over any region. In each case, unobserved grid cells had to be filled.

Inter-Mission Cross Calibration

The previous calculations produced a time series of changes in height per mission. To produce a continuous dataset, biases had to be added between missions. The biasing method used is applied to each grid cell individually, which is known as pixel cross-calibration. In each case, the biasing aimed to bring ERS1, ERS2 and CryoSat-2 data onto the same baseline as the Envisat data.

		<p>CCI Sea Level Budget Closure ESA/ESRIN contract 4000119910/17/I-NB</p> <p>Reference: ESA_SLBC_cci_D2.3.2 Version: v1.2 Date: 22.11.2018 Page: 72 of 119</p>
---	---	--

Conversion from Volume to Mass

As radar altimeters penetrate some (unknown) depth into the snow surface, direct application of a firm correction to the elevation change measurement, and then derivation of mass at the density of ice from the residual signal, has known issues in Antarctica. Therefore we use a time-evolving density mask to delimit the region where we convert volume to mass at the density of snow (350kg/m³) and ice (917kg/m³). To derive mass change, grid cells are identified as containing changing amounts of either snow or ice, using a time-dependent density mask. In this study the density mask was derived from the pixel cross-calibrated timeseries and the Berkeley Ice Sheet Initiative for Climate Extremes (BISICLES) ice velocity map (Cornford et al., 2013).

Down sampling of mass change time series at annual temporal resolution

The mass change time series is provided with an epoch of 140 day and we additionally provide the mass change time series at annual temporal resolution. The annual estimates are computed using a moving weighted average with a window size of 3 years. The time series of annual estimates is truncated by half the window size.

6.3 Product Specification

6.3.1 Product geophysical data content

Greenland Ice Sheet mass changes from GRACE

Ice mass changes for the entire ice sheet (Figure 6.2) and for the single basins (cf. Figure 6.3) are estimated and provided. The drainage basins used are an aggregation of those described by Zwally et al. (2012). The mass change is the mass anomaly in Gt (relative to a chosen zero level) with the associated errors (see Forsberg et al., 2013).

The time series for the entire ice sheet is constructed so that the estimate also includes the signal from outlying Glaciers and ice caps, while the individual basin estimates are derived in a way that aims at leaving those out of the solution. Therefore, there is a difference between the mass balance derived from the total time series and the sum of the individual basins. For further information on how ice sheet and the surrounding glaciers and ice caps are separated see Khvorostovsky et al. (2016).

The data provided here are given in a simple ASCII format and have a format slightly different from those provided in the GIS CCI. In fact we added the starting and ending epoch for each monthly solution.

Files provided are stored in a zipped file (CCI_GMB_RL06_time_series_NO_GIA.zip)

and are named: GIS**_grace.dat

		CCI Sea Level Budget Closure ESA/ESRIN contract 4000119910/17/I-NB Reference: ESA_SLBC_cci_D2.3.2 Version: v1.2 Date: 22.11.2018 Page: 73 of 119
---	---	---

where ** denotes the number of the basin (see Figure 6.3), "00" stands for the entire GrIS.

Geophysical Variable	Column in file	Unit
Time	1	decimal year
Mass change	2	Gt
Error on mass change	3	Gt
Start epoch for estimating the monthly mean mass change	4	decimal year
End epoch for estimating the monthly mean mass change	5	decimal year

Greenland Ice Sheet mass changes from lidar altimetry

Mass changes from lidar altimetry were taken from version 0 data of the SLBC_cci project. The file provided is a copy of the D2.1.1 delivery (version 0 data product) and is named SLBC_ICESat_mass_2003_2009_v0.txt .

The geophysical data content is a grid of mass changes given in ASCII format:

Geophysical Variable	Column in file	Unit
Point location: Latitude	1	degree east
Point location: Longitude	2	degree north
Mass change	3	kg/year
Standard deviation of mass change	4	kg/year
area of the grid cell over which the mass change is calculated	5	km ²

The sum of the mass changes over the whole grid (Greenland ice sheet + outer glaciers and ice caps) is -238.5 Gt/yr (cf. Table 6.1).

Greenland Ice Sheet mass changes from radar altimetry

We provide a grid of mass change rates at 100x100 km² resolution. Figure 6.2 shows the resulting mass change estimate for the main Greenland ice sheet, excluding weakly-connected ice and peripheral glaciers.

		CCI Sea Level Budget Closure ESA/ESRIN contract 4000119910/17/I-NB
		Reference: ESA_SLBC_cci_D2.3.2 Version: v1.2 Date: 22.11.2018 Page: 74 of 119

Content of file SLBC_GrIS_RA_MB_vers2.nc

Geophysical Variable	Name in product	Unit
Cartesian x-coordinate - easting	x	m
Cartesian y-coordinate - northing	y	m
Time	t	year (integer)
Latitude	lat	degrees_north
Longitude	lon	degrees_east
Mass change rate	mass_change_rate	Gt/year
Uncertainty of mass change rate	mass_change_rate_uncertainty	Gt/year
Ice sheet area in cell	Ice_area	km ²
Projection Type (Name of projection and parameters used)	EPSG 3413	

Antarctic Ice Sheet mass changes from GRACE

Mass change time series are provided for a number of drainage basins, based on the boundary definitions by Zwally et al. (2012). They describe the evolution of ice mass relative to a modelled reference value. This reference value is defined to be the GRACE-derived mass as of 2009-01-01. Respective time series are also derived for the total areas of the West Antarctic Ice Sheet, the East Antarctic Ice Sheet, the Antarctic Peninsula and the Antarctic Ice Sheet (AIS) as a whole.

The gridded changes are given in millimetres of equivalent water height (mm w.eq., or kg/m²). The applied algorithm is consistent with the one used for the GMB Basin Product.

The file AIS_GMB_basin.dat is an ASCII file that gives GRACE-derived time series of basin-averaged Antarctic ice mass changes in the form

Geophysical Variable	Column in file	Unit
time	1	decimal year
time	2	modified julian data
Mass change (dm) basin1	3	kg
Uncertainty of mass change (sigma)	4	kg

		CCI Sea Level Budget Closure ESA/ESRIN contract 4000119910/17/I-NB
		Reference: ESA_SLBC_cci_D2.3.2 Version: v1.2 Date: 22.11.2018 Page: 75 of 119

dm) basin1		
dm, sigma dm basin2	5, 6	kg
...	...	
dm, sigma dm basin30	31, 32	kg

The file AIS_GMB_trend.dat gives information, per basin, on the linear trend over the entire time series, on the uncertainties of the linear trends (cf. Section 6.4) and on the GIA correction. This allows, for example, to undo the GIA correction and apply a GIA correction according to a different model. The format is

Variable	Column in file	Unit
Basin number	1	
Mass trend	2	kg / yr
Total standard uncertainty of mass trend	3	kg/year
Applied GIA correction	4	kg/year
Basin area	5	m ²

In addition, gridded AIS mass changes from GRACE are given as a grid file in netCDF format. The NetCDF-4 classic file follows the Climate and Forecast (CF) conventions in version 1.6. Changes in ice mass are stored in the NetCDF variable *dm* [kg/m²]. Beside the projected x- and y-coordinates of the grid cell centres, corresponding ellipsoidal latitudes (*lat*) and longitudes (*lon*) are also given. In addition, each grid cell's area (*area*) on the ellipsoid is provided. Times are indicated in two different formats: modified Julian date (*time*) and decimal years (*time_dec*). Additional information on the product and the generating institution are stored in the global attributes.

Content of AIS_GMB_grid.nc

Geophysical Variable	Name in product	Unit
x-coordinate, y-coordinate	x, y	m
Modified Julian Date	time	days
Decimal year	time_dec	year

		CCI Sea Level Budget Closure ESA/ESRIN contract 4000119910/17/I-NB
		Reference: ESA_SLBC_cci_D2.3.2 Version: v1.2 Date: 22.11.2018 Page: 76 of 119

Longitude, Latitude	lon, lat	degrees_east, degrees_north
Change in ice mass	dm	kg/m ²
Grid cell area on the ellipsoid	area	m ²
Projection Type (Name of projection and parameters used)	crs	-

Table 6.1: The summed mass balance

	Full grid	Zwally et al. (2012) basin outlines		
	GrIS + Outer Glaciers and Ice Caps	GrIS	Above 1500 m	Below 1500 m
Total mass balance [Gt/yr]	-238.5	-204.9	-62.1	-142.7
Uncertainty [+/- Gt/yr]	28	28	15	18

Antarctic Ice Sheet mass changes from altimetry

We provide mass change time series for West Antarctica, East Antarctica and the Antarctic Peninsula as well as for the whole continent. This data is delivered as a comma separated text file for each region, with columns containing information on time, cumulative mass balance, and the measurement uncertainty respectively. Figure 6.4 shows the resulting mass change estimate for the Antarctic ice sheet. The time series is provided with an epoch of 140 days.

The mass change time series are provided in CSV text files

<NNN>_timeseries_and_uncertainty_varying_err_dens.csv

where <NNN> specifies the region covered:

- AIS ... (entire) Antarctic Ice Sheet
- APIS ... Antarctic Peninsula
- EAIS ... East Antarctic Ice Sheet
- WAIS ... West Antarctic Ice Sheet

Geophysical Variable	Column in file	Unit
Epoch mid-time	1	Decimal year
Cumulative mass change	2	Gt

		CCI Sea Level Budget Closure ESA/ESRIN contract 4000119910/17/I-NB Reference: ESA_SLBC_cci_D2.3.2 Version: v1.2 Date: 22.11.2018 Page: 77 of 119
---	---	---

Uncertainty associated to mass change	3	Gt
---------------------------------------	---	----

The mass change time series down sampled at annual resolution are provided in CSV text files for two different subregions. Time series of mass change are provided by the files:

annual_mean_v1_<NNN>.csv

where <NNN> specifies the region covered:

EAIS ... East Antarctic Ice Sheet

WAIS ... West Antarctic Ice Sheet

Geophysical Variable	Name in product	Unit
Year	Year	Year (integer)
Cumulative mass change	Mean_dm_(Gt)	Gt
Uncertainty associated	Sigma_dm_(Gt)	Gt

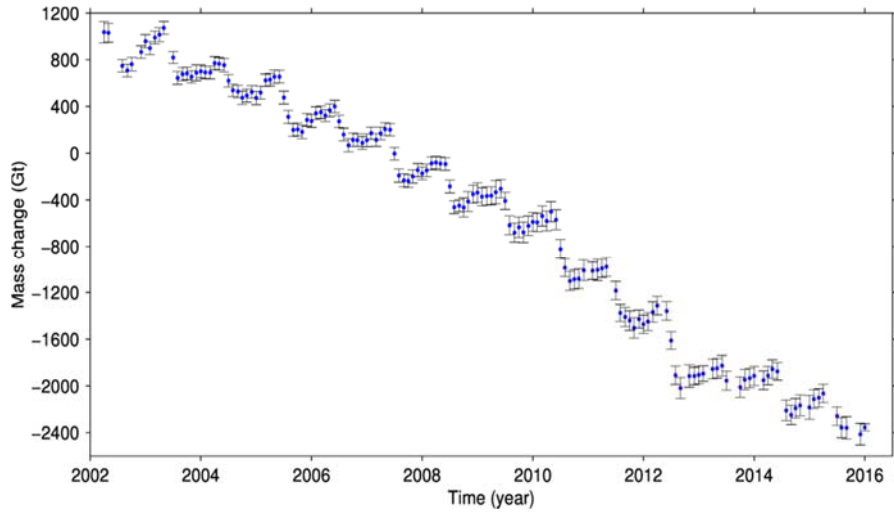


Figure 6.2: Mass change time series from Greenland Ice sheet derived by DTU Space



Figure 6.3: Eight main Greenland Ice Sheet basins (Zwally et al., 2012) colour-coded. Glaciers and ice caps marked with dark blue.

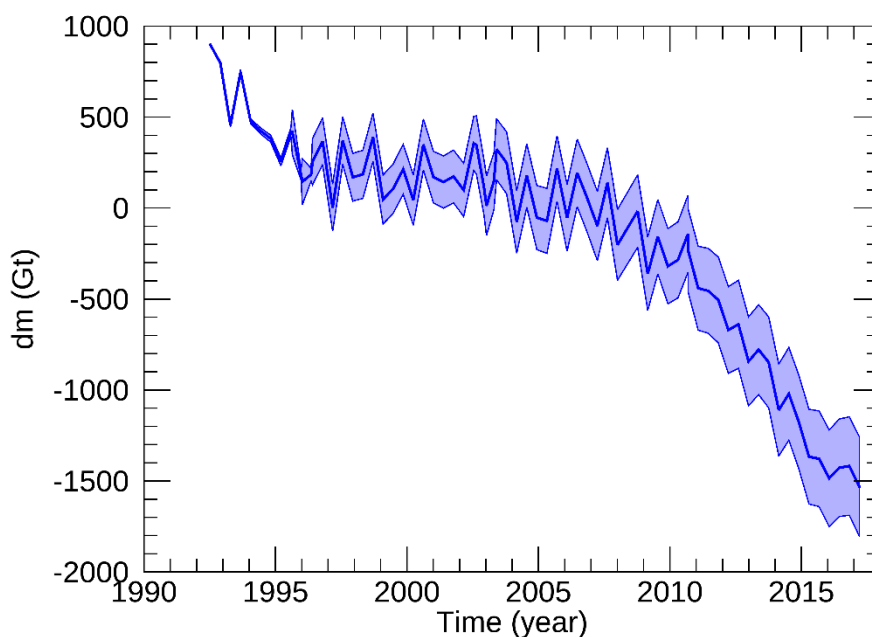


Figure 6.4: Mass change time series from Antarctic Ice sheet derived by CPOM Leeds (Version 1)

6.3.2 Coverage and resolution in time and space

Greenland Ice Sheet mass changes from GRACE

The temporal coverage is constrained by the data availability (2003-2016 for the CSR RLO6 solution), and is continuously extended as data become available. The temporal resolution is monthly estimates (some months are missing due to missing data.)

The spatial coverage for the ice mass balance estimate from GRACE are both the entire ice sheet and basins as shown in Figure 6.3.

Greenland Ice Sheet mass changes from lidar altimetry

The mass changes are provided on the ice covered areas of Greenland, as defined by the land cover type grid available here: http://websrv.cs.umt.edu/isis/index.php/Present_Day_Greenland. The grid resolution is 5 km x 5 km.

The mass change grid product represents the mean mass change for the period with useful laser altimetry data: Oct 2003–Oct 2009 (2003.75 - 2009.83).

Greenland Ice Sheet mass changes from radar altimetry

The spatial coverage for the yearly mass change rates is the entire ice sheet with a resolution of 100x100 km². The temporal coverage is from 1992 to 2017.

		<p>CCI Sea Level Budget Closure ESA/ESRIN contract 4000119910/17/I-NB</p> <p>Reference: ESA_SLBC_cci_D2.3.2 Version: v1.2 Date: 22.11.2018 Page: 80 of 119</p>
---	---	--

Antarctic Ice Sheet mass changes from GRACE

AIS mass changes from GRACE cover the entire ice sheet and the period 2002-2016.

Antarctic Ice Sheet mass changes from altimetry

The altimetry time series provided cover West Antarctica (WAIS), East Antarctica (EAIS) and the Antarctic Peninsula (AP) mass change from 1992 to 2017.

Temporal resolution of the time series is 140 days.

6.3.3 Product data format

Greenland Ice Sheet mass changes from GRACE

The data provided here are given in a simple ASCII format.

Greenland Ice Sheet mass changes from lidar altimetry

The file is given as a text file in ASCII format.

Greenland Ice Sheet mass changes from radar altimetry

The mass change grid is given in NetCDF4-format at 100x100 km² resolution:

Antarctic Ice Sheet mass changes from GRACE

AIS ice mass changes and mass change trends are given for a number of drainage basins in the ASCII files AIS_GMB_basin.dat and AIS_GMB_trend.dat.

In addition, gridded AIS mass changes from GRACE are given as a grid file in netCDF format (AIS_GMB_grid.nc).

Antarctic Ice Sheet mass changes from altimetry

The mass change time series are provided in CSV text files.

6.3.4 Product grid and projection

Greenland Ice Sheet mass changes from lidar altimetry

The mass changes are provided on the ice-covered areas of Greenland, as defined by the land cover type grid available here: http://websrv.cs.umt.edu/isis/index.php/Present_Day_Greenland.

		<p>CCI Sea Level Budget Closure ESA/ESRIN contract 4000119910/17/I-NB</p> <p>Reference: ESA_SLBC_cci_D2.3.2 Version: v1.2 Date: 22.11.2018 Page: 81 of 119</p>
---	---	--

Greenland Ice Sheet mass changes from radar altimetry

The data product is given in EPSG:3413, at 100x100 km² grid.

The mass changes are provided on the ice-sheet covered areas of Greenland, as defined by the ice sheet definition (#4) in the grid¹, the grid resolution is 5x5 km². Counting the 5 x5 km² grid-cells within the 100x100 km² grid gives the estimate of ice sheet area within the given grid-resolution.

Antarctic Ice Sheet mass changes from GRACE

For the map projection utilized for the GMB gridded product a polar stereographic projection with reference latitude at 71°S, reference meridian at 0°, and based on the ellipsoid WGS84 (EPSG3031) is used.

Antarctic Ice Sheet mass changes from altimetry

No grid definitions apply, since integrated mass changes are provided.

6.4 Uncertainty Assessment

For the Greenland Ice Sheet mass changes the uncertainty assessment is described in the Greenland Ice Sheet CCI Comprehensive Error Characterisation Report (Forsberg et al., 2013).

For the Antarctic Ice Sheet mass changes the uncertainty assessment is described in the Antarctic Ice Sheet CCI Comprehensive Error Characterisation Report (CECR) (Nagler et al., 2018b).

6.4.1 Sources of error

Ice Sheet mass changes from GRACE

The error characterization of the GRACE product is provided in detail in Forsberg et al. (2013). Errors in GRACE-derived mass changes have several origins. The three major contributions arise from:

1. GRACE errors in the monthly solutions,
2. Leakage errors due to the limited spatial resolution achieved by GRACE,
3. Errors in models used to reduce superimposed mass signals.

¹ available at http://websrv.cs.umt.edu/isis/index.php/Present_Day_Greenland

		<p>CCI Sea Level Budget Closure ESA/ESRIN contract 4000119910/17/I-NB</p> <p>Reference: ESA_SLBC_cci_D2.3.2 Version: v1.2 Date: 22.11.2018 Page: 82 of 119</p>
---	---	--

Ice Sheet mass changes from altimetry

The sources of errors are

1. Uncertainty in the interpolation of elevation change point estimates into volume change,
 2. error in the firn compaction,
 3. error in bedrock movement,
 4. error from neglecting basal melt and possible ice build-up above the Equilibrium Line Altitude (ELA).
- (5.) Radar altimetry has in addition an error source from changing radar penetration of the firn column.

6.4.2 Methodology for uncertainty assessment

Greenland Ice Sheet mass changes from GRACE

We derive the uncertainties which are related to the data errors provided directly with the GRACE monthly models by using a Monte-Carlo-like approach in which 200 simulations are performed. The simulations are created from Stokes coefficients drawn from normal distributions with zero mean, and the standard deviation provided with the GRACE level-2 data.

In order to give an estimate at basin scale of the effect of the outer glaciers leakage effect, we compute two solutions which represent an upper and lower bound for the mass loss and find that this leakage error is between 4% and 10% of the mass trend.

The GIA error is meaningful only for the linear trends in mass changes. For the entire GrIS we used the value in Barletta et al. (2013) (Table 6.2). For our best value we chose to use the A et al. (2013) model, which is an ICE5g-VM2 compressible model with rotational feedback. This GIA contribution for Greenland is **-5.4 Gt/yr** and the uncertainty is up to +/- 7.2 Gt/yr. Note that the GIA contribution in the submitted v1 time series is not included.

The results of a thorough (mass trend) uncertainty investigation (Forsberg et al., 2103) revealed the numbers provided in Table 6.2. The error source, estimation procedure and expected range in trend values are provided.

Greenland Ice Sheet mass changes from lidar altimetry

Following the error sources above the uncertainty assigned for each of these four sources are:

- Ad 1) The uncertainty of the ice volume changes due to interpolation between the elevation changes along each satellite tracks is estimated by applying a bootstrapping method

		<p>CCI Sea Level Budget Closure ESA/ESRIN contract 4000119910/17/I-NB</p> <p>Reference: ESA_SLBC_cci_D2.3.2 Version: v1.2 Date: 22.11.2018 Page: 83 of 119</p>
---	---	--

(Sørensen et al., 2011). In the bootstrapping approach, 1000 volume change estimates are derived using a randomly chosen subset of the satellite tracks, yielding a distribution of volume changes.

- Ad 2) The uncertainty in the firm compaction model applied is assumed to be 20% of the estimated correction (rate of change of firm air content) applied. This is a conservative estimate of the uncertainty.
- Ad 3) The uncertainty in the bedrock movements beneath the ice sheet is derived from predicting the regional elastic bedrock movement using a model developed by Giorgio Spada (University of Urbino, refer to Sørensen et al., 2011). The uncertainty is proportional to the uncertainty of the regional ice mass change.
- Ad4) The uncertainty of neglecting basal melt was determined by assigning a Greenland-wide average melt rate of 1 mm/year. Such a melt rate corresponds to 0.9 Gt/year above the ELA. An ice sheet model has been used to evaluate the uncertainty of neglecting ice dynamics, which corresponds to 14 Gt/year.

A detailed description of the error calculation is provided in Sørensen et al. (2011).

Greenland Ice Sheet mass changes from radar altimetry

Following the error sources above the uncertainty is given as a conservative estimate based on converting the radar altimetry volume error into mass by ascribing ice densities to all grid cells. This estimate is assumed to be slightly overestimating the combined error of the five error sources, however as seen in Figure 6.1 the estimated uncertainty reconciles the radar altimetry mass balance with the GRACE estimate.

Table 6.2: Sources and ranges of errors in GIS mass variation estimation

Error source	Estimation procedure	Expected range
GRACE solutions	Propagation of the scaled standard deviation	3.2Gt/yr
GIA model	Intercomparison of different models	7.2Gt/yr
Leakage	Analysis of use of different SA	3.2Gt/yr
Degree one	Intercomparison of different degree one time series	3 Gt/yr
Total	Individual components summed in quadrature	9Gt/yr

		CCI Sea Level Budget Closure ESA/ESRIN contract 4000119910/17/I-NB
		Reference: ESA_SLBC_cci_D2.3.2 Version: v1.2 Date: 22.11.2018 Page: 84 of 119

Table 6.3: Error components contributing to the overall error budget of the final GMB products for the entire AIS.

Error source	Estimation procedure	standard uncertainty
Basin averaged mass change time series		
Noise	assessed uncorrelated noise level in the GRACE time series	65 Gt
Total		65 Gt
linear trend uncertainty		
GRACE solutions	Propagation of the scaled error rms	2 Gt/yr
GIA model	Intercomparison of different models	32 Gt/yr
Leakage AIS	Analysis of dominant patterns of dynamic mass changes	6 Gt/yr
Leakage non-AIS	Analysis of a global trend pattern (excluding AIS) derived from GRACE	1 Gt/yr
Degree one	Intercomparison of different degree one time series	16 Gt/yr
C20	Intercomparison of different C20 time series	10 Gt/yr
Total	Individual components summed in quadrature	38 Gt/yr

Antarctic Ice Sheet mass changes from GRACE

The uncertainty assessment is described in detail in the Antarctic_Ice_Sheet_cci Comprehensive Error Characterisation Report (Nagler et al., 2016), updated under https://data1.geo.tu-dresden.de/ais_gmb/source/ST-UL-ESA-AISCCI-CECR-Draft_GMB.pdf and are analogous to the assessment described in Section 4. Table 6.3 summarizes the uncertainty assessment for the entire Antarctic Ice Sheet.

Antarctic Ice Sheet mass changes from altimetry

The uncertainty in mass change is estimated by summing in quadrature the uncertainty associated with our elevation change measurements (taking into account systematic errors, time-varying errors and errors associated with the calculation of inter-satellite biases) and the snowfall variability uncertainty to account for the additional error associated to the identification of ice dynamical imbalance. The total uncertainty is then converted to an equivalent mass change with the density of ice (917 kg m^{-3}) or snow (250 kg m^{-3}) based on our map of ice dynamic imbalance areas.

		CCI Sea Level Budget Closure ESA/ESRIN contract 4000119910/17/I-NB Reference: ESA_SLBC_cci_D2.3.2 Version: v1.2 Date: 22.11.2018 Page: 85 of 119
---	---	---

6.4.3 Results of uncertainty assessment

See the individual produce releases.

6.4.4 Uncertainty documentation in the data products

Greenland Ice Sheet mass changes from GRACE

Monthly mass change time series per basin are provided with an average monthly error estimate, see Figure 6.2.

Greenland Ice Sheet mass changes from laser altimetry (version 0)

The uncertainty is provided in the data product (column 4) as the standard deviation of the mass change as predicted by the bootstrapping approach (cf. Table 6.2).

Greenland Ice Sheet mass changes from radar altimetry (version 1)

The uncertainty is provided in the data product as the standard deviation of the elevation change converted into mass as ice densities.

Antarctic Ice Sheet mass changes from GRACE

Uncertainties of monthly values for the basin products are part of the products.

Uncertainties of linear trends are given in the Comprehensive Error Characterisation Report (Nagler et al., 2016) and updated in Table 6.3.

Antarctic Ice Sheet mass change from altimetry

The uncertainty is provided in the data product per epoch as the standard deviation of the error of cumulated mass change.

6.5 References

- A, G., Wahr, J., and Zhong, S. (2013): Computations of the viscoelastic response of a 3-D compressible Earth to surface loading: an application to Glacial Isostatic Adjustment in Antarctica and Canada. *Geophysical Journal International*, 192(2), 557-572.
- Barletta, V. R., Sørensen, L. S., and Forsberg, R. (2013): Scatter of mass changes estimates at basin scale for Greenland and Antarctica. *The Cryosphere*, 7(5), 1411-1432.
- Cornford et al. (2013): Adaptive mesh, finite volume modelling of marine ice sheets, *Journal of Computational Physics*, 232(1):529-549.
- Forsberg, R., L. Sørensen, et al. (2013): *Comprehensive Error Characterisation Report for the Ice_Sheets_cci project of ESA's Climate Change Initiative*, version 1.2, 06 June 2013.
- Hogg, A., et al. (2018): *Product Specification Document (PSD) for the Antarctic_Ice_Sheet_cci project of ESA's Climate Change Initiative*, version 1.2, 05 July 2018. Available from: <http://www.esa-icesheets-antarctica-cci.org/>.

		<p>CCI Sea Level Budget Closure ESA/ESRIN contract 4000119910/17/I-NB</p> <p>Reference: ESA_SLBC_cci_D2.3.2 Version: v1.2 Date: 22.11.2018 Page: 86 of 119</p>
---	---	--

- Horwath, M., and Groh, A. (2016). Evaluation of recent GRACE monthly solution series with an ice sheet perspective. *In EGU General Assembly Conference Abstracts* (Vol. 18, p. 9728). The PDF of the final poster can be downloaded from http://www.egsiem.eu/images/publication/EGU2016/horwath_egu2016_releases_b.pdf.
- Horwath, M., Tranchant, J.-B., van den Broeke, M., Legrésy, B. (2012): Evaluation of GRACE monthly solutions of Release 5 versus Release 4, with an ice sheet perspective. *Proc. GRACE Science Team Meeting*, September 2012, Potsdam, Germany.
- Ivins E., James T., Wahr J., Schrama E., Landerer F., and Simon K. (2013): Antarctic contribution to sea level rise observed by GRACE with improved GIA correction. *J. Geophys. Res.: Solid Earth*, 118(6), 3126-3141.
- Khvorostovsky, et al. (2016): *Algorithm Theoretical Baseline Document (ATBD) for the Greenland_Ice_Sheet_cci project of ESA's Climate Change Initiative*, version 3.1 (ST-DTU-ESA-GISCCI-ATBD-001), 09 Sep 2016.
- Klinger, B., Mayer-Gürr, T., Behzadpour, S., Ellmer, M., Kvas, A., & Zehentner, N. (2016). The new ITSG-Grace2016 release. *Geophys. Res. Abstr.*, 18, EGU2016-11547.
- Langen, P. L., Mottram, R. H., Christensen, J. H., Boberg, F., Rodehacke, C. B., Stendel, M., ... Cappelen, J. (2015): Quantifying energy and mass fluxes controlling Godthåbsfjord freshwater input in a 5 km simulation (1991-2012). *J. of Climate*, 28, 3694-3713 . doi: 10.1175/JCLI-D-14-00271.1.
- Lucas-Picher, P., Wulff-Nielsen, M., Christensen, J. H., Adalgeirsdóttir, G., Mottram, R. H., and Simonsen, S. B. (2012): Very high resolution regional climate model simulations over Greenland: Identifying added value. *Journal of Geophysical Research*, 117(D), 2108. Retrieved from http://adsabs.harvard.edu/cgi-bin/nph-data_query?bibcode=2012JGRD..11702108L&link_type=ABSTRACT
- Mayer-Gürr, Torsten; Behzadpour, Saniya; Ellmer, Matthias; Kvas, Andreas; Klinger, Beate; Zehentner, Norbert (2016): ITSG-Grace2016 - Monthly and Daily Gravity Field Solutions from GRACE. *GFZ Data Services*. <http://doi.org/10.5880/icgem.2016.007>
- McMillan, M., Shepherd, A., Sundal, A., Briggs, K., Muir, A., Ridout, A., Hogg, A., and Wingham, D. (2014). Increased ice losses from Antarctica detected by CryoSat-2. *Geophys. Res. Lett.*, 41(11), 3899-3905.
- Nagler, T., et al. (2016): *Comprehensive Error Characterisation Report (CECR). Antarctic_Ice_Sheet_cci project, ESA's Climate Change Initiative*, version 1.1, 01 May 2016, Available from: <http://www.esa-icesheets-antarctica-cci.org/>.
- Nagler, T., D. Floricioiu, A. Groh, M. Horwath, A. Kusk, A. Muir, J. Wuite (2018a): *Algorithm Theoretical Basis Document (ATBD) for the Antarctic_Ice_Sheet_cci project of ESA's Climate Change Initiative*, version 2.1, 05 July 2018. Available from: <http://www.esa-icesheets-antarctica-cci.org/>.
- Nagler, T., et al. (2018b): *Comprehensive Error Characterisation Report (CECR). Antarctic_Ice_Sheet_cci project, ESA's Climate Change Initiative*, version 2.1, 05 July 2018. Available from: <http://www.esa-icesheets-antarctica-cci.org/>.
- Nielsen, K., Sørensen, S. L. S., Khan, S. A., Spada, G., Simonsen, S. B., and Forsberg, R. (2014): Towards constraining glacial isostatic adjustment in Greenland by GPS observations. *International Association of Geodesy Symposia*, 1-7. JOUR. http://doi.org/10.1007/978-3-642-37222-3_43.
- Nilsson, J., Vallelonga, P., Simonsen, S.B., Sørensen, L.S., Forsberg, R., Dahl-Jensen, D., Hirabayashi, M. (2015): Greenland 2012 Melt Event Effects on CryoSat-2 Radar Altimetry. *Geophysical Research Letters* 42 (10): 3919-26. doi:10.1002/2015GL063296.
- Peltier, W. R., Argus, D. F., and Drummond, R. (2015): Space geodesy constrains ice age terminal deglaciation: The global ICE-6G_C (VM5a) model. *Journal of Geophysical Research (Solid Earth)*, 120, 450-487. doi: 10.1002/2014JB011176.

		<p>CCI Sea Level Budget Closure ESA/ESRIN contract 4000119910/17/I-NB</p> <p>Reference: ESA_SLBC_cci_D2.3.2 Version: v1.2 Date: 22.11.2018 Page: 87 of 119</p>
---	---	--

- Sasgen, I., van den Broeke, M. R., Bamber, J. L., Rignot, E., Sørensen, S. L. S., Wouters, B., ... Sørensen, L. S. (2012): Timing and origin of recent regional ice-mass loss in Greenland. *Earth and Planetary Science Letters*, 333, 293–303. doi: 10.1016/j.epsl.2012.03.033.
- Simonsen, S. B., Stenseng, L., Adalgeirsdóttir, G., Fausto, R. S., Hvidberg, C. ~S., and Lucas-Picher, P. (2013): Assessing a multilayered dynamic firn-compaction model for Greenland with ASIRAS radar measurements. *Journal of Glaciology*, 59(215), 545–558.
- Simonsen, S. B., and Sørensen, L.S: (2017): Implications of Changing Scattering Properties on Greenland Ice Sheet Volume Change from Cryosat-2 Altimetry. *Remote Sensing of Environment* 190 (March). Elsevier Inc.: 207–16. doi:10.1016/j.rse.2016.12.012.
- Sørensen L.S., et al. (2017): *Product Specification Document (PSD) for the Greenland_Ice_Sheet_cci project of ESA's Climate Change Initiative*, version 2.3 (ST-DTU-ESA-GISCCI-PSD-001), 20 March 2017.
- Sørensen, L. S., Simonsen, S. B., Nielsen, K., Lucas-Picher, P., Spada, G., Adalgeirsdóttir, G., ... Hvidberg, C. S. (2011): Mass balance of the Greenland ice sheet (2003-2008) from ICESat data - the impact of interpolation, sampling and firn density. *The Cryosphere*, 5(1), 173–186. <http://doi.org/10.5194/tc-5-173-2011>.
- Sørensen L. S., Simonsen, S.B., Forsberg, R., Khvorostovsky, K., Meister, R., and Engdahl, M. E.. (2018): 25 Years of Elevation Changes of the Greenland Ice Sheet from ERS, Envisat, and CryoSat-2 Radar Altimetry. *Earth and Planetary Science Letters* 495. Elsevier B.V.: 234–41. doi:10.1016/j.epsl.2018.05.015.
- Spada, G. A., and Stocchi, P. (2007): SELEN : A Fortran 90 program for solving the ‘sea-level equation’. *Computers & Geosciences*, 33, 538–562. <http://doi.org/10.1016/j.cageo.2006.08.006>.
- Zwally, H. J., M. B. Giovinetto, M. A. Beckley, J. L. Saba (2012): *Antarctic and Greenland Drainage Systems*, GSFC Cryospheric Sciences Laboratory, at http://icesat4.gsfc.nasa.gov/cryo_data/ant_grn_drainage_systems.php.

		<p>CCI Sea Level Budget Closure ESA/ESRIN contract 4000119910/17/I-NB</p> <p>Reference: ESA_SLBC_cci_D2.3.2 Version: v1.2 Date: 22.11.2018 Page: 88 of 119</p>
---	---	--

7 Total Land Water Storage Change

7.1 Data Access and Requirements

Global and gridded time series of total land water storage (TWS) were obtained with the global hydrological model WaterGAP 2.2c standard, which is currently applied and developed at the Institute of Physical Geography of the Goethe-University of Frankfurt (GUF). This model version includes improvements over WaterGAP 2.2b standard (used for data products version o) that will be discussed in the following section.

7.2 Algorithms

7.2.1 Review of scientific background

WaterGAP, or more specifically the WaterGAP Global Hydrology Model (Müller Schmied et al., 2014), computes total land water storage by accounting for the water in the canopy storage S_c , snow water storage S_{sn} , soil storage S_s , groundwater storage S_g and surface water body (wetlands, rivers, lakes and man-made reservoirs) storages S_{swb} (Eq. 7.1).

$$\frac{dTWS}{dt} = \frac{S_c}{dt} + \frac{S_{sn}}{dt} + \frac{S_s}{dt} + \frac{S_g}{dt} + \frac{S_{swb}}{dt} \quad (\text{Eq. 7.1})$$

The human water use is computed by various water use models and the submodel GWSWUSE as water withdrawal (abstraction) and water consumption for five sectors (irrigation, livestock farming, domestic use, manufacturing industries and cooling of thermal power plants). The submodel GWSWUSE distinguishes the source of abstracted water and computes net abstractions (abstractions minus return flows) from groundwater and from surface water. These net abstractions are input to the WaterGAP Global Hydrology Model.

Since the initial phase of the project, model enhancements related to the reservoir operation algorithm and to the estimation of groundwater depletion were implemented.

7.2.2 Algorithms

Reservoir storage. In order to account for the impoundment of water in man-made reservoirs, a slightly modified version of the reservoir operation algorithm of Hanasaki et al. (2006), which distinguishes irrigation and non-irrigation reservoirs, is implemented in WaterGAP.

The algorithm works under three assumptions (Döll et al., 2009):

- A reservoir can never store water to its total capacity; it is assumed that the inflow above 85% of the total capacity is immediately released, as a measure for flood prevention (flood storage of 15%) (hereafter “assumption 1”).
- When the reservoir storage is very low (e.g. during the filling phase), the release flow is set to only 10% of the mean annual release flow (hereafter “assumption 2”).
- For non-irrigation reservoirs, the monthly release flow is the same throughout the year (hereafter “assumption 3”). For irrigation reservoirs, it varies according to the downstream water demand.

In the previous version of the model, the commissioning year of each reservoir had not yet been included; this means that all reservoirs were assumed to always have existed, which did not allow for the model to simulate the filling phase. Figure 7.1 shows the global annual reservoir storage in mm before and after including the operational years. As can be noted, there was a strong increase in water impoundment in reservoirs during the second half of the 20th century.

In order to have a first idea of the model’s performance at the scale of individual reservoirs after the inclusion of the first operational year, the observed reservoir storage was compared to the simulated reservoir storage at the monthly scale for 16 reservoirs in the USA (listed in Table A 1 from the Appendix). Figure A 1 and Figure A 2 (Appendix) show the observed and simulated monthly reservoir storage for all individual reservoirs. In most cases, the model performs rather poorly compared to the observations. From Figure A 1 and Figure A 2, we could deduct that assumption 1 results in an underestimation of the maximum reservoir storage (e.g. Livingston reservoir, New Melones reservoir) (Figure A 1 and Table 7.1).

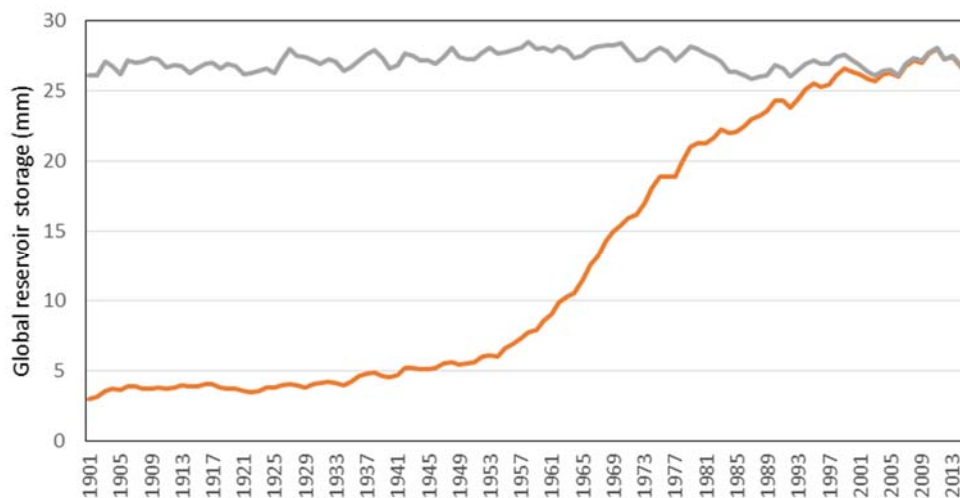


Figure 7.1: Global annual reservoir storage (mm over global land area) as computed by WaterGAP 2.2b standard (grey curve, before inclusion of year of reservoir construction) and by WaterGAP 2.2c standard (orange curve, including year of reservoir construction).

		<p>CCI Sea Level Budget Closure ESA/ESRIN contract 4000119910/17/I-NB</p> <p>Reference: ESA_SLBC_cci_D2.3.2 Version: v1.2 Date: 22.11.2018 Page: 90 of 119</p>
---	---	--

Table 7.1: Comparison between observed and simulated (WaterGAP 2.2c forced by WFDEI-GPCC) monthly reservoir storage for sixteen reservoirs in the USA (see in combination with Figure A 1 and Figure A 2 in the Appendix).

Reservoir name	Start of filling period (observations)	Start of filling period (WaterGAP 2.2c)	Max. storage at 85% of volume	Filling phase	Simulated variability	Comments related to simulated data
Lake Berryessa	1957	1957	/	Reservoir does not fill up.	/	Inflow very underestimated.
Cascade reservoir	1947	1947	Maximum underestimated.	Reservoir fills up too quickly.	Too low at the beginning	
New Don Pedro reservoir	1970	1971	Maximum underestimated.	Reservoir fills up too quickly.	Similar amplitude	Year shift.
Hungry Horse reservoir	1951	1952	Maximum underestimated.	Similar steepness.	Too low	Wrong volume input data. Year shift.
Amistad lake	1968	1969	Maximum underestimated.	Reservoir fills up too quickly.	Too high	Year shift.
Livingston reservoir	1968	1969	Maximum underestimated.	Reservoir fills up too quickly.	Too high	Release overestimated. Year shift.
Mohave lake	1950	1952	/	Similar steepness.	Too high	Inflow underestimated and/or release overestimated. Year shift.
New Melones reservoir	1975	1979	Maximum underestimated.	Reservoir fills up too quickly.	Too high	Release overestimated. Year shift.
Oroville lake	1967	1968	Maximum underestimated.	Similar steepness.	Too high	Release overestimated. Year shift.
Palisades reservoir	1956	1956	Maximum underestimated.	Reservoir fills up too quickly.	Too low	
Pine Flat lake	1951	1954	Maximum underestimated.	Reservoir fills up too quickly.	Similar amplitude	Year shift.
Powell lake	1963	1963	Maximum underestimated.	Reservoir fills up too quickly.	Similar amplitude	Wrong volume input data.
Richland-Chambers reservoir	1988	1987	/	Similar steepness.	Too high	Inflow underestimated and/or release overestimated. Year shift.
Sam Rayburn reservoir	1965	1965	/	Reservoir fills up too quickly.	Too high	Inflow and release overestimated.
San Luis reservoir	1968	1967	/	/	Too low	Inflow very underestimated, reservoir does not fill up. Year shift.
Toledo Bend reservoir	1966	1966	Maximum underestimated.	Similar steepness.	Too high	Release overestimated.

		<p>CCI Sea Level Budget Closure ESA/ESRIN contract 4000119910/17/I-NB</p> <p>Reference: ESA_SLBC_cci_D2.3.2 Version: v1.2 Date: 22.11.2018 Page: 91 of 119</p>
---	---	--

Furthermore, it was noticed that, in some cases, the simulated filling of the reservoir is too fast compared to the observations (e.g. New Melones reservoir, Cascade reservoir), whereas in other cases, this “fast” filling fits well to the observations (e.g. Hungry Horse reservoir, Toledo Bend reservoir) (Figure A 1 and Figure A 2, Table 7.1). The rather fast filling is due to very low release flows during the filling phase (assumption 2). It was also noticed that, in some cases, the model overestimates the release flows during the dry period, leading to a larger seasonal variability of reservoir storage than observed. This is especially striking for the non-irrigation reservoirs (e.g. Livingston reservoir, Mohave lake), for which we apply assumption 3 (Figure A 1 and Figure A 2, Table 7.1).

This first evaluation of the performance of the WaterGAP model with respect to water storage in reservoirs already gives a good insight into what needs to be changed in order to improve the algorithm. For instance, in the next model version assumption 1 will be dropped, as this analysis showed it to be incorrect. Moreover, there are some discrepancies regarding the first year of reservoir filling between the observations and the WaterGAP input data (Table 7.1); this will also need correction in the future.

Groundwater storage. Groundwater depletion (GWD) is often observed in regions with a very high water demand that is mainly satisfied by groundwater water withdrawals. Globally, irrigation is by far the most consumptive water use sector. Assumptions regarding irrigation water use are an important source of uncertainty when estimating GWD in these regions. Using WaterGAP 2.2a, Döll et al. (2014) concluded that assuming that farmers irrigate at approximately 70% of the optimal rate resulted in improved results as compared to independent estimates in GWD regions.

WaterGAP 2.2c was run under the two following irrigation scenarios with three climate forcings (see Section 7.3.1), in order to assess the impact of irrigation water use on groundwater storage (GWS) variations:

- Farmers irrigate at 70% of the optimal rate in GWD regions and at 100% of the optimal rate in non-GWD regions (hereafter “70% deficit irrigation scenario”) (for more details, see Döll et al., 2014)
- Farmers irrigate at 100% of the optimal rate worldwide (hereafter “optimal irrigation scenario”) (for more details, see Döll et al., 2014)

Table 7.2: Global groundwater storage trends computed by WaterGAP 2.2c with two irrigation scenarios and three climate forcings. GWD: groundwater depletion, GWS: groundwater storage. Trends are caused by both climatic variations and human water use.

Period	Irrigation in GWD regions (% of optimal rate)	GWS trend in km ³ /yr (WFDEI-CRU)	GWS trend in km ³ /yr (CRU TS 4.00)	GWS trend in km ³ /yr (WFDEI-GPCC)
1950-2013	70	-62.40	-63.94	-62.04
1992-2013	70	-94.23	-92.10	-92.53
2003-2013	70	-104.76	-92.87	-84.03
1950-2013	100	-91.88	-90.27	-92.80
1992-2013	100	-137.82	-132.96	-137.22
2003-2013	100	-150.48	-136.23	-131.40

As shown in Table 7.2, global GWS trends are considerably lower under the optimal irrigation scenario for all forcings. This reflects a higher irrigation water use under this scenario, which results in a higher groundwater mass loss. Differences in global trends due to different forcings are smaller, except during 2003-2013. However, Figure 7.2, which corresponds to the 70% deficit irrigation scenario, shows that differences due to different forcings can be considerable in terms of relative interannual variability.

Table A 2 and Table A 3 show GWD trends estimated by WaterGAP 2.2a and three variants of WaterGAP 2.2c compared to independent estimates under the 70% deficit irrigation scenario and the optimal irrigation scenario, respectively. The results in both tables were not conclusive as to which irrigation scenario provides better results for WaterGAP 2.2c; for instance, in the High Plains aquifer, simulated GWD is closer to independent estimates under the 70% deficit irrigation scenario, whereas in the Central Valley a better fit is found for all three forcings under the optimal irrigation scenario. Concerning the impact of using different climate forcings at the regional scale, the conclusions differ depending on the case considered. For instance, in the North China Plain, the impact is low, whereas in the Gulf coastal plain it is rather large.

Table A 2 and Table A 3 also show that the previous WaterGAP 2.2a version highly overestimates GWD trends in the North China Plain (NCP) and thus in the Hai river basin, located within the boundaries of the NCP. This is mainly due to an underestimation of groundwater recharge in this region. Based on these results, the runoff coefficient (hereafter gamma), which is the main calibration parameter of the model and varies between 0.1 and 5.0, was optimized at the regional scale in order to improve the model's performance in the NCP. Basically,

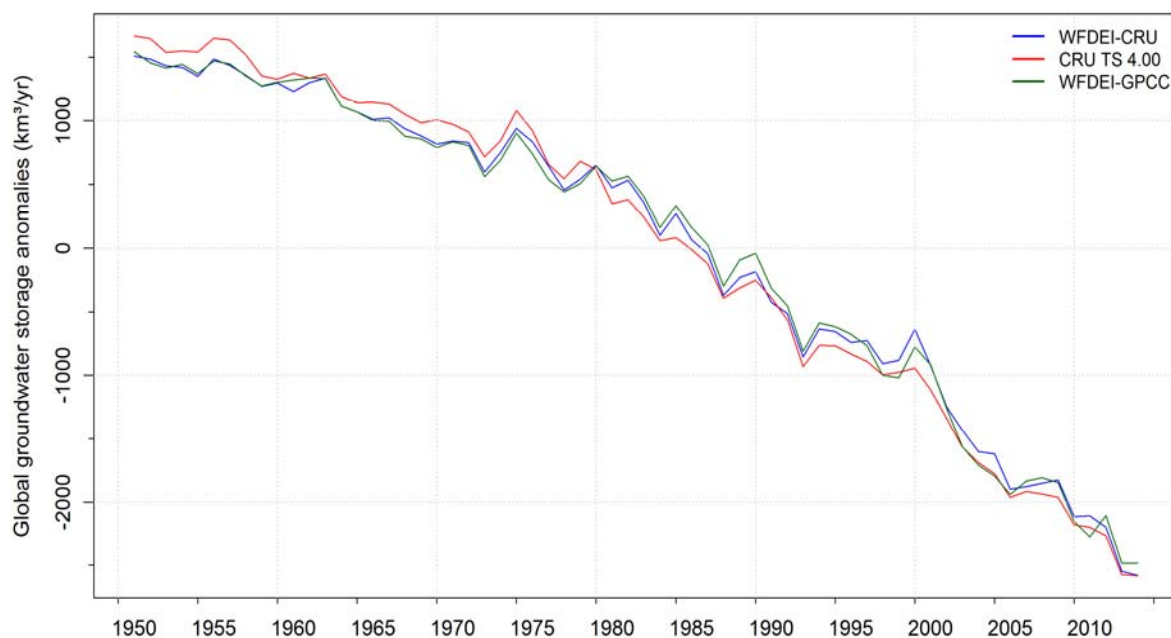


Figure 7.2: Global groundwater storage anomalies in km³/yr computed by three variants of WaterGAP 2.2c corresponding to different climate forcings (70% deficit irrigation scenario).

gamma was decreased from values between 3.0 and 5.0 to 0.1 in all grid cells of the NCP; this resulted in an increased groundwater recharge, and thus a decreased GWD for the three variants of WaterGAP 2.2c that now fits well to observations. Furthermore, WaterGAP 2.2a highly underestimates GWD trends in the Gulf coastal plain, which is mainly due to an overestimation of groundwater recharge. In WaterGAP 2.2c, the fraction of runoff recharging the aquifer was reduced from 0.8-0.9 to 0.1 in this region, which resulted in an increased GWD for the three variants of WaterGAP 2.2c, and a good fit to observations in case of the two WFDEI-based climate forcings. Despite the adjustments performed for the NCP and the Gulf coastal plain, Table A 2 and Table A 3 also show several regions for which the model still performs poorly (e.g. Atlantic coastal plain).

Glacier storage. WaterGAP 2.2c does not include a glacier compartment and thus cannot compute glacier water storage variations. However, in a former version of the model, daily output time series of the global glacier model HYOGA2 (glacier area, glacier mass, glacier runoff; Hirabayashi et al., 2013, 2010) were integrated to better simulate river discharge downstream of glaciers. However, HYOGA2 does not represent the state-of-the-art in glacier modeling anymore. Moreover, as shown in Hirabayashi et al. (2010), HYOGA2 cannot simulate well the observed seasonality of winter accumulation and summer ablation, which is essential for the hydrological seasonal cycle. Therefore, in the frame of this project, the experience will be repeated with monthly time series of the state-of-the-art Open Global

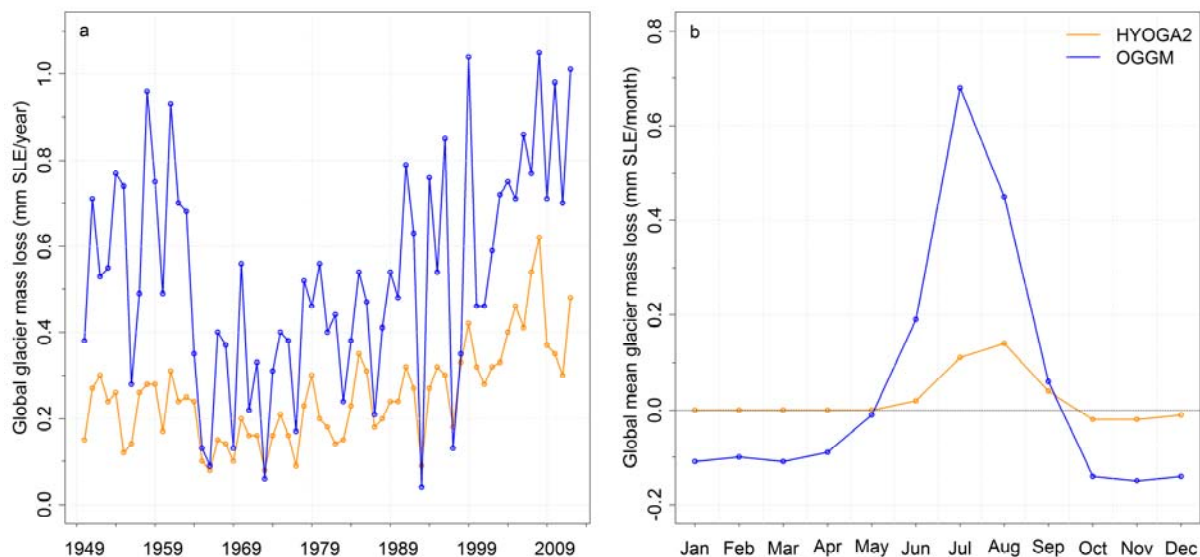


Figure 7.3: Global annual (a) and mean monthly (b) glacier mass loss during 1949-2011 as computed by HYOGA2 (yellow curve) and OGGM (blue curve).

Glacier Model (OGGM) (Marzeion et al., 2012), which will be disaggregated into daily data to fit with the computation time step of WaterGAP.

A first comparison between HYOGA2 and OGGM in terms of glacier mass variations was performed at the global scale. Figure 7.2Figure 7.3 (left) shows the global glacier annual mass loss between 1949 and 2011; it can be seen that even if the two models agree in terms of general trend, OGGM computes higher glacier annual mass losses and shows a higher interannual variability. Figure 7.3 (right) shows the global mean glacier monthly mass loss during 1949-2011; it shows that HYOGA2 computes very low glacier mass loss during summer and shows basically no mass gain during winter. OGGM, on the other hand, shows higher mean seasonal amplitude.

In order to test OGGM performance in terms of seasonal glacier mass variations at the scale of individual glaciers, model output was compared to observations for 31 glaciers worldwide (see Table A 4) from the World Glacier Monitoring Service (2017). In general, the model shows a good performance among the glacier sample, as evidenced by the efficiency criteria results in Table A 4. Only two glaciers, the “Devon Ice Cap NW” and the “Vernagt F.”, show a negative Nash-Sutcliffe efficiency. In the case of the first one, this might be related to calving processes (marine-terminating ice cap) that the model cannot capture with enough accuracy. Figure 7.4 shows the correlation between observed and modeled mean annual and seasonal (winter and summer) glacier mass balance for all glaciers (this figure can be compared with Figure 4 of Hirabayashi et al. (2010), which was made in a similar way). It shows that OGGM can

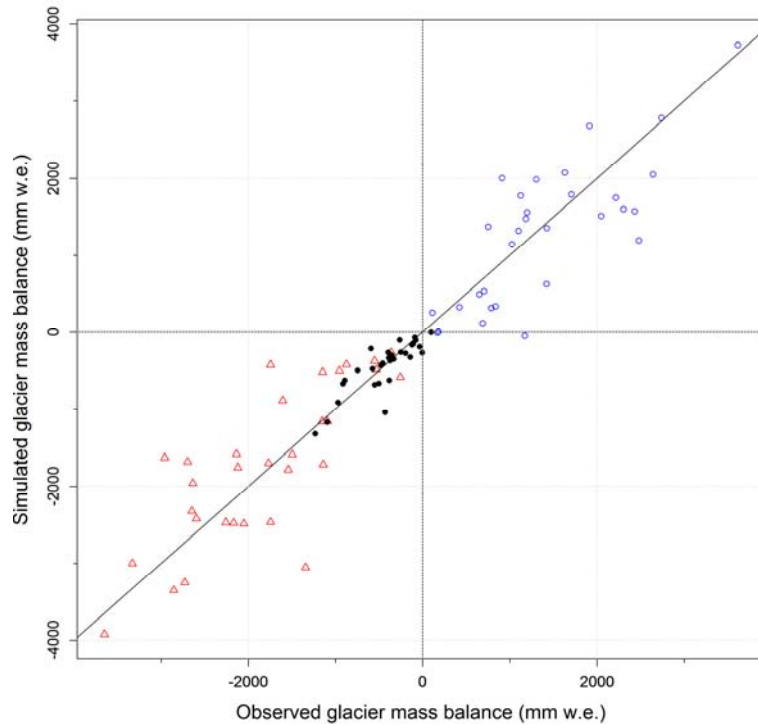


Figure 7.4: Correlation plot between observed and modeled mean annual and seasonal (winter and summer) glacier mass balance in mm of water equivalent (all glaciers are included). Filled circles: mean annual mass balance, open blue circles: mean winter mass balance, open red triangles: mean summer mass balance.

reasonably reproduce the observed mean seasonality, which gives us confidence for the next phase of the project, for which the output data of OGGM will be implemented into WaterGAP.

7.3 Product Specification

7.3.1 Product geophysical data content

Two variants of WaterGAP 2.2c, corresponding to two irrigation scenarios (“70% deficit irrigation scenario” and “optimal irrigation scenario”, see Section 7.2.2) were run with the three following state-of-the-art climate forcings:

- daily WFDEI (“WATCH Forcing Data methodology applied to ERA-Interim data”) dataset (Weedon et al. 2014) with precipitation bias-corrected using GPCP monthly precipitation sums (Schneider et al. 2015) (hereafter “WFDEI-GPCP”)
- daily WFDEI dataset with precipitation bias-corrected using CRU TS 3.23 monthly precipitation sums (Harris et al. 2014) (hereafter “WFDEI-CRU”)

		<p>CCI Sea Level Budget Closure ESA/ESRIN contract 4000119910/17/I-NB</p> <p>Reference: ESA_SLBC_cci_D2.3.2 Version: v1.2 Date: 22.11.2018 Page: 96 of 119</p>
---	---	--

- monthly CRU TS 4.00 (University of East Anglia Climatic Research Unit et al. 2017) (hereafter “CRU”)

Six datasets (2 irrigation scenarios * 3 climate forcings) of TWS are provided. In addition, six datasets of river discharge (generated from the same model runs) are provided (request from WP260 Arctic Ocean) (see Table 7.3). As complementary information, a gridded dataset with continental area information for each grid cell, as well as a gridded dataset to identify the cells from the coastal line with discharge to the ocean are provided (see Table 7.3 and Table 7.4).

Time series of globally averaged TWS are provided as text files and are described in Table 7.5 and Table 7.6.

Table 7.3: Files of monthly gridded data provided for sea level budget assessment version 1.

Geophysical Variable	Name in product	Unit	Period	File name
Total water storage forced by WFDEI-GPCC	tws	mm	1992-2013	tws_WaterGAP22c_WFDEI_GPCC_mm_irr70_version1.nc tws_WaterGAP22c_WFDEI_GPCC_mm_irr100_version1.nc
Total water storage forced by WFDEI-CRU	tws	mm	1992-2015	tws_WaterGAP22c_WFDEI_CRU_mm_irr70_version1.nc tws_WaterGAP22c_WFDEI_CRU_mm_irr100_version1.nc
Total water storage forced by CRU TS 4.00	tws	mm	1992-2015	tws_WaterGAP22c_CRU_mm_irr70_version1.nc tws_WaterGAP22c_CRU_mm_irr100_version1.nc
River discharge forced by WFDEI-GPCC	Q	km ³ /month	1992-2013	Q_WaterGAP22c_WFDEI_GPCC_irr70_version1.nc Q_WaterGAP22c_WFDEI_GPCC_irr100_version1.nc
River discharge forced by WFDEI-CRU	Q	km ³ /month	1992-2015	Q_WaterGAP22c_WFDEI_CRU_irr70_version1.nc Q_WaterGAP22c_WFDEI_CRU_irr100_version1.nc
River discharge forced by CRU TS 4.00	Q	km ³ /month	1992-2015	Q_WaterGAP22c_CRU_irr70_version1.nc Q_WaterGAP22c_CRU_irr100_version1.nc
Continental area	contarea	km ²	-	contarea_wghm_wlm.nc
Cells with river discharge into ocean	outcell	-	-	outcell_wghm_wlm.nc

		<p>CCI Sea Level Budget Closure ESA/ESRIN contract 4000119910/17/I-NB</p> <p>Reference: ESA_SLBC_cci_D2.3.2 Version: v1.2 Date: 22.11.2018 Page: 97 of 119</p>
---	---	--

Table 7.4: Geophysical data content of gridded files

File name	Geophysical Variable	Name in product	Unit
all files	Latitude	lat	degrees north
	Longitude	lon	degrees east
Q_*.nc	Time	time	months since 1992-01-01
	River discharge (excluding Greenland)	Q	km ³ /month
tws_*.nc	Time	time	months since 1992-01-01
	total water storage (excluding Greenland)	tws	mm (over grid cell continental area, see contarea_wghm_wlm.nc)
contarea_*.nc	Time	time	not used
	continental area (excluding Greenland)	contarea	km ²
outcell_*.nc	Time	time	not used
	cells with river discharge into ocean (excluding Greenland)	outcell	--

		CCI Sea Level Budget Closure ESA/ESRIN contract 4000119910/17/I-NB
		Reference: ESA_SLBC_cci_D2.3.2 Version: v1.2 Date: 22.11.2018 Page: 98 of 119

Table 7.5: Files of globally averaged data provided for sea level budget assessment version 1.

Geophysical Variable	Unit	Time step	Period	File name
Total water storage forced by WFDEI-GPCC	mm	monthly and annual	1992-2013	tws_WaterGAP22c_WFDEI_GPCC_mm_irr70_version1_month1992_2013.txt tws_WaterGAP22c_WFDEI_GPCC_mm_irr70_version1_year1992_2013.txt tws_WaterGAP22c_WFDEI_GPCC_mm_irr70_version1_yearinmonth1992_2013.txt tws_WaterGAP22c_WFDEI_GPCC_mm_irr100_version1_month1992_2013.txt tws_WaterGAP22c_WFDEI_GPCC_mm_irr100_version1_year1992_2013.txt tws_WaterGAP22c_WFDEI_GPCC_mm_irr100_version1_yearinmonth1992_2013.txt
Total water storage forced by WFDEI-CRU	mm	monthly and annual	1992-2015	tws_WaterGAP22c_WFDEI_CRU_mm_irr70_version1_month1992_2015.txt tws_WaterGAP22c_WFDEI_CRU_mm_irr70_version1_year1992_2015.txt tws_WaterGAP22c_WFDEI_CRU_mm_irr70_version1_yearinmonth1992_2015.txt tws_WaterGAP22c_WFDEI_CRU_mm_irr100_version1_month1992_2015.txt tws_WaterGAP22c_WFDEI_CRU_mm_irr100_version1_year1992_2015.txt tws_WaterGAP22c_WFDEI_CRU_mm_irr100_version1_yearinmonth1992_2015.txt
Total water storage forced by CRU TS 4.00	mm	monthly and annual	1992-2015	tws_WaterGAP22c_CRU_mm_irr70_version1_month1992_2015.txt tws_WaterGAP22c_CRU_mm_irr70_version1_year1992_2015.txt tws_WaterGAP22c_CRU_mm_irr70_version1_yearinmonth1992_2015.txt tws_WaterGAP22c_CRU_mm_irr100_version1_month1992_2015.txt tws_WaterGAP22c_CRU_mm_irr100_version1_year1992_2015.txt tws_WaterGAP22c_CRU_mm_irr100_version1_yearinmonth1992_2015.txt

Table 7.6: Geophysical data content of globally averaged files

File name	Geophysical Variable	Name in product	Unit
month.txt	Time	month	month counted with reference epoch 1992-01
	TWS (globally averaged per month)	value	mm over global continental area (sum of grid cell continental areas from contarea_wghm_wlm.nc)
year.txt	Time	year	year (integer)
	TWS (globally averaged per year)	value	mm over global continental area
yearinmonth.txt	Time	year	month counted with reference epoch 1992-01
	TWS (globally averaged per year)	value	mm over global continental area

		<p>CCI Sea Level Budget Closure ESA/ESRIN contract 4000119910/17/I-NB</p> <p>Reference: ESA_SLBC_cci_D2.3.2 Version: v1.2 Date: 22.11.2018 Page: 99 of 119</p>
---	---	--

7.3.2 Coverage and resolution in time and space

Gridded monthly time series of TWS and river discharge are given for the global land area, with the exception of Antarctica and Greenland. For the globally averaged monthly and annual time series of TWS, an area-weighted average was used. Weighting areas are so-called “continental areas” that in case of coastal cells exclude the part of the $0.5^{\circ} \times 0.5^{\circ}$ grid cell that is ocean (see file `contarea_wghm_wlm.nc`, Table 7.4).

The time series obtained with WFDEI-GPCC forcing only extend until the end of 2013 because the GPCC precipitation product has not yet been released at the global scale for more recent years. The rest of the time series are provided until the end of 2015.

7.3.3 Product data format

Gridded time series of TWS and river discharge, as well as complementary gridded data are provided in a NetCDF format. Globally averaged time series of TWS are provided in a text format.

7.3.4 Product grid and projection

The WATCH-CRU ocean-land mask, covering 67420 $0.5^{\circ} \times 0.5^{\circ}$ grid cells, was used for the simulations, as opposed to the ocean-land mask used for data products version 0, which covers only 66896 $0.5^{\circ} \times 0.5^{\circ}$ grid cells.

7.4 Uncertainty Assessment

7.4.1 Sources of error

For data products version 1, the uncertainty in simulated TWS variations due to spatially distributed climate input data and to the modeling approach with respect to irrigation water use in groundwater depletion regions was considered by running different model variants.

7.4.2 Methodology for uncertainty assessment

In order to assess the uncertainty due to the two sources of error mentioned above, the following model variants were used to compute monthly time series of TWS:

- WaterGAP 2.2c, 70% deficit irrigation, WFDEI-GPCC forcing
- WaterGAP 2.2c, 70% deficit irrigation, WFDEI-CRU forcing
- WaterGAP 2.2c, 70% deficit irrigation, CRU TS 4.00 forcing
- WaterGAP 2.2c, optimal irrigation, WFDEI-GPCC forcing

- WaterGAP 2.2c, optimal irrigation, WFDEI-CRU forcing
- WaterGAP 2.2c, optimal irrigation, CRU TS 4.00 forcing

The two irrigation scenarios are considered equally plausible.

7.4.3 Results of uncertainty assessment

Figure 7.5 shows that absolute total water storages of CRU forcing are higher than those computed with WFDEI-GPCC and WFDEI-CRU. This can be attributed to differences in global averages of precipitation. Furthermore, Figure 7.5 also shows that absolute TWS corresponding to the optimal irrigation scenario are slightly lower than those corresponding to the 70% deficit irrigation scenario for all forcings. This is not surprising, since irrigation water use in GWD regions is higher under the optimal irrigation scenario (Döll et al., 2014).

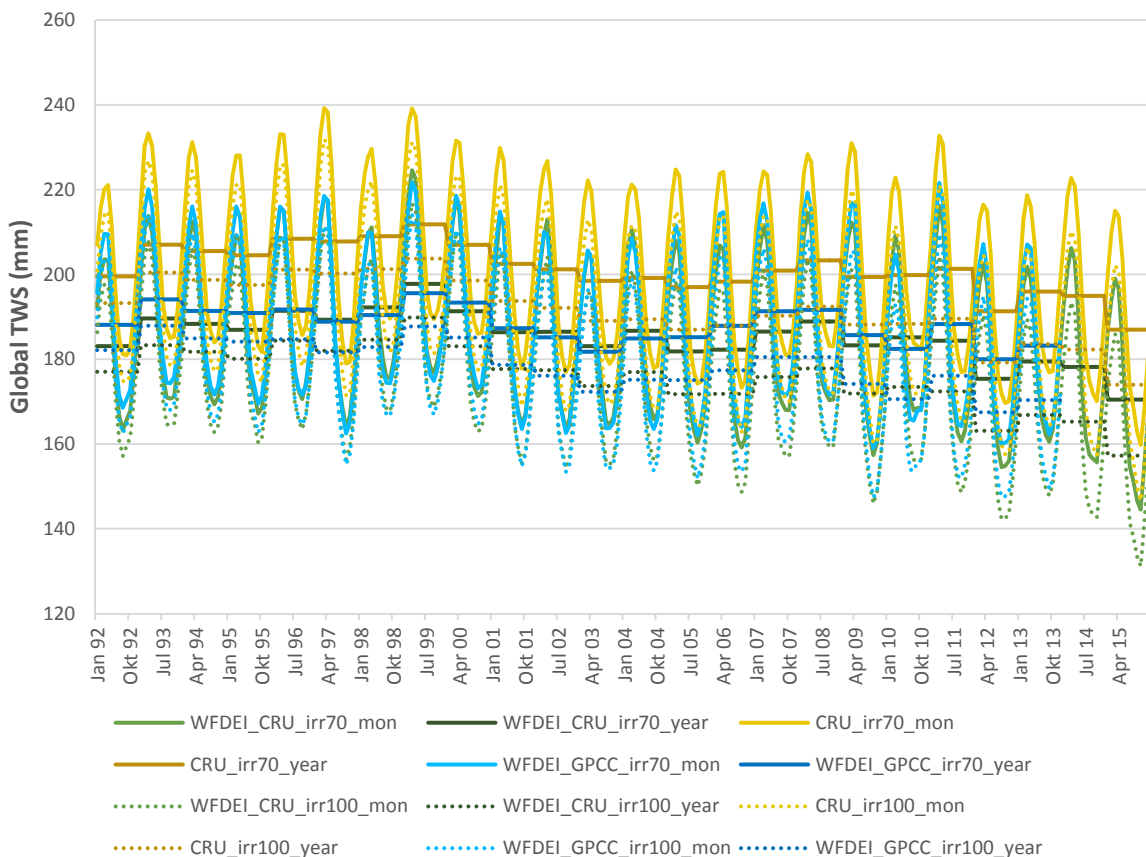


Figure 7.5: Global average for land area (except Antarctica and Greenland) in mm of monthly and annual total water storage for three climate data sets and two irrigation scenarios between 1992 and 2015 (time series with WFDEI-GPCC forcing only extend until the end of 2013). Full curves; 70% deficit irrigation scenario, dotted curves; optimal irrigation scenario.

Figure 7.6 shows that, in relative terms or amplitudes, global TWS is not very dependent on climate forcing. Also, the impact of using different irrigation scenarios on global TWS is rather small, even if more apparent at the annual scale. This is partly due to the fact that the two irrigation scenarios differ only at the scale of groundwater depletion regions, not at the scale of the global land area.

7.4.4 Uncertainty documentation in the data products

No uncertainty ranges are provided in the data products.

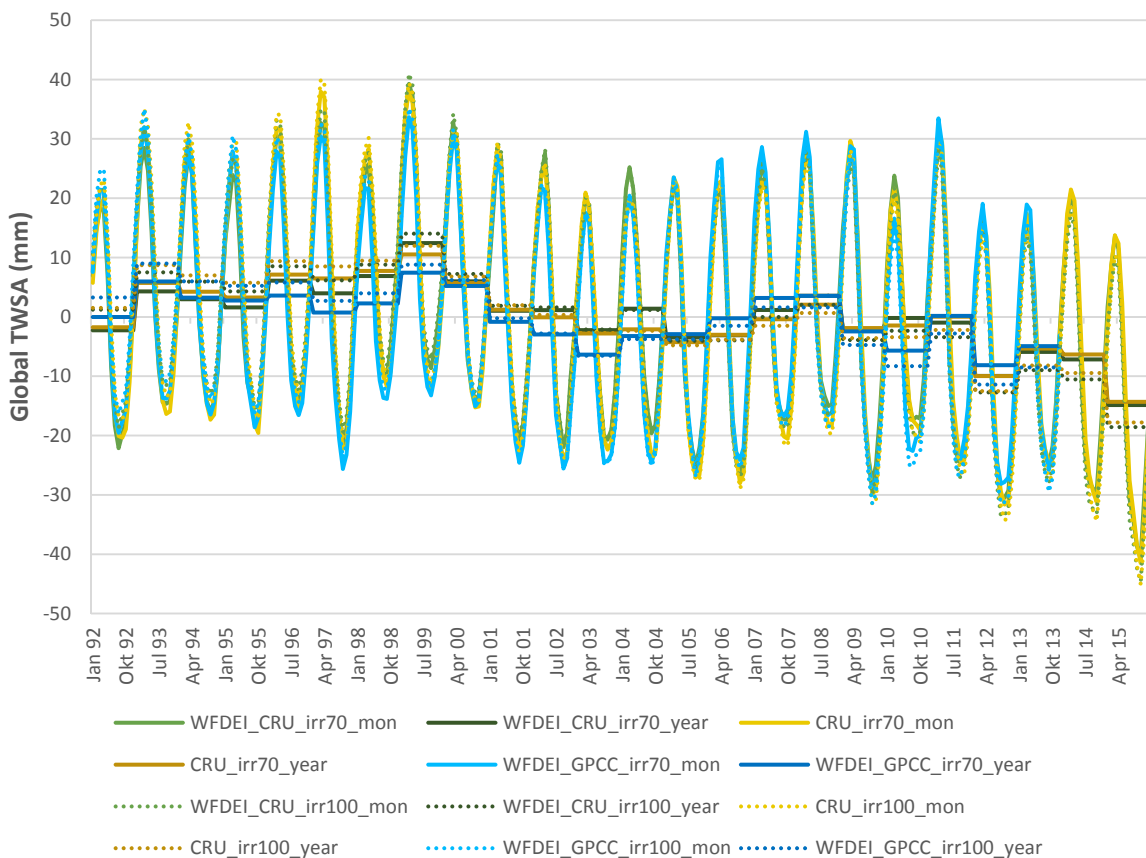


Figure 7.6: Global average for land area (except Antarctica and Greenland) in mm of monthly and annual total water storage anomalies (TWSA) for three climate data sets and two irrigation scenarios between 1992 and 2015 (time series with WFDEI-GPCC forcing only extend until the end of 2013). Here, relative values were calculated by removing the mean value of each dataset. Full curves; 70% deficit irrigation scenario, dotted curves; optimal irrigation scenario.

		<p>CCI Sea Level Budget Closure ESA/ESRIN contract 4000119910/17/I-NB</p> <p>Reference: ESA_SLBC_cci_D2.3.2 Version: v1.2 Date: 22.11.2018 Page: 102 of 119</p>
---	---	---

7.5 References

- Döll, P.; Fiedler, K.; Zhang, J. (2009): Global-scale analysis of river flow alterations due to water withdrawals and reservoirs. *Hydrol. Earth Syst. Sci. Discuss.* 6 (4), S. 4773–4812. DOI: 10.5194/hessd-6-4773-2009.
- Döll, P.; Müller Schmied, Hannes; Schuh, Carina; Portmann, Felix T.; Eicker, Annette (2014): Global-scale assessment of groundwater depletion and related groundwater abstractions: Combining hydrological modeling with information from well observations and GRACE satellites. *Water Resour. Res.* 50 (7), S. 5698–5720. DOI: 10.1002/2014WR015595.
- Hanasaki, Naota; Kanae, Shinjiro; Oki, Taikan (2006): A reservoir operation scheme for global river routing models. *Journal of Hydrology* 327 (1-2), S. 22–41. DOI: 10.1016/j.jhydrol.2005.11.011.
- Harris, I.; Jones, P.D; Osborn, T.J; Lister, D.H (2014): Updated high-resolution grids of monthly climatic observations - the CRU TS3.10 dataset. *Int. J. Climatol.* 34 (3), S. 623–642. DOI: 10.1002/joc.3711.
- Hirabayashi, Yukiko; Döll, P.; Kanae, Shinjiro (2010): Global-scale modeling of glacier mass balances for water resources assessments. Glacier mass changes between 1948 and 2006. *Journal of Hydrology* 390 (3-4), S. 245–256. DOI: 10.1016/j.jhydrol.2010.07.001.
- Hirabayashi, Yukiko; Zang, Yong; Watanabe, Satoshi; Koirala, Sujun; Kanae, Shinjiro (2013): Projection of glacier mass changes under a high-emission climate scenario using the global glacier model HYOGA2. *Hydrological Research Letters* 7 (1), S. 6–11. DOI: 10.3178/hrl.7.6.
- Marzeion, B.; Jarosch, A. H.; Hofer, M. (2012): Past and future sea-level change from the surface mass balance of glaciers. In: *The Cryosphere* 6 (6), S. 1295–1322. DOI: 10.5194/tc-6-1295-2012.
- Müller Schmied, H.; Eisner, S.; Franz, D.; Wattenbach, M.; Portmann, F. T.; Flörke, M.; Döll, P. (2014): Sensitivity of simulated global-scale freshwater fluxes and storages to input data, hydrological model structure, human water use and calibration. In *Hydrol. Earth Syst. Sci.* 18 (9), pp. 3511–3538. DOI: 10.5194/hess-18-3511-2014.
- Schneider, Udo; Becker, Andreas; Finger, Peter; Meyer-Christoffer, Anja; Rudolf, Bruno; Ziese, Markus (2015): GPCC Full Data Reanalysis Version 7.0 at 0.5°: Monthly Land-Surface Precipitation from Rain-Gauges built on GTS-based and Historic Data. *Research Data Archive at the National Center for Atmospheric Research*, Computational and Information Systems Laboratory, Boulder, Colo. (Updated irregularly.). DOI: 10.5676/DWD_GPCC/FD_M_V7_050.
- University of East Anglia Climatic Research Unit; Harris, Ian C.; Jones, Philip D. (2017): *CRU TS4.00. Climatic Research Unit (CRU) Time-Series (TS) version 4.00 of high resolution gridded data of month-by-month variation in climate (Jan. 1901- Dec. 2015)*. In cooperation with Centre for Environmental Data Analysis und Ian C. Harris.
- Weedon, Graham P.; Balsamo, Gianpaolo; Bellouin, Nicolas; Gomes, Sandra; Best, Martin J.; Viterbo, Pedro (2014): The WFDEI meteorological forcing data set. WATCH Forcing Data methodology applied to ERA-Interim reanalysis data. *Water Resour. Res.* 50 (9), S. 7505–7514. DOI: 10.1002/2014WR015638.
- World Glacier Monitoring Service (2017): *Fluctuations of Glaciers Database*. In cooperation with WGMS scientific collaboration network of national correspondents and principal investigators as listed in the related publications above, last visited 07.03.2018.

		<p>CCI Sea Level Budget Closure ESA/ESRIN contract 4000119910/17/I-NB</p> <p>Reference: ESA_SLBC_cci_D2.3.2 Version: v1.2 Date: 22.11.2018 Page: 103 of 119</p>
---	---	---

8 Arctic Sea Level Change

For the Arctic, sea level heights from satellite altimetry as well as sea level heights and steric sea level from the TOPAZ4 model are provided and described in the following sections. Note, that the sea level heights from the TOPAZ4 model are a copy of the version 0 data product (D2.1).

8.1 Data Access and Requirements



The altimetric sea level anomaly (SLA) record is obtained from ERS-2, Envisat, and CryoSat-2 data north of 65°N. Measuring the range between the satellite altimeter and the underlying sea surface yields the sea surface height, which then is referenced to a mean sea surface to obtain SLA. The more homogenous and flat the underlying surface is, the easier it is to estimate the correct range from the altimeter waveform. Large parts of the Arctic Ocean have a permanent or seasonal sea ice cover, which makes accurate range estimation difficult. For the v1 time series, we therefore used a newly developed physical retracker, which adapts to the surface in order to appropriately fit the received waveform.

In addition, data on both sea level change and steric sea level change are also obtained from the TOPAZ4 data assimilation system operated at NERSC. This system represents the Arctic Marine Forecasting Center of the Copernicus Marine Services (<http://marine.copernicus.eu/>). The system delivers routinely products and information used for analyses, forecast (up to 10 days) and reanalyses.

8.2 Algorithms

8.2.1 Review of scientific background

DTU Arctic Altimetric Sea Level Record: To obtain the altimetric SLA record, ERS-2 and Envisat data have been retracked using the Adaptive Leading Edge Subwaveform (ALES+) retracker. The ALES+ (Passaro et al., 2018) retracker is similar to the original ALES retracker (Passaro et al., 2014), but has been adjusted to fit waveform returns from all types of water surfaces, i.e. not only open ocean, but also coastal areas, lakes and rivers, and sea ice covered areas. 1 Hz CryoSat-2 data in LRM and SAR mode were taken from the Radar Altimetry Database System (RADS, Scharoo et al., 2013). However, 20 Hz CryoSat-2 SAR and SARIn data have been retracked by the Lars Advanced Retracking System (LARS) system (Stenseng, 2011), since RADS is not able to handle 20 Hz data, which is necessary in order to retrieve height estimates from sea ice leads.

		<p>CCI Sea Level Budget Closure ESA/ESRIN contract 4000119910/17/I-NB</p> <p>Reference: ESA_SLBC_cci_D2.3.2 Version: v1.2 Date: 22.11.2018 Page: 104 of 119</p>
---	---	---

The retracking methods used for the v1 data have been chosen due to the need for a better height retrieval in the Arctic Ocean, where traditional retrackers are not sufficient for extracting accurate height estimates in sea ice leads. In addition, not only a higher quality of data is needed, but definitely also a higher quantity of data. At the moment, most data are acquired during the late summer season, where peaky waveforms from melt ponds on top of sea ice might be mistaken for the desired waveforms stemming from sea ice leads.

Hopefully, using the ALES+ retracker as well as utilizing the retracking of CryoSat-2 SAR and SARIn data in the LARS system at DTU Space will provide a higher quality and quantity of data compared to standard ocean retracking.

NERSC TOPAZ4: NERSC TOPAZ4 is a coupled ocean and sea ice data assimilation system for the North Atlantic and the Arctic Ocean that is based on the Hybrid Coordinate Ocean Model (HYCOM) and the Ensemble Kalman Filter data assimilation (Sakov et al. 2012). HYCOM is using 28 hybrid z-isopycnal layers at a horizontal resolution varying from 16 km in North Atlantic to 12 km in the Arctic Ocean. The TOPAZ4 system is forced by the ECMWF ERA Interim reanalysis and assimilates most available measurements including along-track altimetry data, sea surface temperatures, sea ice concentrations and sea ice drift from satellites along with in-situ temperature and salinity profiles from Argo floats and research cruises. For validation results and more details see Sakov et al. (2012) and Xie et al. (2017).



8.2.2 Algorithms

ALES+

ALES+ is a subwaveform retracking algorithm that takes into account the sea state and the slope of the trailing edge. The retracking algorithm itself is based on the Brown-Hayne model (Brown, 1977 and Hayne, 1980) and contains a preliminary step in order to estimate the most appropriate length of the trailing edge contained by the subwaveform. For very specular waveforms, the trailing edge is much shorter, which is taken into account during the fitting of the procedure if the waveform is found to be a “non-standard” ocean waveform. Non-standard ocean waveforms are detected by identifying waveforms with a pulse peakiness (PP) higher than 1 (PP>1). The PP value is determined as defined by Peacock and Laxon (2014):

$$PP = 31.5 \frac{p_{max}}{\sum_{i=5}^{64} p_i} ,$$

where pmax is the maximum power of the waveform and p_i is the power in range bin number i . More on the retracking algorithms can be found in Passaro et al. (2014) and Passaro et al. (2018).

		<p>CCI Sea Level Budget Closure ESA/ESRIN contract 4000119910/17/I-NB</p> <p>Reference: ESA_SLBC_cci_D2.3.2 Version: v1.2 Date: 22.11.2018 Page: 105 of 119</p>
---	---	---

LARS

For 20 Hz SAR and SARIn data from LARS we are only including waveforms retrieved over ice leads. Within the LARS database, the waveforms are retracked using a simple threshold retracker. Ice lead waveforms are then found to be those with a PP higher than 0.35 for SAR and 0.25 for SARIn, and a stack standard deviation lower than 4. For the CryoSat-2 SAR and SARIn data, PP is defined as in Armitage and Davidson (2014):

$$PP = \frac{p_{max}}{\sum_1^N p_i} ,$$

where p_{max} is the maximum power of the waveform, N is the number of range bins in the waveform (128 for SAR, 512 for SARIn), and p_i is the power in bin number i .

Intermission bias

To make a seamless transition between the three satellite missions, the intermission biases were estimated and minimized. The following steps were completed to handle the intermission biases:

1. Diurnal means were calculated for each mission for the entire region covered by the data set.
2. For overlapping mission pairs (either ERS-2 and Envisat, or Envisat and CryoSat-2), coinciding days were detected and extracted.
3. The trend was removed for each data set containing coinciding diurnal means.
4. For each data set, the median was determined.
5. For each overlapping pair, the median difference was calculated and the data sets were aligned.
6. The data sets were corrected corresponding to the RADS reference.

For CryoSat-2, RADS and LARS data have been corrected using the same procedure, although only using data between 70°N to 88°N and -70°E to -20°E. This region was chosen due to its multi-year sea ice (above 82°N), making the data more stable and appropriate for long-term comparisons.

A time series showing the weekly mean SLA for the entire Arctic region is shown in Figure 8.1. The time series has been constructed by taking a weighted average of each weekly mean grid from the netCDF file. The weights were derived from the inverse of the uncertainty, e , multiplied by cosine of the latitude, for each grid point, i , out of all N grid points:

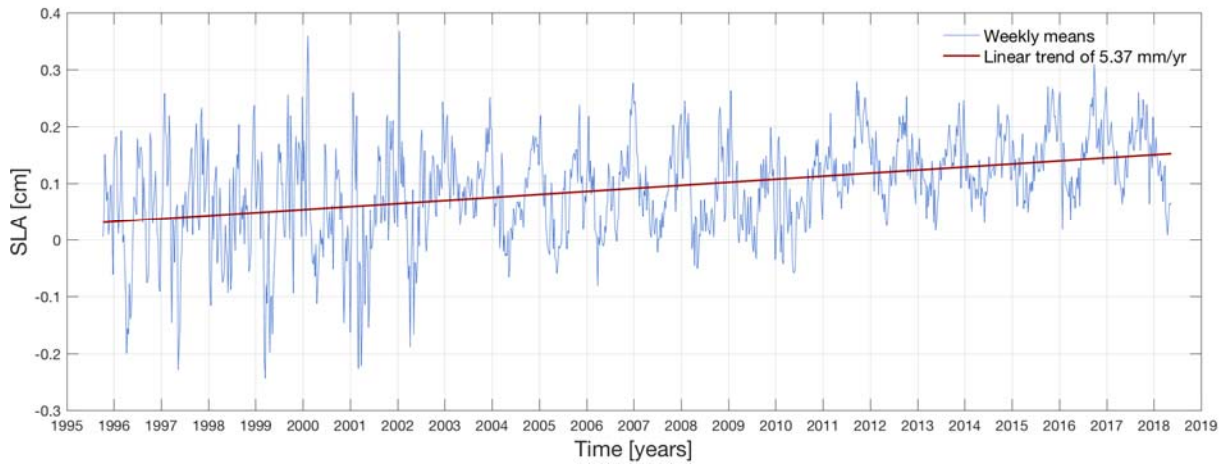


Figure 8.1: DTU/TUM Arctic sea level record

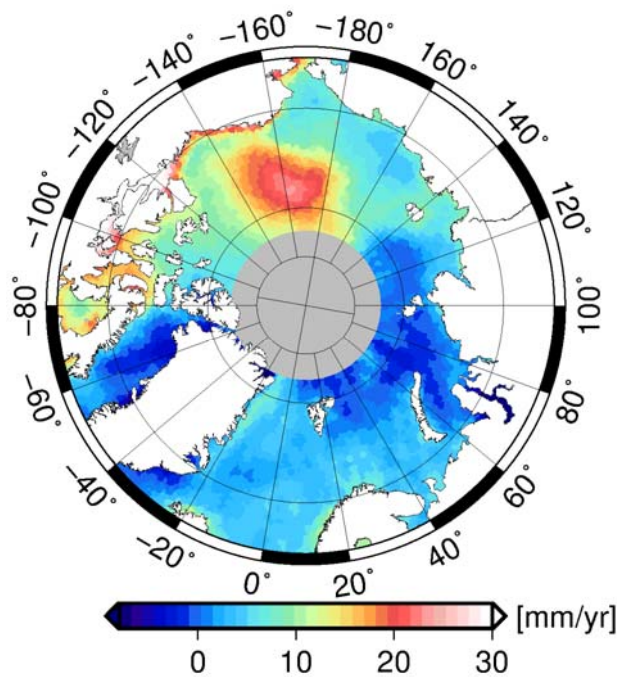


Figure 8.2: Trend of DTU/TUM Arctic sea level record between 1995 and 2018

		<p>CCI Sea Level Budget Closure ESA/ESRIN contract 4000119910/17/I-NB</p> <p>Reference: ESA_SLBC_cci_D2.3.2 Version: v1.2 Date: 22.11.2018 Page: 107 of 119</p>
---	---	---

$$w_i = \frac{\frac{1}{e_i} * \cos(lat_i)}{\sum_i^N \frac{1}{e_i} * \cos(lat_i)}$$

The average SLA for each week, t , was then found to be:

$$\overline{SLA}_t = \sum_i^N w_i * SLA_i$$

The time series have a mean trend of 5.4 mm/year for the entire Arctic region. The spatial distribution of the trend can be seen in Figure 8.2.

8.3 Product Specification

8.3.1 Product geophysical data content

DTU Arctic Altimetric Sea Level Record: The data con SLA record was corrected for all geophysical corrections and is referenced to the DTU15MSS. The ocean tides are from FES2014. Since all corrections have been applied (in particular tides and atmospheric pressure effects), the SLA data are not directly comparable to tide gauge data.

Weekly mean SLA covering the region from 65°N-82°N and 180°W-180°E are provided for the period October 1995 and May 2018 with the file

ARCTIC_SLA_v1.1.nc

Geophysical Variable	Name in product	Unit
Longitude	lon	degrees east
Latitude	lat	degrees north
Date of weekly mean SLA estimate	date	YYYYMMDD
SLA above DTU15MSS	sla	m
uncertainty of SLA	sla_error	m
Mission initials	source_mission	Mission Initials: e = ERS-2 n = Envisat c = CryoSat-2

		CCI Sea Level Budget Closure ESA/ESRIN contract 4000119910/17/I-NB Reference: ESA_SLBC_cci_D2.3.2 Version: v1.2 Date: 22.11.2018 Page: 108 of 119
---	---	--

NERSC TOPAZ4: The TOPAZ4 products contain gridded sea surface height (meters; relative to geoid), and steric height (meters).

Files: (1) topazssh20032015.nc (sea surface height, SSH)
(2) topazstht20032015.nc (steric height)

Geophysical Variable	Name in product	Unit
Longitude	LONGITUDE	degrees_east
Latitude	LATITUDE	degrees_north
Time	TAX	months since 1901-01-15 00:00:00
(1) Sea Surface Height	SSHTOP	m
(2) Steric Sea Level	STERICHT	m

8.3.2 Coverage and resolution in time and space

DTU Arctic Altimetric Sea Level Record: The SLA data cover the region from 65°N-82°N and 180°W-180°E with a resolution of 0.25° in latitudinal direction and 0.5° in longitudinal direction, respectively. Data are given in weekly intervals between October 1995 and May 2018. Until July 2003, data are from ERS-2, from August 2003 to mid-October 2010 data are from Envisat, and from mid-October 2010 to May 2018, data are from CryoSat-2.

There are fewer data points from ERS-2 and Envisat compared to CryoSat-2, and for all of the missions, the data coverage is highest during summer/fall.

NERSC TOPAZ4: The TOPAZ4 covers the North Atlantic and entire Arctic Oceans bounded by 20°N - 90°N and 180°W to 180°E with a spatial resolution of 0.125°. The temporal coverage is from 2003-2015 at a monthly resolution.

8.3.3 Product data format

DTU Arctic Altimetric Sea Level Record: The Arctic SLA record is provided in a netCDF file.

NERSC TOPAZ4: The format of the TOPAZ4 fields is in NetCDF CF 1.0. Dimensions are 2881 in longitude and 561 in latitude and 156 in time, and variables are SSHTOP and STERICHT.

8.3.4 Product grid and projection

DTU Arctic Altimetric Sea Level Record: The data are provided in a grid with a resolution of 0.25 degrees in the latitudinal direction and 0.5 degrees in the longitudinal direction. Data points are located at -180:0.5:180 degrees longitude and 65:0.25:82 degrees latitude.

		<p>CCI Sea Level Budget Closure ESA/ESRIN contract 4000119910/17/I-NB</p> <p>Reference: ESA_SLBC_cci_D2.3.2 Version: v1.2 Date: 22.11.2018 Page: 109 of 119</p>
---	---	---

NERSC TOPAZ4: The TOPAZ4 is provided on a regular $0.125^\circ \times 0.125^\circ$ latitude-longitude grid.

8.4 Uncertainty assessment

8.4.1 Sources of error

DTU Arctic Altimetric Sea Level Record: When it comes to satellite altimetry in the Arctic Ocean there are multiple error sources:

- Erroneous range estimates caused by highly reflective melt ponds on sea ice (mostly during summer).
- Inaccurate range corrections from atmospheric models – e.g. the dynamic atmospheric correction.
- Inaccurate tide models. The tidal models are based on altimetry, and in an area with less altimetry data, such as sea ice covered regions in the Arctic Ocean, it is to be expected that the tidal model (in this case FES2014) is less accurate.

However, not all of the above listed error sources are directly quantifiable, and those that are, are difficult to keep track of during interpolation and transformation to polar stereographic coordinates. Therefore, the uncertainty estimates included in this altimetry SLA product is the sum of the interpolation errors and an estimated uncertainty of 2 cm to account for range and geophysical corrections.

The interpolation error itself only says something about the availability of data. When there is less data, the error is higher, i.e. in winter and spring in regions where the sea ice cover does not allow for retrieval of sea level heights. In general, the geophysical corrections will also be more uncertain in these areas. E.g., tidal models are tuned and validated with altimetry data from earlier missions – hence, regions with less data available from altimetry will be prone to inaccurate tidal signals.

By adding 2 cm to the interpolation error, we hope to capture the uncertainty of the various geophysical corrections applied to obtain the final SLA, but more work should be put into quantifying the uncertainties linked to satellite altimetry in the Arctic Ocean.

NERSC TOPAZ4: The sources of error come predominantly arise from deficiency in the TOPAZ4 model system and lack of in-situ data for assimilation.

8.4.2 Methodology for uncertainty assessment

Firstly, it was necessary to look at the interpolation errors from the gridding procedure.

Figure 8.3 shows the median interpolation error as a function of time for the weekly gridded SLA product. For the ERS-2 and Envisat periods, the time series behave in a similar manner with a strong seasonal signal. Higher errors during winter and spring, and lower in summer/autumn. This seasonality can be explained by sea ice cover, making it difficult for the conventional altimeter to retrieve sea level heights. When CryoSat-2 is introduced in 2010, the seasonal signal disappears, most likely because the new SAR altimeter, which has a higher along-track resolution, is able to capture sea level retrievals in leads and is generally less affected by the presence of sea ice in the along-track direction.

However, for fairness it should also be mentioned, that since the launch of CryoSat-2, the amount of sea ice cover in the Arctic has been fairly low compared to normal (1981-2010 median, <https://nsidc.org/arcticseaicenews/charctic-interactive-sea-ice-graph/>).

From Figure 8.3 it can also be seen that the median error usually ranges between 1.5 cm to 3.5 cm, which is a little low compared to the error we expect in this area. In the Arctic Ocean, we would expect a total uncertainty of around 4-5 cm. We therefore add 2 cm to all interpolation errors in order to arrive at a total uncertainty, which is expected to account for both the temporal and spatial distribution of the data and for the uncertainties associated with range measurements, geophysical corrections, etc.

8.4.3 Results of uncertainty assessment

Figure 8.4 shows two examples of the uncertainties related to the weekly gridded SLA data. The left plot shows the uncertainty linked to CryoSat-2 SLA estimates from the first week of March 2015. During spring, many areas are covered with sea ice, which leads to fewer data points, and thereby a higher interpolation error. The interpolation error is visibly lower near the CryoSat-2 tracks with errors down to around 3 cm. The plot on the right-hand side in Figure 8.4 shows the uncertainties given for the ERS-2 SLA estimates retrieved in the first week of October 1998. Compared to springtime, the uncertainties are much lower – most likely due to a lesser extent of sea ice. It is also worth noticing the difference in track patterns compared to CryoSat-2.

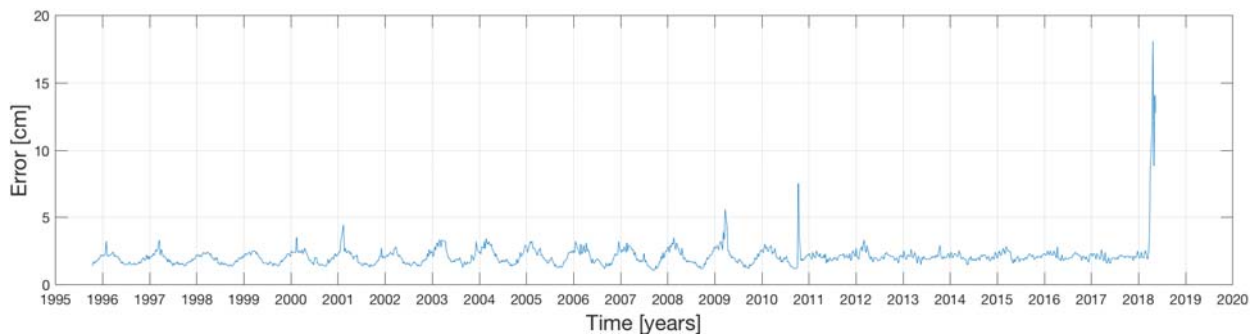



Figure 8.3: Median interpolation error for the entire Arctic region.

		<p>CCI Sea Level Budget Closure ESA/ESRIN contract 4000119910/17/I-NB</p> <p>Reference: ESA_SLBC_cci_D2.3.2 Version: v1.2 Date: 22.11.2018 Page: 111 of 119</p>
---	---	---

8.4.4 Uncertainty documentation in the data products

The estimated uncertainties associated with the SLA are given as a separate variable in the netCDF file. The uncertainty estimate is the sum of the interpolation error and the 2 cm added to account for uncertainties related to range and geophysical corrections.

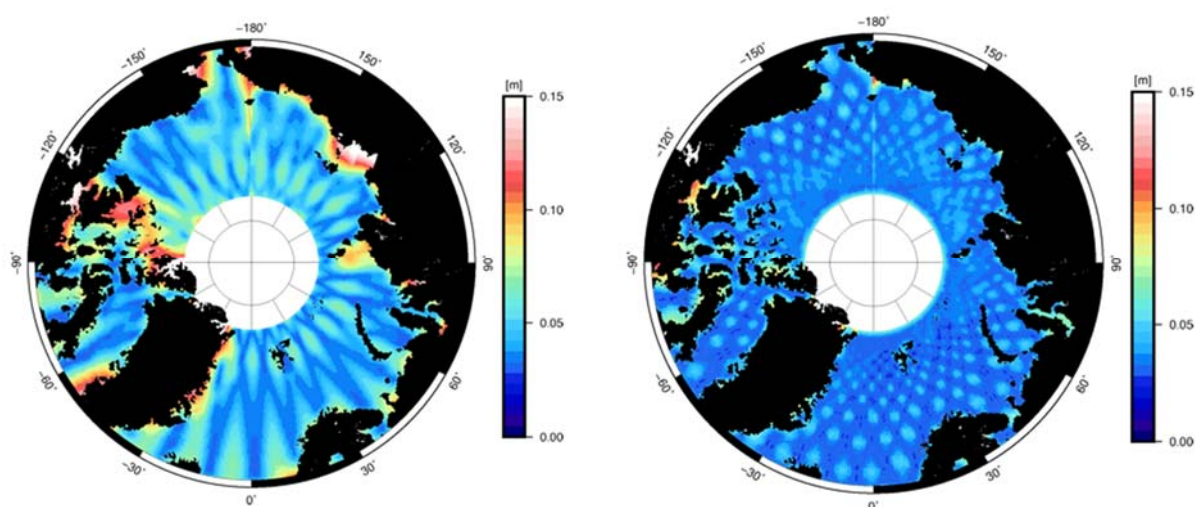


Figure 8.4: Maps of total uncertainty from CryoSat-2 for the first week of March 2015 (left) and ERS-2 for the first week of October 1998 (right).

8.5 References

- Armitage, T. W. K., and M. W. J. Davidson (2014): Using the Interferometric Capabilities of the ESA CryoSat-2 Mission to Improve the Accuracy of Sea Ice Freeboard Retrievals, *IEEE Transactions on Geoscience and Remote Sensing*, vol. 52, no. 1, pp. 529-536, Jan. 2014. doi: 10.1109/TGRS.2013.2242082. <http://ieeexplore.ieee.org/stamp/stamp.jsp?tp=&arnumber=6479282&isnumber=6675822>
- Brown, G.S. (1977): The average impulse response of a rough surface and its applications. *IEEE Trans. Antennas Propag.* 25, 67–74. <http://dx.doi.org/10.1109/TAP.1977.1141536>.
- Hayne, G.S. (1980): Radar altimeter mean return waveforms from near-normal-incidence ocean surface scattering. *IEEE Trans. Antennas Propag.* 28, 687–692. doi: 10.1109/TAP.1980.1142398.
- Passaro, M., Cipollini, P., Vignudelli, S., Quartly, G., and Snaith, H. (2014): ALES: A multimission subwaveform retracker for coastal and open ocean altimetry. *Remote Sens. Environ.* 145, 173–189. doi: 10.1016/j.rse.2014.02.008.

		<p>CCI Sea Level Budget Closure ESA/ESRIN contract 4000119910/17/I-NB</p> <p>Reference: ESA_SLBC_cci_D2.3.2 Version: v1.2 Date: 22.11.2018 Page: 112 of 119</p>
---	---	---

- Passaro, M., S. K. Rose, O. B. Andersen, E. Boergens, F. M. Calafat, D. Dettmering, and J. Benveniste (2018): ALES+: Adapting a homogenous ocean retracker for satellite altimetry to sea ice leads, coastal and inland waters. *Remote Sens. Environ.*, 211, 456-471. doi: 10.1016/j.rse.2018.02.074.
- Peacock, N.R., and Laxon, S.W. (2004): Sea surface height determination in the Arctic ocean from ERS altimetry. *J. Geophys. Res. Oceans* 109. doi: 10.1029/2001JC001026.
- Sakov, P., F. Counillon, L. Bertino, K. A. Lisæter, P. R. Oke, and A. Korabely (2012) TOPAZ4: an ocean-sea ice data assimilation system for the North Atlantic and Arctic. *Ocean Science*, 8:633-656, doi:10.5194/os-8-633-2012.
- Scharroo, R., Leuliette, E. W., Lillibridge, J. L., Byrne, D., Naeije, M. C., and Mitchum, G. T. (2013): RADS: Consistent multi-mission products, *Proceedings of the Symposium on 20 Years of Progress in Radar Altimetry*, Venice: ESA Spec. Publ., ESA SP-710, 4.
- Stenseng, L. (2011): *Polar Remote Sensing by CryoSat-type Radar Altimetry*. Ph.D. thesis. National Space Institute, Technical University of Denmark.
- Xie, J., L. Bertino, F. Counillon, K. A. Lisæter, and P. Sakov (2017): Quality assessment of the TOPAZ4 reanalysis in the Arctic over the period 1991-2013, *Ocean Sci.*, 13(1), pp. 123-144, doi:10.5194/os-2016-38, 2016 doi:10.5194/os-13-123-2017.

Appendix

Complementary material for Chapter 7 “Total Land Water Storage Change”

Table A 1: Efficiency criteria values derived from comparison between observed and simulated monthly reservoir storage. r : correlation coefficient, NSE: Nash-Sutcliffe efficiency, KGE: Kling-Gupta efficiency, KGE_r : correlation coefficient component, KGE_{Beta} : mean bias component, KGE_{Gamma} : coefficient of variation component.

Reservoir name	r	NSE	KGE	KGE_r	KGE_{Beta}	KGE_{Gamma}
Lake Berryessa	0.37	-12.68	-0.25	0.37	0.17	1.7
Cascade reservoir	0.07	-0.59	0.06	0.07	0.99	0.86
New Don Pedro reservoir	0.81	0.52	0.78	0.81	0.89	0.99
Hungry Horse reservoir	0.45	-0.97	0.37	0.45	0.73	0.85
Amistad lake	0.72	0.33	0.7	0.72	1.05	1.08
Livingston reservoir	0.24	-3.15	-0.17	0.24	0.74	1.85
Mohave lake	0.36	-15.03	-0.75	0.36	0.54	2.56
New Melones reservoir	0.57	0.23	0.56	0.57	1.01	0.88
Oroville lake	0.67	-2.31	-0.24	0.67	0.55	2.1
Palisades reservoir	0.48	-0.04	0.39	0.48	0.77	0.76
Pine Flat lake	0.71	0.46	0.61	0.71	1.09	0.76
Powell lake	0.54	-0.53	0.43	0.54	0.68	0.92
Richland-Chambers reservoir	0.6	-5.61	0.03	0.6	0.64	1.81
Sam Rayburn reservoir	0.7	-9.22	0.26	0.7	1.62	1.24
San Luis reservoir	-0.18	-4.75	-0.5	-0.18	0.09	0.82
Toledo Bend reservoir	0.53	-1.37	0.16	0.53	0.83	1.68

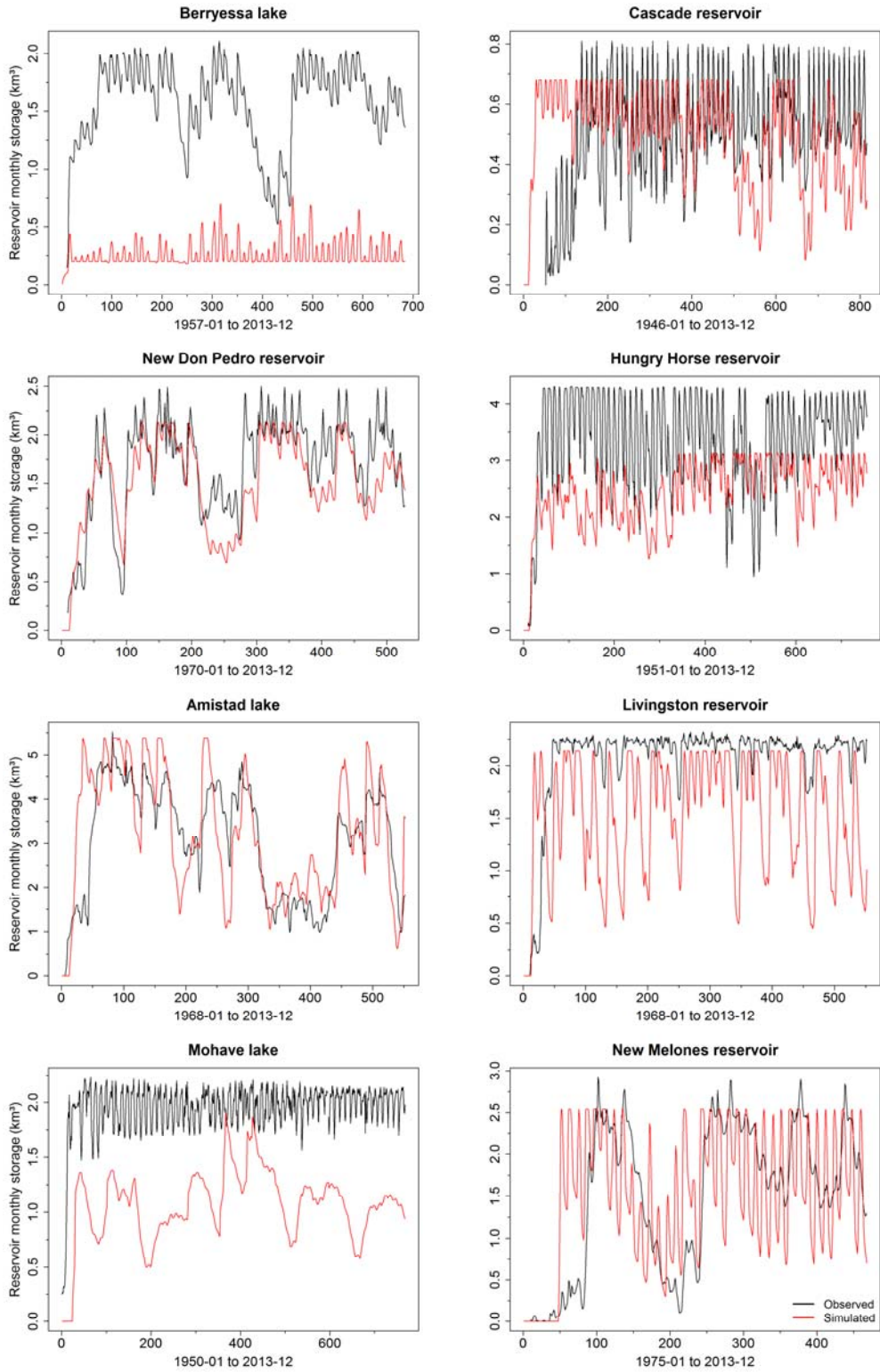


Figure A 1: Comparison of observed to simulated (WaterGAP 2.2c forced by WFDEI-GPCC dataset) reservoir monthly storage for eight reservoirs in the USA. Black curves; observations, red curves; simulated data.

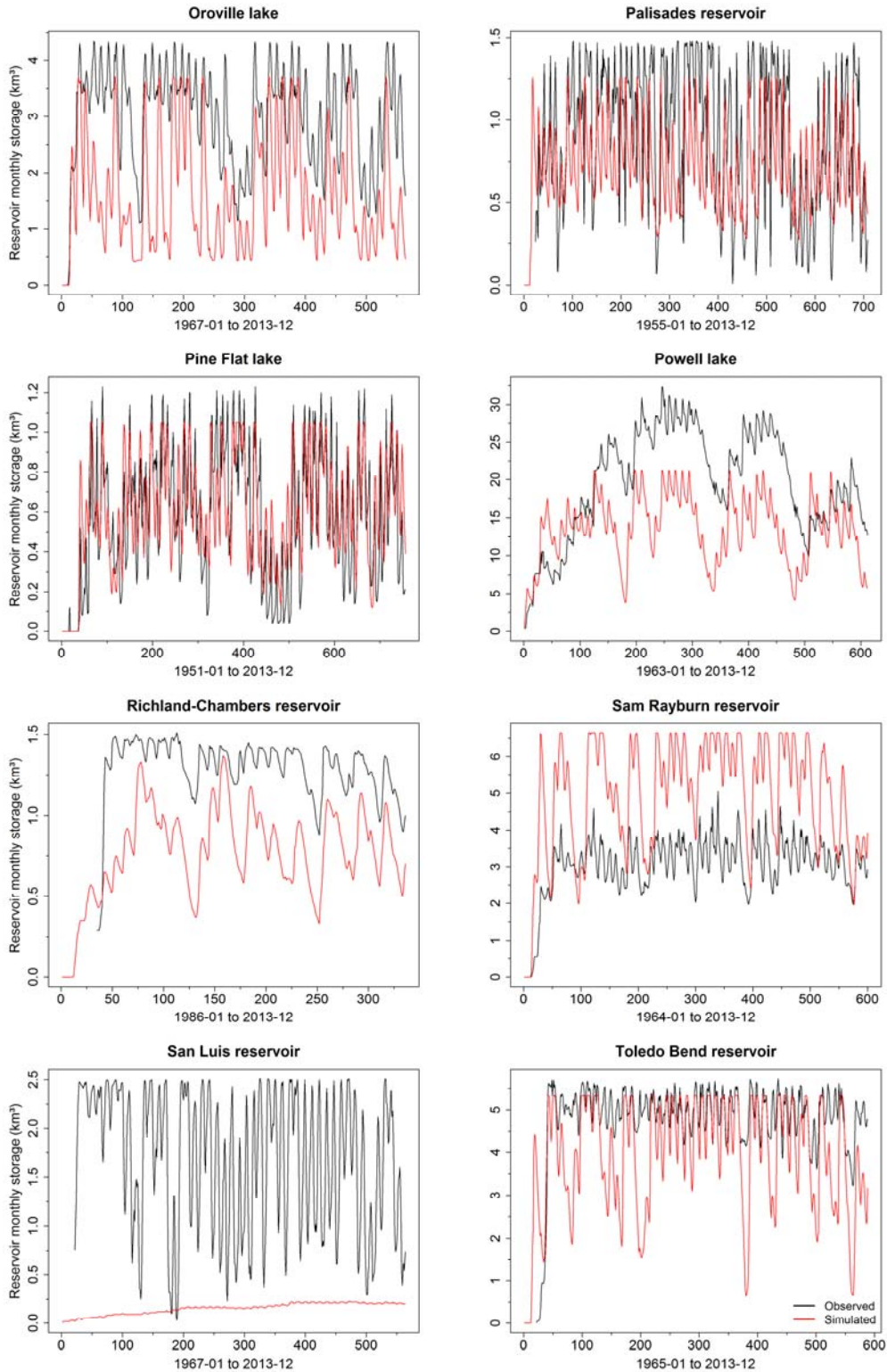


Figure A 2: Comparison of observed to simulated (WaterGAP 2.2c forced by WFDEI-GPCC dataset) reservoir monthly storage for eight reservoirs in the USA. Black curves: observations, red curves: simulated data.

		<p>CCI Sea Level Budget Closure ESA/ESRIN contract 4000119910/17/I-NB</p> <p>Reference: ESA_SLBC_cci_D2.3.2 Version: v1.2 Date: 22.11.2018 Page: 116 of 119</p>
---	---	---

Table A 2: Comparison of groundwater depletion computed by WaterGAP 2.2a and WaterGAP 2.2c (70% deficit irrigation scenario) to independent estimates for selected regions. W: groundwater well observations; M: modeling; G: derived from GRACE TWS data; O: other methods. Observed data from Döll et al. (2014).

Study region	Area [1000 km ²]	Period	Independently estimated GWD [mm/yr (km ³ /yr)]	Modeled GWD [mm/yr (km ³ /yr)]			
				WG22a (70% irr.)	WG22c (70% irr.)	WG22c (70% irr.)	WG22c (70% irr.)
				CRU TS 3.10	WFDEI-GPCC	WFDEI-CRU	CRU TS 4.00
USA							
High Plains aquifer	488	1950-2000	10 (5) W	15 (7)	17 (8)	18 (9)	13 (6)
	488	2000-2009	21 (10) W	20 (10)	25 (12)	27 (13)	20 (10)
Central Valley aquifer	53	1961-2000	26 (1) M	14 (0.8)	19 (1)	18 (0.9)	16 (0.8)
	53	2001-2009	73 (4) M, G	21 (1)	27 (1)	24 (1)	23 (1)
Gulf coastal plain	518	1961-2000	8 (4) O	0.8 (0.4)	7 (4)	7 (4)	2 (1)
	518	2001-2008	16 (8) O	-0.2 (-0.1)	9 (5)	10 (5)	2 (1)
Atlantic coastal plain	265	1961-2000	0.7 (0.2) O	4 (1)	17 (4)	16 (4)	16 (4)
	265	2001-2008	1 (0.3) O	4 (1)	13 (3)	11 (3)	12 (3)
Northeastern China							
North China Plain	140	2000-2008	27 (4) M	127 (18)	29 (4)	25 (3)	19 (3)
Hai river basin	330	1958-1998	7 (2) W	24 (8)	2.7 (0.9)	3 (1)	3 (1)
	330	1999-2006	13 (4) W	58 (19)	15 (5)	14 (5)	12 (4)
	330	2003-2006	23 W / 12 G (8 W / 4 G)	59 (20)	12 (4)	12 (4)	10 (3)
	330	2003-2010	25 ± 3 (8 ± 1) G	67 (22)	12 (4)	12 (4)	11 (3)

		CCI Sea Level Budget Closure ESA/ESRIN contract 4000119910/17/I-NB Reference: ESA_SLBC_cci_D2.3.2 Version: v1.2 Date: 22.11.2018 Page: 117 of 119
---	---	--

Table A 3: Comparison of groundwater depletion computed by WaterGAP 2.2a and WaterGAP 2.2c (optimal irrigation scenario) to independent estimates for selected regions. W: groundwater well observations; M: modeling; G: derived from GRACE TWS data; O: other methods. Observed data from Döll et al. (2014).

Study region	Area [1000 km ²]	Period	Independently estimated GWD [mm/yr (km ³ /yr)]	Modeled GWD [mm/yr (km ³ /yr)]			
				WG22a (100% irr.)	WG22c (100% irr.)	WG22c (100% irr.)	WG22c (100% irr.)
				CRU TS 3.10	WFDEI-GPCC	WFDEI-CRU	CRU TS 4.00
USA							
High Plains aquifer	488	1950-2000	10 (5) W	23 (11)	27 (13)	28 (14)	20 (10)
	488	2000-2009	21 (10) W	32 (15)	40 (19)	42 (20)	29 (14)
Central Valley aquifer	53	1961-2000	26 (1) M	20 (1)	26 (1)	24 (1)	21 (1)
	53	2001-2009	73 (4) M, G	27 (1)	36 (2)	32 (2)	29 (2)
Gulf coastal plain	518	1961-2000	8 (4) O	1 (0.5)	7 (4)	7 (4)	2 (1)
	518	2001-2008	16 (8) O	#-0.1 (-0.1)	9 (5)	10 (5)	2 (1)
Atlantic coastal plain	265	1961-2000	0.7 (0.2) O	4 (1)	17 (4)	16 (4)	16 (4)
	265	2001-2008	1 (0.3) O	4 (1)	13 (3)	11 (3)	12 (3)
Northeastern China							
North China Plain	140	2000-2008	27 (4) M	152 (21)	53 (7)	44 (6)	31 (4)
Hai river basin	330	1958-1998	7 (2) W	32 (11)	7 (2)	7 (2)	5 (2)
	330	1999-2006	13 (4) W	71 (23)	25 (8)	22 (7)	17 (6)
	330	2003-2006	23 W / 12 G (8 W / 4 G)	71 (23)	22 (7)	19 (6)	15 (5)
	330	2003-2010	25 ± 3 (8 ± 1) G	81 (27)	23 (7)	21 (7)	16 (5)



		CCI Sea Level Budget Closure ESA/ESRIN contract 4000119910/17/I-NB Reference: ESA_SLBC_cci_D2.3.2 Version: v1.2 Date: 22.11.2018 Page: 118 of 119

Table A 4: List of glaciers considered for the comparison between observed and simulated (OGGM) glacier seasonal mass balance. The observational data was obtained from the World Glacier Monitoring Service (2017). NSE: Nash-Sutcliffe efficiency, r: correlation coefficient.

Glacier name	RGI Region	Is tidewater	Area (km ² , 1950)	r	NSE	Glacier name	RGI Region	Is tidewater	Area (km ² , 1950)	r	NSE
Gulkana	01: Alaska	False	17.57	0.97	0.23	Storglaciaeren	08: Scandinavia	False	3.16	0.94	0.68
Wolverine	01: Alaska	False	0.03	0.97	0.86	Engabreen	08: Scandinavia	False	42.95	0.98	0.93
Melville South Ice Cap	02: Western Canada and US	False	1.24	0.9	0.77	Aalfotbreen	08: Scandinavia	False	4.86	0.99	0.97
Helm	02: Western Canada and US	False	0.98	0.99	0.91	Vodopadnyy	10: North Asia	False	0.76	0.9	0.8
Place	02: Western Canada and US	False	3.02	0.99	0.98	Maliy Aktru	10: North Asia	False	2.62	0.89	0.57
Peyto	02: Western Canada and US	False	9.70	0.97	0.72	Leviy Aktru	10: North Asia	False	5.67	0.95	0.68
South Cascade	02: Western Canada and US	False	3.55	0.99	0.97	Careser	11: Central Europe	False	2.84	0.97	0.91
Devon Ice Cap NW	03: Arctic Canada North	True	765.44	0.94	-0.68	Gries	11: Central Europe	False	5.29	0.98	0.84
Meighen Ice Cap	03: Arctic Canada North	False	92.93	0.88	0.73	Sarennes	11: Central Europe	False	0.44	0.96	0.85
Midtre Lovénbreen	07: Svalbard	False	5.21	0.96	0.9	Vernagt F.	11: Central Europe	False	8.56	0.96	-1.23
Austre Broeggerbreen	07: Svalbard	False	9.81	0.96	0.9	Silvretta	11: Central Europe	False	2.88	0.97	0.92
Rembedalskaaka	08: Scandinavia	False	16.83	0.97	0.88	Hintereis F.	11: Central Europe	False	8.04	0.99	0.94
Storbreen	08: Scandinavia	False	5.21	0.98	0.97	Djankuat	12: Caucasus and Middle East	False	1.76	0.99	0.85
Graasubreen	08: Scandinavia	False	2.00	0.96	0.48	TS. Tuyuksuyskiy	13: Central Asia	False	2.84	0.93	0.52
Hellstugubreen	08: Scandinavia	False	3.28	0.98	0.94	Echaurren Norte	17: Southern Andes	False	0.34	0.96	0.71
Nigardsbreen	08: Scandinavia	False	38.10	0.97	0.91	-	-	-	-	-	-

End of document